HYDRODYNAMIC MODELING OF NETS AND TRAWLS

By

M. KRISHNAMURTHY

A DISSERTATION PRESENTED TO THE GRADUATE COUNCIL OF
THE UNIVERSITY OF FLORIDA
IN PARTIAL FULFILLMENT OF THE REQUIREMENTS FOR THE
DEGREE OF DOCTOR OF PHILOSOPHY

UNIVERSITY OF FLORIDA

1975

ACKNOWLEDGEMENTS

The author wishes to express his sincere gratitude to Dr. B. A. Christensen, under whose guidance this work was carried out, for his advice and invaluable suggestions throughout the study. This work would not have been accomplished but for his patient guidance.

The author would like to thank Dr. Pop-Stojavanic for his discussions during the course of the study. Thanks are also due to Dr. Huber for serving on the supervisory committee of the author.

Appreciation is extended to all of his friends in the hydraulics laboratory, especially to Fred Morris and Tracy Lenocker for their help during the period of experiments. Assistance from the Marine Extension Center of the University of Georgia is acknowledged. Mr. W. H. Burbank of Fernandina Beach has provided invaluable suggestions and assistance in the net designs.

The author appreciates the financial support received from the National and Oceanic and Atmospheric Administration Office of Sea Grant.

The typing of this dissertation has been ably performed by Mrs. Carolyn Lyons.

TABLE OF CONTENTS

		Page
ACKNOWLEDGEMENTS		ii
LIST OF TABLES		vi
LIST OF FIGURES		vii
LIST OF SYMBOLS		xi
ABSTRACT		xvii
Chapter		
1	INTRODUCTION	1
	1.1 Statement of Problem	1
	1.2 Objectives	7
2	COMPONENTS OF A GEAR	9
	2.1 Net	9
	2.2 Ropes	28
	2.3 Sweeplines	32
	2.4 Doors	33
	2.5 Towing Warp	36
3	LITERATURE REVIEW	41
	3.1 Mathematical Modeling of Fish Nets	41
	3.2 Physical Modeling of Nets and Trawls	44
	3.3 Prototype Experiments	70
	3.4 Pitfalls in Existing Physical Model Laws	71
4	DEVELOPMENT OF MODEL LAWS	74
	4.1 Froude Modeling	74
	4.2 Mesh-Twine Distortion	74
	4.3 Elongation of Twine	80
	4.4 Modeling of Ropes	84
	4.5 Modeling of Floats and Sinkers	86
	4.6 Modeling of Doors	88

TABLE OF CONTENTS—Continued

Chapter		Page
5	PROTOTYPE FIELD TESTS	89
	5.1 Parameters Measured	89
	5.2 Net and Towing Site	90
	5.3 Instrumentation	91
	5.4 Test Procedure	107
	5.5 Test Results	109
6	MODEL EXPERIMENTS	113
	6.1 Selection of Scale Ratios	113
	6.2 Instrumentation of Model Net	123
	6.3 Description of Experimental Apparatus	131
	6.4 Test Procedure	140
7	DISCUSSION OF RESULTS	160
	7.1 Validity of Model Laws	160
	7.2 Effect of the Movable Belts	164
	7.3 Comparison Between Physical and Mathematical Models	166
8	APPLICATION OF MODEL APPROACH IN DESIGNING A BEAM TRAWL	171
	8.1 Introduction	171
	8.2 Description of the Beam Trawl	172
	8.3 Design of the Beam Trawl	175
	8.4 Model and Field Experiments	181
	8.5 Discussion and Results	185
9	CONCLUSIONS AND RECOMMENDATIONS	191
Appendix		
A	BIBLIOGRAPHY ON CHARACTERISTICS OF FISHING TWINES AND THEIR TESTING	195
B	BIBILOGRAPHY ON MODEL LAW	198
C	BIBLIOGRAPHY ON MODEL EXPERIMENTS	201
D	BIBLIOGRAPHY ON PROTOTYPE EXPERIMENTS	209
E	CALCULATION OF FISHING NET DRAG BY THE NUMERICAL METHOD DEVELOPED BY KOWALSKI AND GIANNOTTI (1974)	214

TABLE OF CONTENTS—Continued

Page

REFERENCES 220

BIOGRAPHICAL SKETCH 223

LIST OF TABLES

Table		Page
2.1	VALUES OF COEFFICIENT OF FRICTION	32
3.1	BASIC AND DERIVED MODEL SCALES FOR HYDRAULIC MODELS	54
5.1	SPECIFICATIONS OF BURBANK FLAT NET	91
5.2	RESULTS OF FIELD TESTS	110
6.1	SUMMARY OF SCALE RATIO	127
6.2	MODEL RESULTS WITH MOVABLE BEDS	157
6.3	MODEL RESULTS WITHOUT MOVABLE BEDS	159
7.1	PROJECTED FIELD DATA FROM THE RESULTS OF MODEL EXPERIMENTS WITH MOVABLE BEDS	162
7.2	PROJECTED FIELD DATA FROM THE RESULTS OF MODEL EXPERIMENTS WITHOUT MOVABLE BEDS	165
7.3	COMPARISON BETWEEN PREDICTED VALUE OF NET DRAG BY NUMERICAL METHOD AND MEASURED VALUE IN THE FIELD TEST	170
8.1	MODEL TEST RESULTS OF BEAM TRAWL	183
8.2	RESULTS OF FIELD EXPERIMENTS	185

LIST OF FIGURES

Figure		Page
1.1	Components of a gear research program	2
1.2	Physical elements of a fishing operation	3
1.3	Iterative procedure in trawl and trawler design and selection	4
2.1	Components of a gear	10
2.2	A netting twine	11
2.3	Load elongation curves	13
2.4	Load elongation curves for polyamide netting twine	15
2.5	Logarithmic linearization of load-strain curve for polyamide	16
2.6	The mesh	17
2.7	Net panels	20
2.8	Net diagram of Burbank flat net	21
2.9	Drag coefficient for nets as a function of Reynolds number	25
2.10	Hanging the net on the headrope	29
2.11	Equilibrium condition of door	34
2.12	Forces acting on a towing warp	38
3.1	Force polygon of a fluid flow	46
3.2	Force polygon in the model and full-scale net	59

LIST OF FIGURES—Continued

Figure		Page
4.1	Idealized mesh and twine in prototype and model	76
4.2	Typical stress-strain curve for polyamide twine	81
4.3	Evaluation of average stress in a twine	83
4.4	Headrope	85
4.5	Attachments in a rope	86
5.1	Net diagram of Burbank flat net	92
5.2	Dimensions of door	93
5.3	Site of prototype field study	94
5.4	Instrumentation of prototype net	95
5.5	Attachment of bolt to the cable	97
5.6	Bolt load cell, its attachments and the recorder	99
5.7	Underwater load cell	100
5.8	Attachment of underwater load cell to the footrope and headrope	101
5.9	Attachment of underwater load cell to the door	102
5.10	Twine load cell	103
5.11	Twine load cells in the net	105
5.12	Channel selector switch and strain indicator for the twine load cells	106
5.13	Relationship between warp tension and trawler speed	112
6.1	Tension testing of twines	115

LIST OF FIGURES—Continued

Figure		Page
6.2	Grip for testing of twines	116
6.3	Elastic characteristics of twines	117
6.4	Model net diagram	119
6.5	Elastic characteristics of ropes	122
6.6	Dimensions of model door	124
6.7	Model doors	125
6.8	Model net	126
6.9	Load cell to measure warp tensile force	128
6.10	Load cell to measure the tensile force in the rope between door and net	129
6.11	Load cell to measure tensile force of the midsection of headrope	130
6.12	Gate, main and return flumes	132
6.13	Storage tank, pump and bypass pipe	133
6.14	Relationship between weir head and flume discharge	134
6.15	Electric point gauges for measurement of the head on the weir	135
6.16	Weir and flow straighteners	136
6.17	Sand filter for the flume	138
6.18	Mounting of motor and regulator for the movable belt	139
6.19	Movable bed	141
6.20	Velocity distribution at center section of right belt	142
6.21	Isovel for run 1	144

LIST OF FIGURES—Continued

Figure		Page
6.22	Isovel for run 2	145
6.23	Isovel for run 3	146
6.24	Isovel for run 4	147
6.25	Isovel for run 5	148
6.26	Isovel for run 6	149
6.27	Point gauge and Ott current propeller	150
6.28	Net profile during testing	151
6.29	Plan view of net during testing	152
6.30	Side view of net during testing	153
6.31	Front view of net during testing	154
6.32	Side view of door during testing	156
7.1	Prediction of warp tensile force from model results	167
7.2	Prediction of drag force acting on a net	168
8.1	Beam trawl	173
8.2	Trawl head	174
8.3	Continuous beam	176
8.4	Prototype net for beam trawl	180
8.5	Model net diagram for beam trawl	182
8.6	Ocean testing of beam trawl	184
8.7	Relationship between net spread and trawler speed for otter door trawler	186
8.8	Relationship between warp tensile force and trawler speed for otter door trawler	187
8.9	Relationship between warp tensile force and trawler speed for beam trawler	188

LIST OF SYMBOLS

a - Half of wing spread

$\vec{a}$ - Acceleration

A - Elastic constant, area

b - Half of headline height

B - Elastic constant of twine

B - Buoyant force

B.M. - Bending moment

c - Length of net

C_a - Cauchy number

C_D - Drag coefficient

C_f - Friction coefficient of flow

c_1, c_2, c_3 - Constants
c_4, c_5, c_6

d - Subscript denoting door

D - Twine diameter

D_i - Inside diameter

D_o - Outside diameter

D_w - Depth of water

E - Float diameter

E' - Modulus of elasticity

E_u - Euler number

f - Coefficient of friction, subscript denoting float

F - Force

F_r - Froude number

$\vec{g}$ - Acceleration due to gravity

H - Horizontal dimension

H_r - Rope diameter

I - Moment of inertia

k_1, k_2 - Float constants

K - Bulk modulus of elasticity

l - Length

L - Characteristic length

L_c - Length of towing cable

m - Subscript denoting model

m' - Number of meshes (depth wise)

m'' - Mass

M - Bar length, moment

M_a - Mach number

n - Number of floats or sinkers per unit length of rope

n_f - Frequency of vortices

n' - Number of meshes (lengthwise)

n_l - A factor considering the rate of filling of fish

N - Number of meshes

N_f - Total number of floats or sinkers

N_{bd} - Reaction of ocean bottom to door

O - Surface tension

p - Subscript denoting prototype

p' - A factor denoting twine porosity

p'' - Pressure

P - Power

r - Resistant force, subscript denoting rope

R - Tensile force in towing cable at door

R_e - Reynolds number

s - Cable length, subscript denoting solid

S - Solidity

S' - Circumference

S_n - Strouhal number

t - Time

T - Characteristic time

T_l - Cable tension

T_f - Tensile force

$\vec{v}$ - Velocity of flow

v - Velocity at depth y

V - Trawler velocity, subscript denoting vertical dimension

w - Weight per unit length or area or volume, subscript denoting water

W - Total apparent weight

W_n - Weber number

x - Longitudinal axis (along the width of net)

X - Total force in the x direction

y - Vertical axis

Y - Total force in the y direction

z - Transverse axis (flow axis)

Z - Total force in the z direction

Z_m - Sectional modulus

Greek Symbols

α - Angle of incidence

γ_w - Unit weight of water

γ_s - Unit weight of twine

γ_s' - Unit weight of float or sinker

γ_r - Unit weight of rope

ε - Strain

η - Mesh number scale

κ - Force scale

λ - Length scale

λ_D - Twine diameter scale

λ_E - Float or sinker size ratio

λ_H - Rope size ratio

λ_M - Mesh size ratio

2ϕ - Total angle between two adjacent bars

μ - Dynamic viscosity of water

ν - Kinematic viscosity of water

ρ - Density

σ - Stress

τ - Time scale

ω - Frequency

Abbreviations

cfs - Cubic feet per second

°F - Fahrenheit

fps - Feet per second

ft - Feet

gf - Gram force

hp - Horsepower

in - Inch

lb - Pounds

OD - Outside diameter

rpm - Revolutions per minute

Abstract of Dissertation Presented to the Graduate Council
of the University of Florida in Partial Fulfillment
of the Requirements for the Degree of
Doctor of Philosophy

HYDRODYNAMIC MODELING OF NETS AND TRAWLS

By

M. Krishnamurthy

December, 1975

Chairman: B. A. Christensen
Major Department: Civil Engineering

Design of efficient fish nets by means of small-scale hydrodynamic models is of relatively recent origin in the United States. While investigators have developed basic equations for modeling flow around fish nets by considering the intertia and gravity forces as primary forces, they assume that the elongation of twines and ropes in the net is negligible. However, the shape of the fish net and, therefore, the forces acting on it are affected by the stretching of twines and ropes under load. In order to permit the correct numerical transfer of model observations to the prototype, it is necessary to establish special hydrodynamic model laws which take the stress-strain characteristics of the model and prototype materials into consideration. Such model laws were developed in this study.

These developed model laws were verified by full-scale ocean tests and by laboratory experiments. A movable bed was

constructed in the laboratory flume in order to obtain uniform velocity profiles similar to the uniform velocity profiles in the prototype. Experiments conducted in the flume yielded results comparable to those of the field tests, thereby, confirming the validity of the developed model laws.

Using the model approach, a beam trawl was designed to harvest deep-water shrimp. The results of laboratory tests and field trials indicated that a substantial decrease in the overall drag force was achieved with the designed beam trawl in comparison to a conventional otter door trawl. The major benefit of the reduction in the drag force would be a decrease in the fuel consumption of the trawler.

CHAPTER 1

INTRODUCTION

1.1 Statement of Problem

The manufacture of nets and trawls is an art which has been handed down from father to son through generations. Fishing gears of the past were designed by trial and error. Nowadays an attempt is being made to supplement this empirical approach with analytical theory and with physical tests in the laboratory and in the oceans.

The optimum performance of a fish-trawling operation depends on the efficiency of the gear and the behavior of fish. Therefore, any research program of gear design should include the biological study of fish reaction. The components of one such program are shown in Figure 1.1.

The major physical elements of a fishing operation are the net, the otter doors, the sweep-lines, the towing warps, and the ship or the trawler as indicated schematically in Figure 1.2. The design of these elements is an iterative process, an outline of which is given by Dickson (1971) and is shown in Figure 1.3.

From Figures 1.1 and 1.3, it can be seen that fish biology should also be considered in the iterative design

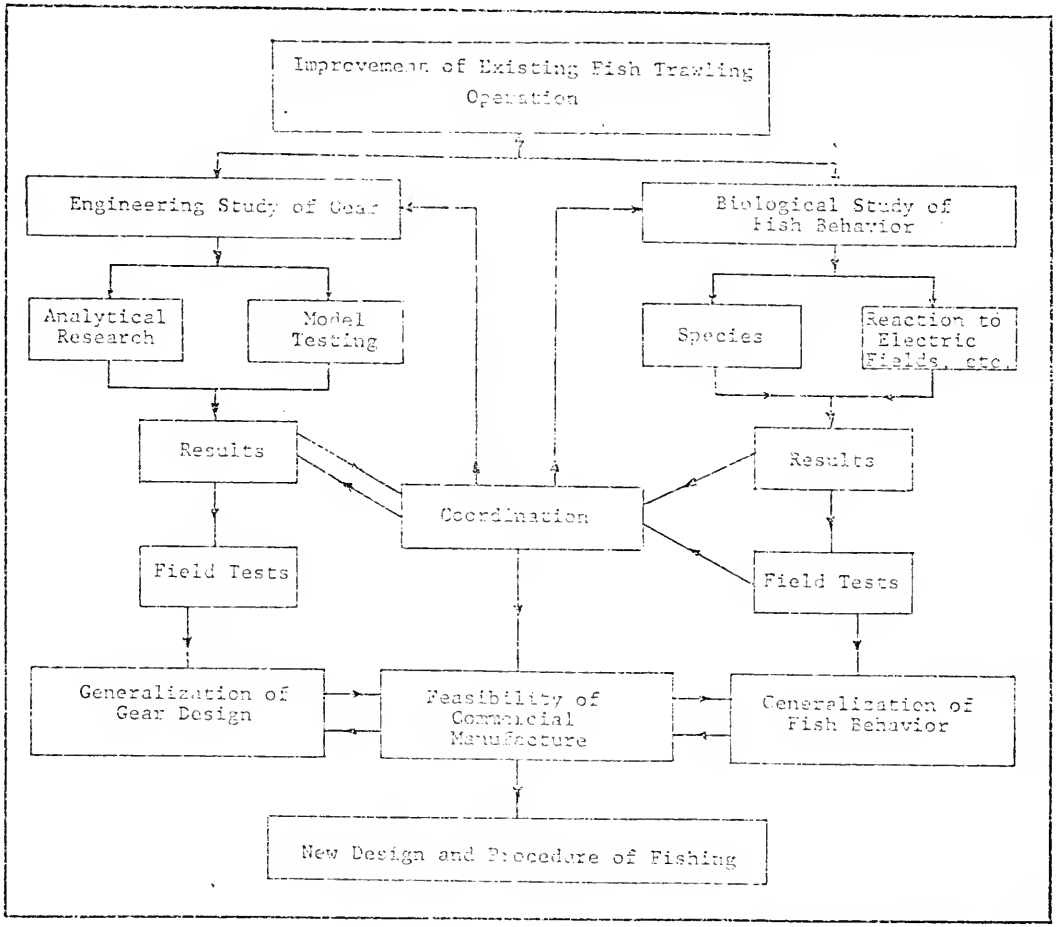

Figure 1.1. Components of a gear research program.

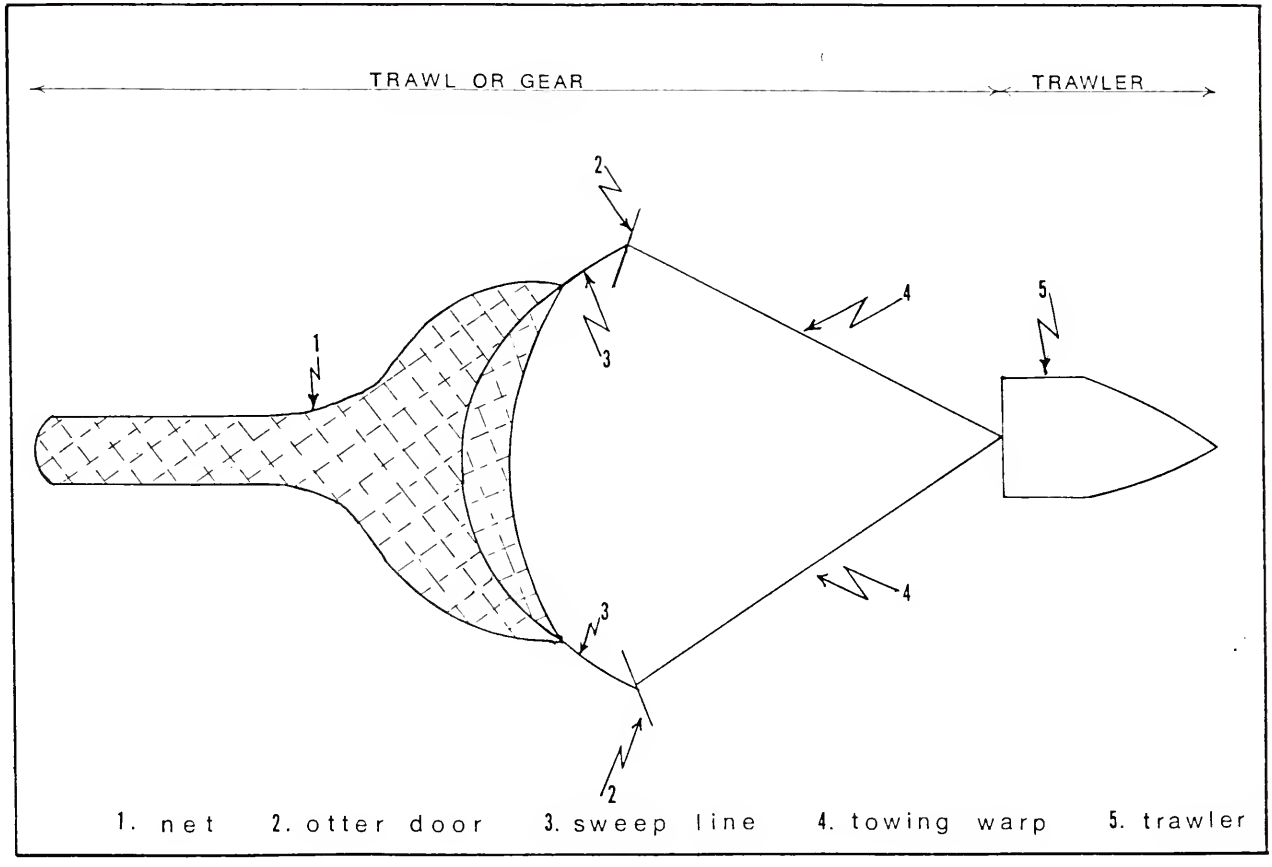

Figure 1.2. Physical elements of a fishing operation.

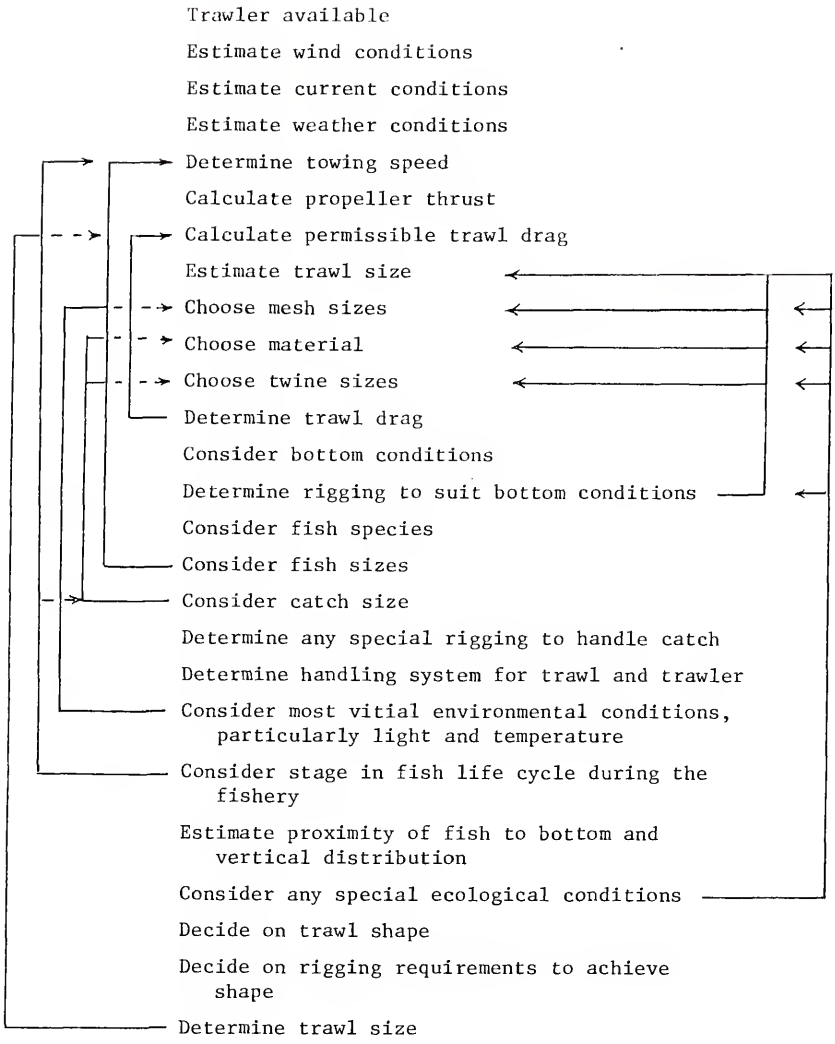

Figure 1.3. Iterative procedure in trawl and trawler design and selection.

Source: Dickson, 1971.

of a trawl and a trawler. However, these aspects are beyond the scope of the present investigation. Also, the interaction of the propulsive system of the trawler with the performance of the trawl is itself a major study. Therefore, the current research focuses attention on the engineering behavior of the gear. This behavior of the gear can be studied (1) by analytical approaches, (2) by physical tests in the ocean and (3) by model experiments in the laboratory.

Analytical gear design requires a knowledge of the hydrodynamic resistance of the net, bottom friction of the otter doors and the behavior of the rigging under different towing conditions. The literature on mathematical modeling indicates that this design procedure involves long and tedious numerical computations. Further analytical approaches to these problems are to be made before this approach may be considered practical.

Ocean tests of fishing gear are expensive and time consuming. Determination of the shape of the net under various conditions is cumbersome because underwater observations of the net depends upon the clearness of water. The outcome of field tests also depends on such factors as weather conditions, shark problems, etc.

Another method of designing the fish net is by small-scale model experimentation in the laboratory. Hydraulic models and laws governing their use have been applied successfully to the problems of dams, spillways, energy

dissipators and ships. The hydraulic model has proved to be a powerful research tool even in the study of fluvial phenomena (Graf 1971), where the interaction between water and sediment is considerably more complex than the case of nets and trawls. Therefore, the fishing industry may reap substantial benefits through improved net structure and improved performance derived from the hydraulic model concept in net and trawl research.

Physical model tests in the laboratory offer various advantages over ocean tests. Costs: Whereas field testing for one net may require $5,000, laboratory costs may be only $500, with fewer logistic problems such as weather and ship-time (Hillier 1974). Visual observation: It is possible to detect easily the deficiencies in net design and to implement modifications immediately. Time factors: A model test requires by far less hours than a field test. At least a week is needed to conduct a particular aspect of a gear test in the ocean whereas the laboratory tests covering the same modifications can be done in a day. However, model test results should be extrapolated with caution because of scale effects of the models. Therefore, an ideal gear design would be a method which combines the analytical approach with model and full-scale experiments.

Summarizing, a simple method is necessary to design and to test efficient fishing gear. Though not satisfactory, existing mathematical analyses can be applied to the initial

and preliminary gear design. At the present time, however, physical scale modeling in the laboratory seems to be the only reliable alternative tool in the evaluation of gear performance. Development of such a tool is the general objective of the present investigation.

1.2 Objectives

The specific objectives of the research are a review of literature on mathematical and physical models of fishing gear and their deficiencies, the development of adequate model laws and the verification of the developed laws and procedures by field and model tests.

The presentation of the objectives is as follows. The gear and the behavior of its elements under fluid motion are introduced in Chapter 2. In Chapter 3, the literature on mathematical analyses of fishing gear, physical modeling in the laboratory and full-scale field experiments is presented. The pitfalls in the existing analyses are brought out. Development of adequate model laws is presented in Chapter 4. To verify the model laws, prototype experiments were conducted in the Gulf of Mexico as explained in Chapter 5. Chapter 6 illustrates the model experiments in the hydraulic flume. The validity of model laws is given in Chapter 7. Using the model approach, a special beam trawl was designed for deep-water shrimping. The design and testing of this trawl in the laboratory and in the field are given in Chapter 8. Conclusions on the experimental

results in the laboratory and in the field are presented in Chapter 9. Suggested future research is mentioned also in the same chapter.

CHAPTER 2

COMPONENTS OF A GEAR

In Chapter 1 the main components of a gear were briefly mentioned and shown in Figure 1.2. Their physical structure and behavior, when towed through water, are described below.

2.1 Net

A net consists of three sections, namely cod end, belly and wings (Fig. 2.1). Each section may be of different netting twine and may have different mesh dimension. The net is usually treated by dipping it in a solution of tar to give greater resistance to wear, tear and aging due to storage in the sun.

2.1.1 Netting Twine

Netting twine may be of a natural fiber such as cotton and coir, or of synthetic polymers like nylon (polyamide) and polyethylene. Single yarns are plied together and twisted to make a netting twine (Fig. 2.2). The voids in a twine depend on the amount of twist and the diameter of plied yarns. Nylon is widely used in the United States in making a net.

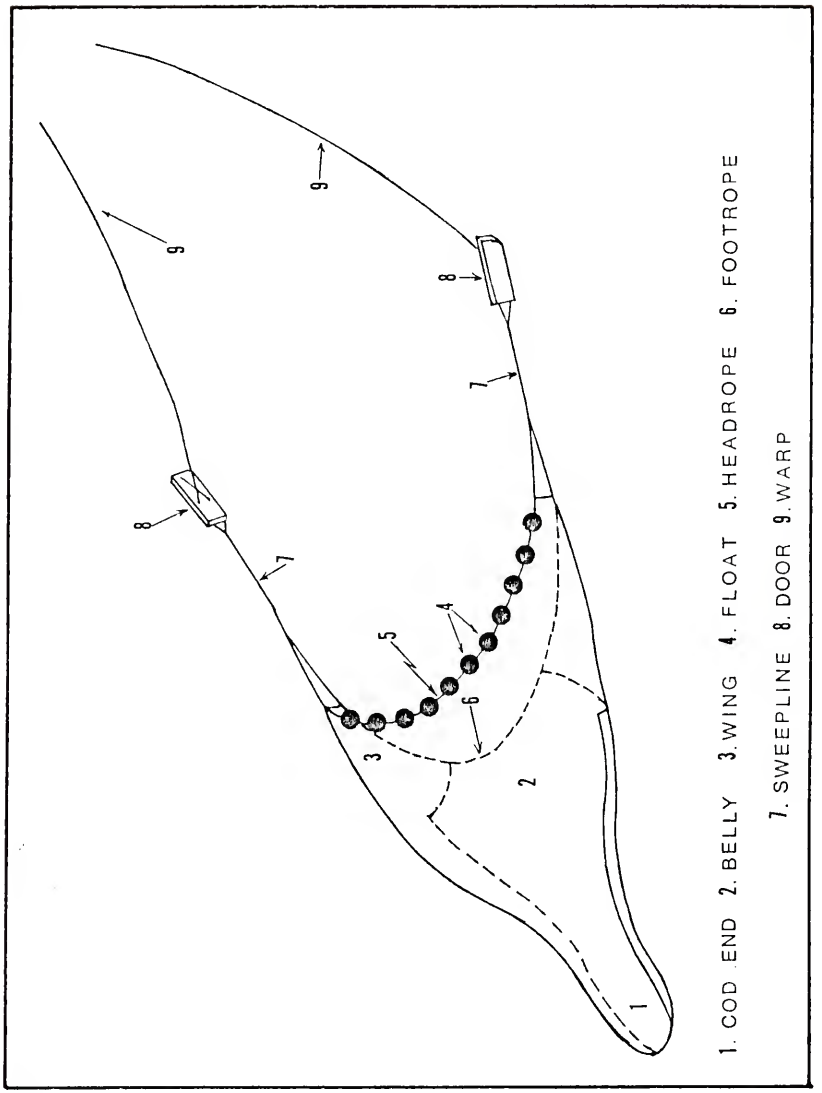

Figure 2.1. Components of a gear.

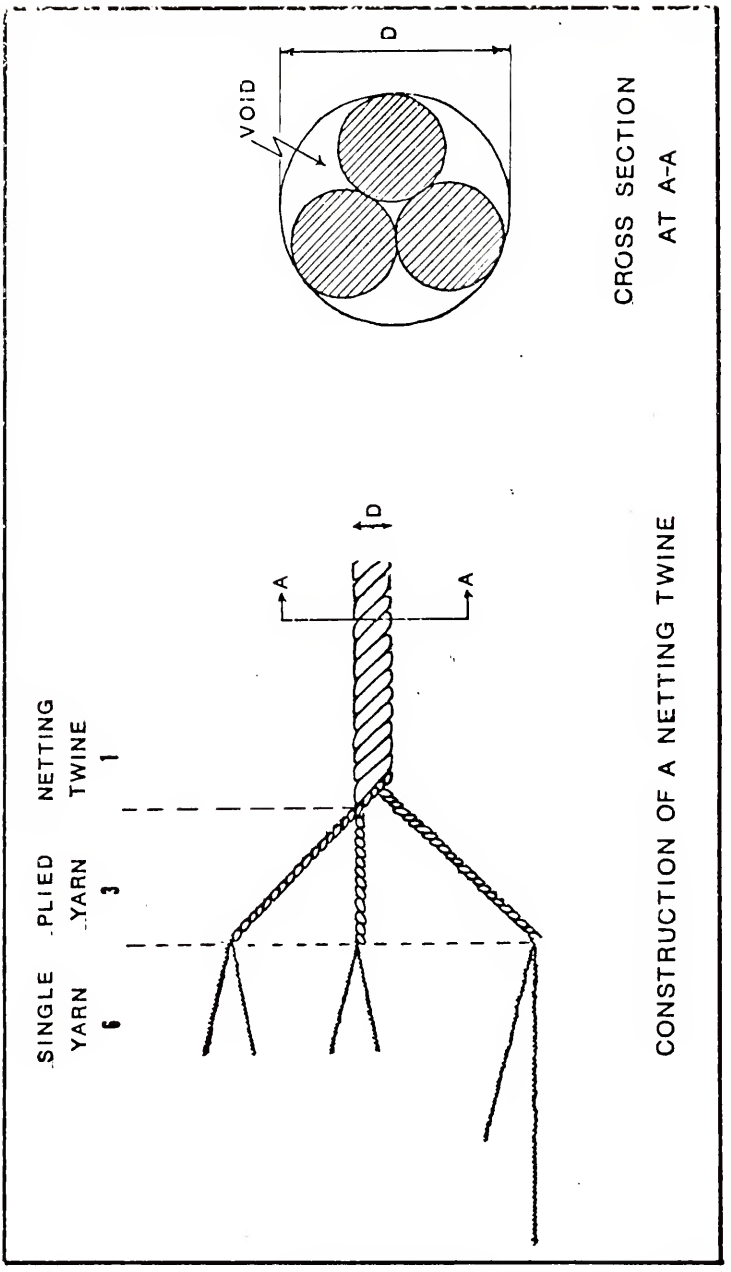

Figure 2.2. A netting twine.

The cross-sectional shape of twine and plied yarns may be approximated by a circle (Fig. 2.2). The solid area of a twine consisting of three plied yarns may then be found from the expression

$$A_{solid} = 0.508\ D^2 \qquad (2.1)$$

where

A_{solid} = Area of solid mass

D = Diameter of the netting twine

Therefore, the ratio of solid area to the total twine area and porosity in the twine are equal to 0.646 and 0.354, respectively.

Properties of the twine that are specially important in the fishing industry are density, tenacity, tensile strength, knot strength, loop strength, elasticity, toughness, stiffness, water absorption, resistance to heat, sunlight, seawater and mildew. The definition and determination of these properties are described by von Brandt and Carrothers (1964). Additional information on characteristics of fishing twines and their testing may be found in the bibliography which is given in Appendix A.

The elastic behavior of a netting twine under a load is described by its stress-strain curve or load-strain curve. Figure 2.3 shows the relationship between load and strain of man-made fibers used in making nets. This relationship for

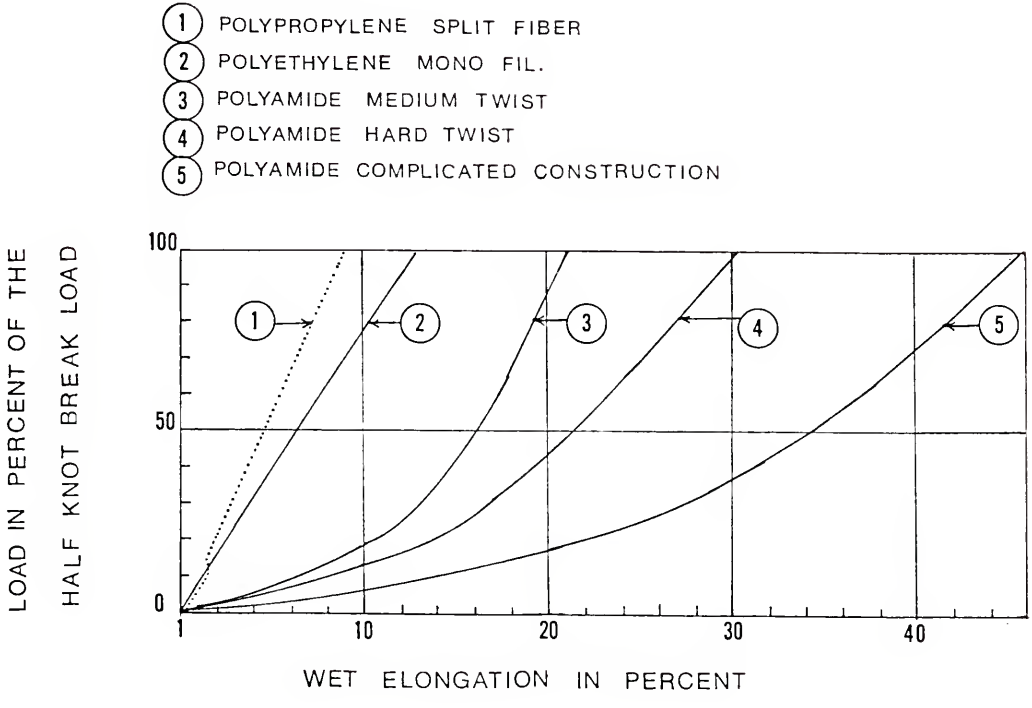

Figure 2.3. Load elongation curves.

Source: Brandt and Klust, 1971.

polyamide netting twines of different linear density is drawn in Figure 2.4. It can be seen from Figures 2.3 and 2.4 that the fibers do not obey the linear Hooke's law. However, a nonlinear law is expressed by

$$\sigma = A\varepsilon^B \tag{2.2}$$

where

σ = Stress

ε = Strain

A and B are constants which may be derived from the log-log plot shown in Figure 2.5. The value of stress is obtained by dividing the load by the original solid area of the twine. This definition of stress is used without exception in this study.

2.1.2 Mesh

The basic structure of a net is the mesh. A mesh is defined by Kawakami (1964) as a rhombic opening enclosed by four bars of twine of equal length firmly knotted at the four corners. Since one bar is common to two meshes and one knot to four meshes, a mesh consists of two bars and a knot. The area of a single mesh depends on the angle between two adjacent bars (Fig. 2.6). This angle may be changed by different hanging or mounting of the webbing to the frame line. The surface area of a mesh can be calculated from the geometry of the mesh and is given by the simple formula

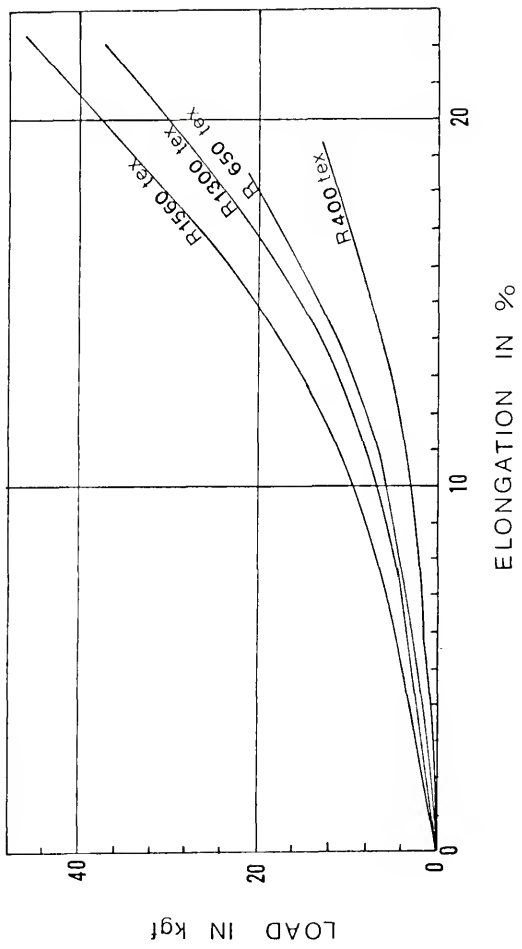

Figure 2.4. Load elongation curves for polyamide netting twine.

Source: Brandt and Klust, 1971.

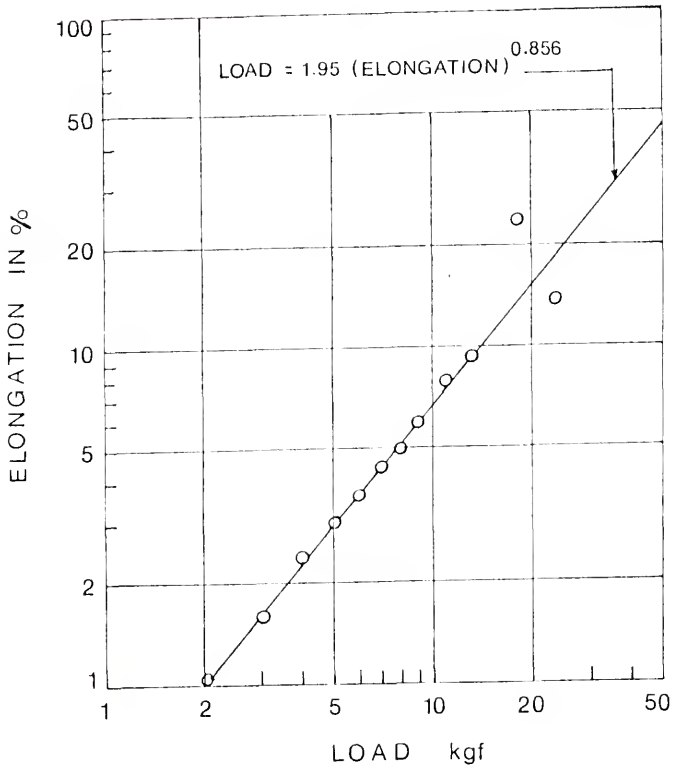

Figure 2.5. Logarithmic linearization of load-strain curve for polyamide.

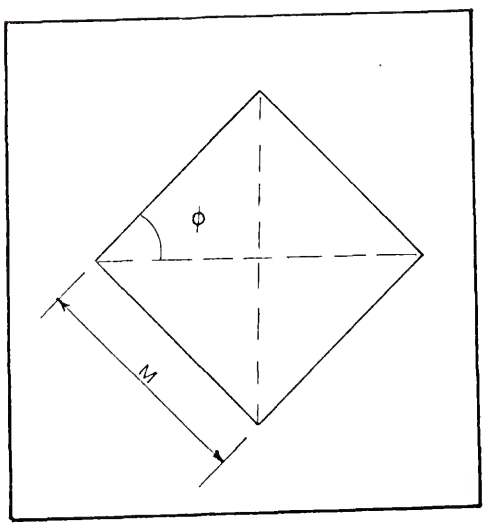

Figure 2.6. The mesh.

$$A_{mesh} = 2M^2 \sin \phi \cos \phi \qquad (2.3)$$

where

A_{mesh} = Surface area of the mesh

M = Bar length

2ϕ = Total angle between two adjacent bars

The weight of one dry mesh W, in air, is the sum of the weight of its two bars and the knot.

$$W = 2\left(\frac{\pi D^2}{4}\right)\left(M \cdot p' \cdot \gamma_s\right) + \left(\frac{\pi D_k^2}{4}\right)\left(M_k \cdot p_k' \cdot \gamma_s\right) \qquad (2.4)$$

where

γ_s = Unit dry weight of twine

$1-p'$ = Porosity of the twine

D_k = Diameter of the knot

$1-p_k'$ = Porosity of the knot

M_k = Length of twine included in one knot

Since the density of the fiber is unaltered by tightening of the knots,

$$\frac{\pi D^2}{4} \cdot p' = \frac{\pi D_k^2}{4} \cdot p_k' \qquad (2.5)$$

and

$$D_k = D\left(\frac{p'}{p_k'}\right)^{1/2} \qquad (2.6)$$

From Equations (2.3) to (2.6), the apparent weight, w, of one mesh in water per unit area is obtained:

$$w = \left(\frac{\pi D^2}{4}\right)\left(\frac{p'}{\sin 2\phi}\right)\left(\frac{2}{M} + \frac{M_k}{M^2}\right)(\gamma_s - \gamma_w) \cdot \qquad (2.7)$$

where

γ_w = Unit weight of water

2.1.3 Net Panel

A net panel is an array of meshes. It is either straight or tapered (Fig. 2.7). A net consists of a combination of straight and tapered panels sewed together. The combination and tapering of panels depends on the judgment of the net maker who uses a net diagram to show this combination. For example, Figure 2.8 is the net diagram of a "Burbank Flat Net" which is widely used by Florida and Texas shrimpers.

The length and depth of a rectangular panel of n' by m' meshes (m' meshes deep) can be computed from the geometry and hanging of the net panel

$$L_H = 2n'M \cos \phi \qquad (2.8)$$

and

$$L_V = 2m'M \sin \phi \qquad (2.9)$$

where

L_H = Length of panel

L_V = Depth of panel

When a net panel is placed in a current with a uniform velocity, a hydrodynamic force acts on the panel in a

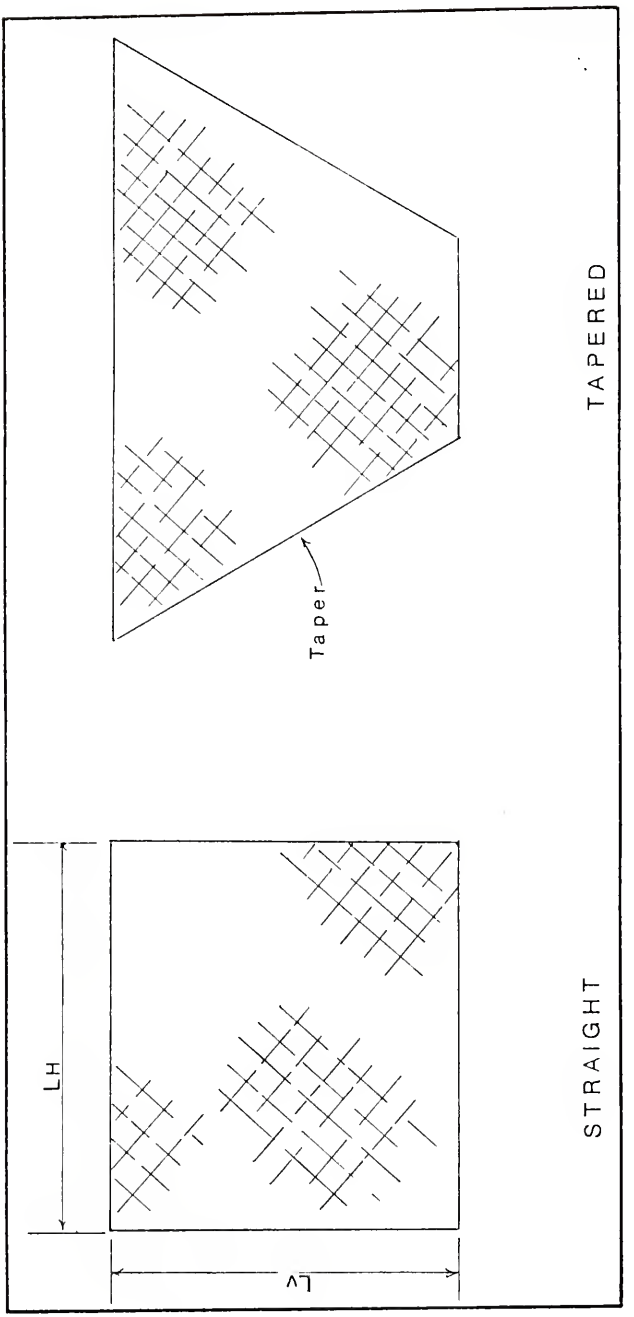

Figure 2.7. Net panels.

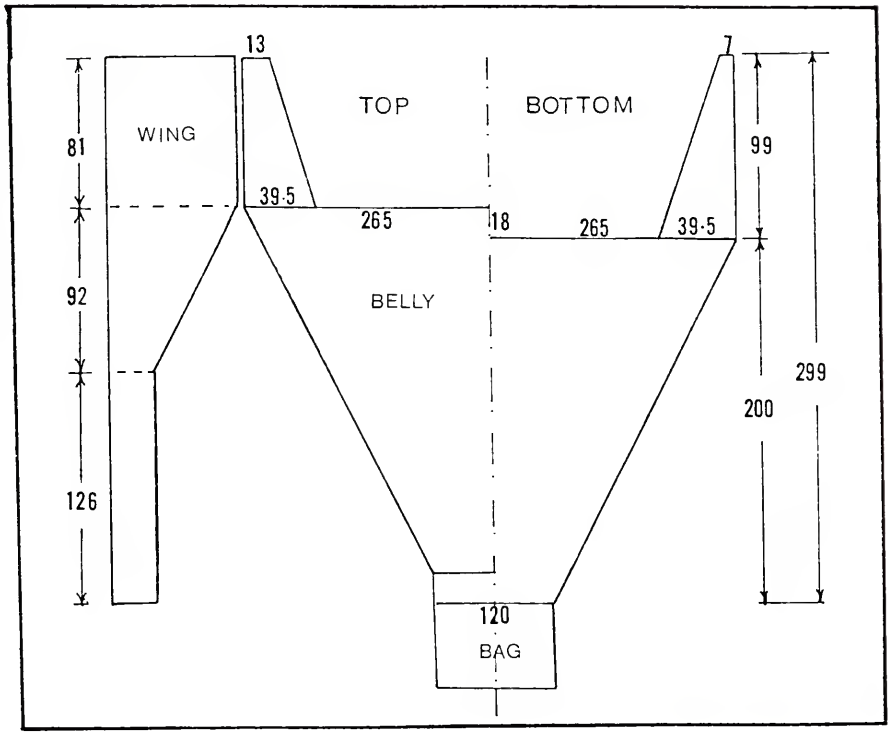

Figure 2.8. Net diagram of Burbank flat net.

direction normal to the panel. The component of this force to the current is the drag force. The magnitude of drag force is calculated by

$$F = C_{Db} \cdot \frac{\rho V^2}{2} \cdot A_b + C_{Dk} \cdot \frac{\rho V^2}{2} \cdot A_k \qquad (2.10)$$

where

F = Drag force

C_{Db} = Drag coefficient of bar

C_{Dk} = Drag coefficient of knot

ρ = Density of water

V = Velocity

A_b = Projected area of bars on a plane normal to current

A_k = Projected area of knots on a plane normal to current

The first and second terms in Equation (2.10) represent the drag to the bars and knots, respectively.

The values of drag coefficient for the bar and the knot depend on the Reynolds number of the bar and knot, respectively. The Reynolds number is defined as

$$R_e = \frac{VL}{\nu} \qquad (2.11)$$

where

ν = Kinematic viscosity of water

L = Characteristic length

Kowalski and Giannotti (1974) consider the bar length as the characteristic length. In the turbulent region where the

Reynolds number is greater than 20,000, a value of 2.02 for C_{Db} is given. Taking the diameter of the knot as the characteristic length, a value of 0.47 for C_{Dk} is shown.

For a net panel placed normal to the current, the drag on the panel is

$$F = C_{D\ panel} \cdot \frac{\rho V^2}{2} \cdot A_{surface} \cdot S \tag{2.12}$$

where

$C_{D\ panel}$ = Drag coefficient of the panel

$A_{surface}$ = Total projected area on a plane normal to the current

S = Solidity, the projected solid area per unit surface area of the panel.

The values of S and $C_{D\ panel}$ are

$$S = \frac{\left(2MD + \frac{\pi}{4} D_k^2\right)}{M^2 \sin 2\phi} \tag{2.13}$$

and

$$C_{D\ panel} = \frac{\left(C_{Dk} A_k N_k + C_{Db} N_b A_b\right)}{A_k N_k + A_b N_b} \tag{2.14}$$

where

N_k = Number of knots

N_b = Number of bars

Fridman (1973, p. 63) considers the diameter of the bar as the characteristic length and defines the Reynolds number as

$$R_{eD} = \frac{VD}{\nu} \tag{2.15}$$

From the results of the laboratory experiments, he establishes a relation between R_{eD} and $C_{D\ panel}$ (Fig. 2.9). The values of $C_{D\ panel}$ were averaged from the drag coefficients for net panels with $\frac{D}{M}$ values ranging from 0.0024 to 0.1500.

Carrothers and Baines (1975) present an empirical equation to compute the value of $C_{D\ panel}$ for $R_{eD} > 500$.

$$C_{D\ panel} = \frac{1.26}{1 - S} \qquad \text{for} \quad S < 0.1 \tag{2.16}$$

If the axis of the net panel is inclined at an angle α with the velocity vector, the corresponding drag coefficient of the net panel can be found experimentally. Carrothers and Baines (1975) analyzed the experimental results of various investigators and concluded:

$$C'_{D\ panel} = C_{D\ panel} \sin^2 \alpha \tag{2.17}$$

where

$C_{D\ panel}$ = Drag coefficient for the panel for $\alpha = 90°$

$C'_{D\ panel}$ = Drag coefficient when the panel is inclined at an angle α with the velocity vector

For values of α approaching 90°, Tauti (1934) approximates the value of $\sin^2 \alpha$ and gives an expression for the drag coefficient.

$$C'_{D\ panel} = C_{D\ panel} \sin \alpha \tag{2.18}$$

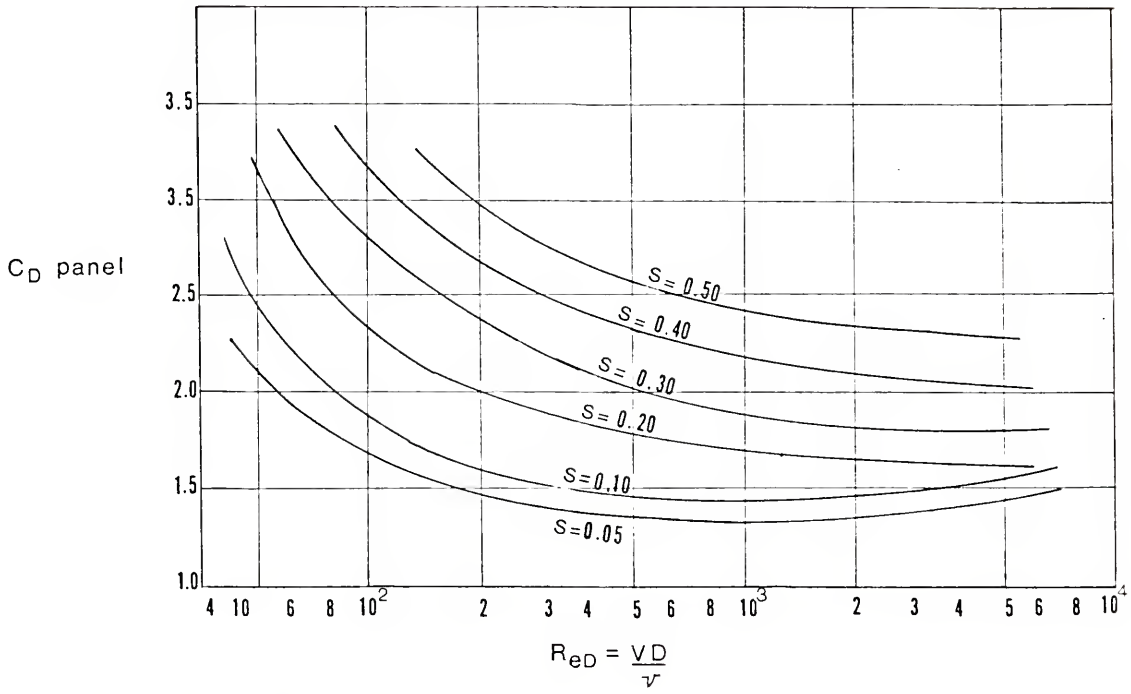

Figure 2.9. Drag coefficient for nets as a function of Reynolds number.

Source: Fridman (1973, p. 63).

Miyake (1927), Revin (1959) and Kanamori (1960) verified this approximation by laboratory experiments. Giannotti (1973) has conducted wind tunnel tests on two different net frames and given results which support this approximation.

However, at low values of α, the component of resistance normal to the net becomes small. The predominant force will be the component parallel to the frame. Carrothers and Baines (1975) have found that Equation (2.18) predicts low values of drag coefficient for low values of α and, therefore, cannot be applied to compute the drag force. For this case, Kawakami and Nakasai (1968) determined the magnitude of the force acting along the length of the panel by

$$F = C''_{D\ panel} \left(\frac{\rho V^2}{2}\right) \cdot \left(\frac{D}{M} \cdot \tan \phi\right) \cdot \cos \alpha \qquad (2.19)$$

where

$C''_{D\ panel}$ = Drag coefficient for the net panel for $\alpha = 0$

Equation (2.19) considers the resistance of the knots to the flow to be small compared with the resistance of the bars.

2.1.4 The Cod End

The cod end is the tail of the net where the catch is collected. It has a thicker twine and smaller mesh compared with the other parts of the net. To protect the cod end from wear and tear, soft strands of twines known as chaff are attached to each knot.

During a tow, Kowalski and Giannotti (1974) consider the cod end a hollow cylinder with its longitudinal axis parallel to the flow. To compute the drag force acting on the cod end, they suggest:

$$F_{cod} = (0.82) \left(\frac{\rho V^2}{2}\right)\left(\frac{\pi}{4} d_{cod}^2\right) n_1 + C_f \cdot \frac{\rho V^2}{2} \times \left(N_b \cdot \pi \cdot MD + N_k \pi D_k^2\right) \cdot \left(1 - n_1\right) \qquad (2.20)$$

where

F_{cod} = Drag

d_{cod} = Diameter of the cylindrical cod end

C_f = Friction coefficient

n_1 = Factor which considers rate of fish filling in cod end: $n_1 = 0$ for $t = 0$, and $n_1 = 1$ for $t > 0$

Equation (2.20) holds good for Reynolds number, $R_{eM} = \frac{VM}{\nu}$ greater than 10^7 and with an aspect ratio greater than 2. The aspect ratio is the ratio of the length to the diameter of the cylindrical cod end.

2.1.5 Belly

The belly refers to the top and the bottom tapered part of the net extending from wing to wing and from the hanging lines to the cod end. The shape of the belly during a tow is complicated. Kowalski and Giannotti (1974) approximate the belly by a conical net with an elliptical mouth, where the major axis of the ellipse is given by the

wingspread and the minor axis by the headline height. They compute the resistance of the belly to the flow by Equation (2.18).

2.1.6 Wings

The wings are the sides of the net, tapered along the top seam and straight along the bottom seam. The wings facilitate the required mouth opening of the net.

2.2 Ropes

2.2.1 Headrope

After the sections of the net are sewed, the top portion of the net is hung on a headrope (Fig. 2.10). The headrope is a combination rope of steel and manila. The floats are attached to the headrope when a larger mouth opening is required.

Fridman (1973, p. 73) analyzes the shape of the headrope under towing conditions. He assumes a catenary shape for the rope and presents a procedure to compute the magnitude of the tension along the length of the rope.

The resistance of a rope lying at an angle α to the flow is computed by

$$F_{rope} = C_{D\ rope} \left[\sin^3 \alpha\right] \left[\frac{\rho V^2}{2}\right] H_r \cdot \ell_r \qquad (2.21)$$

where

H_r = Diameter of the rope

ℓ_r = Length of the rope

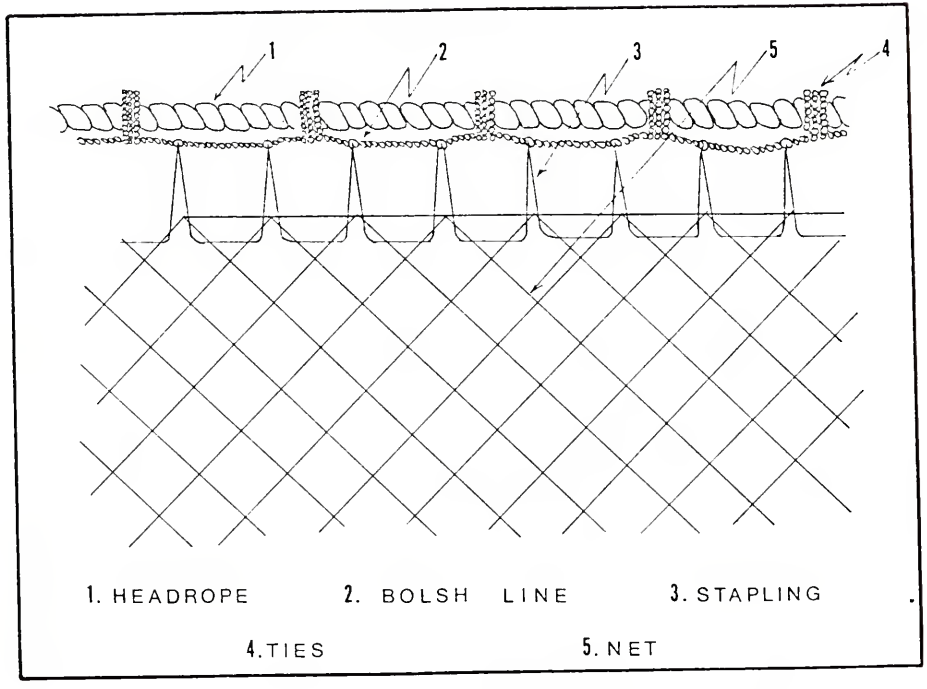

Figure 2.10. Hanging the net on the headrope.

$C_{D\ rope}$ = Drag coefficient of the rope when it is lying perpendicular to the flow

The value of $C_{D\ rope}$ is given as 1.1 by Kowalski and Giannotti (1974), whereas, Fridman (1973, p. 56) offers a value ranging from 1.2 to 1.3. The resistance of the headrope can be computed by Equation (2.21).

2.2.2 Floats

To achieve a larger fishing height, floats are attached on the headrope. They may be hollow cast aluminum or plastic spheres or solid bodies made of plastic foams. The drag acting on the floats is determined by

$$F_{float} = N_f \cdot C_{D\ float} \cdot \frac{\rho V^2}{2} \cdot A_f \qquad (2.22)$$

where

N_f = Number of floats

$C_{D\ float}$ = Drag coefficient for spherical float

A_f = Projected area of float to a plane normal to flow

For a single spherical float, Fridman (1973, p. 51) expresses a value of 0.475 for $C_{D\ float}$ when the float Reynolds number is greater than $(2.0)(10^5)$. The float Reynolds number is defined as

$$R_{ef} = \frac{VD_f}{\nu} \qquad (2.23)$$

where

D_f = Diameter of the spherical float

However, if the floats are grouped together, there is an interaction of flow between the floats and, for this case, Fridman gives a value of 0.93 for $C_{D\ float}$.

2.2.3 Ground or Footrope

The bottom portion of the net is hung on the footrope. Sinkers are attached to the footrope to keep the net in contact with the bottom. Spacing and weight of the sinkers vary with the type of the net.

Kawakami and Suzuki (1959) and Suzuki and Kawakami (1960) studied the shape of the footrope during a tow and its load distribution. The resistance of the footrope to the flow are the drag and friction forces. The magnitude of the drag force may be computed from Equation (2.21) if the angle between the rope and flow direction is known. However, the magnitude of the friction force depends on the bottom condition and the material of the rope. Fridman (1973) estimates the friction force as

$$F_{friction} = f \cdot W \tag{2.24}$$

where

$F_{friction}$ = Friction force

W = Apparent weight of the rope

f = Coefficient of friction between the soil and the rope

The values of f for two different bottom conditions and for different materials are given in Table 2.1. The

coefficient of friction is dependent on the angle between the flow direction and the rope. Fridman (1973) establishes a graphical relation between α and f.

TABLE 2.1

VALUES OF COEFFICIENT OF FRICTION

Material	Coefficient of Friction	
	Gravel with Sand	Fine Sand
Cast iron	0.47	0.61
Wood	0.51	0.73
Stone	0.54	0.70
Lead	0.44	0.53
Sand bags	0.63	0.76
Vegetable ropes (hemps)	0.70	0.80

Source: Fridman (1973, p. 38).

2.3 Sweeplines

To increase the wingspread, it is customary to insert extra lengths of rope between the door and the wing. These ropes are known as sweeplines. They may be the same material as the footrope, the headrope or the towing warp. The length of the sweeplines depend on the fishing conditions and the towing speed.

2.4 Doors

The doors in a trawl provide the all-important fishing spread of the net. The doors of the bottom trawls used in Florida are rectangular in shape. They are wooden boards reinforced with iron strips and no attempt on streamlining is made. At the lower edge of the door, a heavy metal shoe plate is fitted for stability and for protection of doors against the hard bottom. The towing warp is connected to the doors by a chain and a shackle arrangement. If the sweeplines are used in the net, they are connected to the backstops of the door by shackles.

Figure 2.11 shows the equilibrium condition of the door. The forces acting on the door are the tensile force in the towing warp R_1; the hydrodynamic force, R_2; the tensile force in the sweepline, R_3; the apparent weight of the door, W; and the friction of the door against the bottom, F. The governing equations for the equilibrium conditions are

$$\begin{aligned} \Sigma X &= 0 & \Sigma M_x &= 0 \\ \Sigma Y &= 0 & \Sigma M_y &= 0 \\ \Sigma Z &= 0 & \Sigma M_z &= 0 \end{aligned} \qquad (2.25)$$

where

ΣX, ΣY and ΣZ = Sum of components of all forces of x, y and z directions, respectively

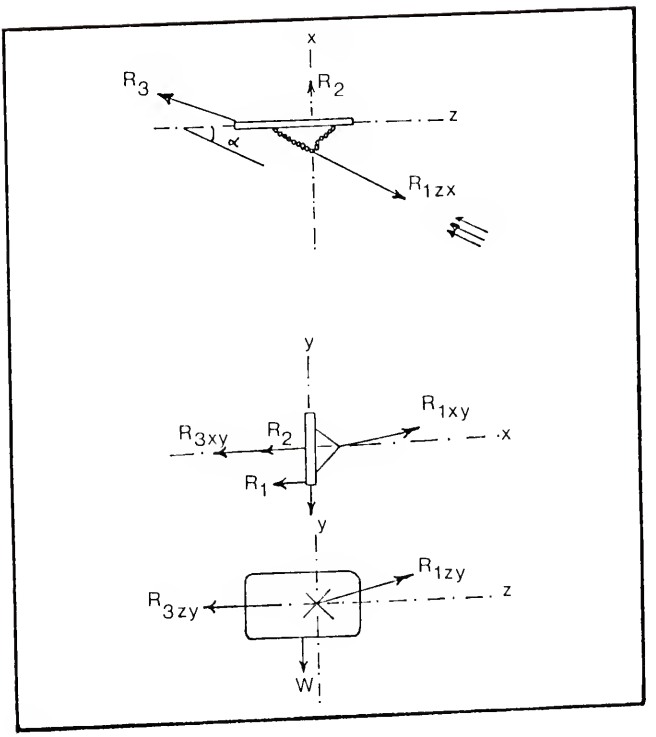

Figure 2.11. Equilibrium condition of door.

Source: Fridman, 1973.

ΣM_x, ΣM_y and ΣM_z = Moment of forces about x, y and z axis, respectively

The equilibrium condition of the doors is detailed by Crewe (1964) and by Fridman (1973).

The resistance of the door to the flow arises from the drag of the door and the component of the friction force. The hydrodynamic drag of the doors is

$$F_{door} = C_{D\ door} \left(\frac{\rho V^2}{2}\right) \cdot A \tag{2.26}$$

where

F_{door} = Drag force acting on doors

$C_{D\ door}$ = Drag coefficient for door

A = Area of door

The drag coefficient for the door depends on the door Reynolds number which is defined as

$$R_{ed} = \frac{V\ell_d}{\nu} \tag{2.27}$$

where

ℓ_d = Length of door

It also depends on the angle of incidence of the flow, the shape of the door and the ratio of the length to height of the door. For $R_{ed} > (0.8) \cdot (10^6)$, Fridman (1973, p. 276) presents the values of the drag coefficient for oval and rectangular doors with angles of incidence ranging from 20°

to 40°. The $C_{D\ door}$ values vary from 0.5 to 1.0 for a rectangular door. This range agrees with the trials of Crewe (1964) and Scharfe (1959).

The friction force of the door against the bottom depends on the apparent weight of the doors and the soil condition. Literature on the evaluation of this friction force is scarce. As a first-order approximation, the magnitude of the friction force may be evaluated from Equation (2.24) and by using Table 2.1

2.5 Towing Warp

Towing warps are steel wire ropes, the diameter of which depends on the towing power of the trawler and the type of trawl. Length of the warps is determined by fishing conditions, trawl type and drum capacity.

Drag force acting on a towing warp is a function of its (warp) shape which, in turn, is determined by the system of forces acting on it. The hydrodynamic drag F of a straight circular cable inclined at angle α to the flow is

$$F = C_{D\ warp} \cdot \left(\frac{\rho V^2}{2}\right) \cdot \left(\sin^2 \alpha\right) \cdot \left(H_r \ell_r\right) \qquad (2.28)$$

where

$C_{D\ warp}$ = Drag coefficient for warp

For steel cables, the value of $C_{D\ warp}$ is 1.1 (Fridman 1973, p. 57). However, if the frequency of the vortices forming behind the cable is equal to the natural

frequency of the cable system, the value of $C_{D\ warp}$ will be greater than 1.1. Literature on the evaluation of this value is not presently available and research is wanting.

Figure 2.12 shows the forces acting on a towing cable system. The tangent at any point to the cable makes an angle α to the incident flow. Therefore, the towing velocity can be resolved into V sin α and V cos α as the normal and tangential velocity components, respectively. Let F_n be the drag force per unit length of the cable when the cable lies normal to the flow and F_t be the drag force when the cable is tangential to the flow. For the flow system represented in Figure 2.12, the force acting normal to the cable is $F_n \sin^2 \alpha$. Similarly, the force tangential to the cable is $F_t \cos^2 \alpha$. But Streeter (1961) approximates the value of $F_t \cos^2 \alpha$ to $F_t \cos \alpha$ to fit the experimental data. The forces acting on an element of length ds are given in the free body diagram of Figure 2.12. By resolving these forces in the tangential and normal direction, the equilibrium condition of the cable system is obtained.

$$\frac{dT_f}{ds} + F_t \cos \alpha - w \sin \alpha = 0$$

$$T_f \frac{d\alpha}{ds} - F_n \sin^2 \alpha + w \cos \alpha = 0$$

$$\frac{dz}{ds} = \cos \alpha; \quad \frac{dy}{ds} = \sin \alpha \tag{2.29}$$

where

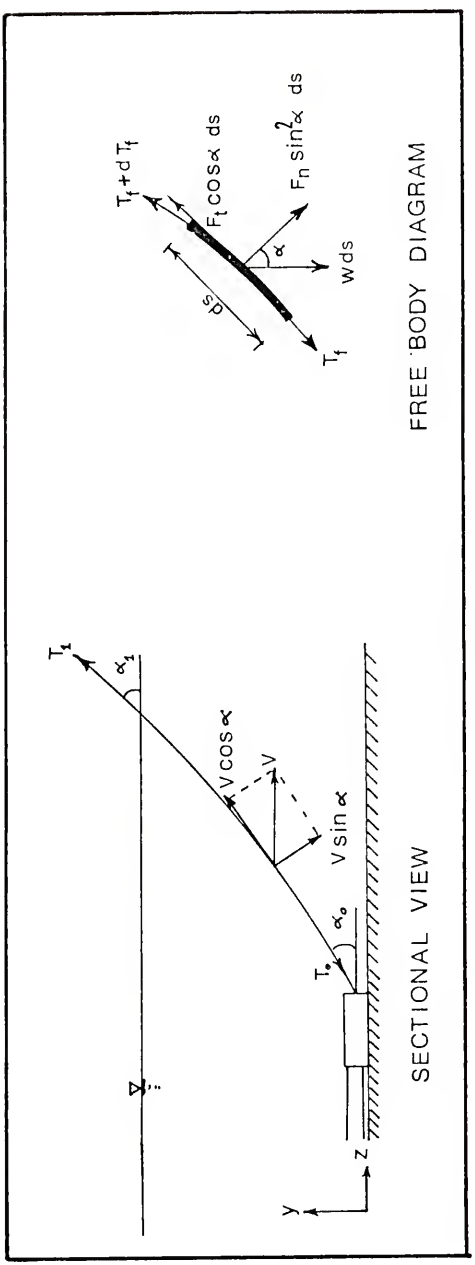

Figure 2.12. Forces acting on a towing warp.

w = Weight of cable per unit length

T_f = Tensile force per unit length

The solution of Equation (2.29), for the values of z, y, α and T_f as a function of the length of the cable, yields (Streeter 1961)

$$T_f = T_0 - F_t z + wy$$

$$\ell n \frac{T_f}{T_0} = \int_{\alpha_0}^{\alpha_1} \frac{w \sin \alpha - F_t \cos \alpha}{F_n \sin^2 \alpha + w \cos \alpha} \, d\alpha$$

$$z = \int_{\alpha_0}^{\alpha_1} \frac{T_f \cos \alpha}{F_n \sin^2 \alpha + w \cos \alpha} \, d\alpha$$

$$y = \int_{\alpha_0}^{\alpha_1} \frac{T_f \sin \alpha}{F_n \sin^2 \alpha + w \cos \alpha} \, d\alpha \qquad (2.30)$$

The magnitude of the tension T_0 in the warp at the point of attachment to the door can be computed by assuming that the warp lies in the vertical plane z - y (Fig. 2.12).

$$T_0 = \sqrt{\left(\frac{F_{net}}{2} + F_{door}\right)^2 + F_v^2} \qquad (2.31)$$

where

F_{net} = Drag of the net

F_{door} = Drag of the door

F_v = Vertical component of tension in cable which is given as

$$F_v = W + F_{v\ door} - N_{bd} \tag{2.32}$$

where

W = Apparent weight of door

$F_{v\ door}$ = Vertical component of hydrodynamic resistance

N_{bd} = Reaction of the bottom to door

From Figure 2.12, it is seen that the hydrodynamic drag of the warps is computed by the following expression:

$$F_{warp} = T_1 \cos \alpha_1 - T_0 \cos \alpha_0 \tag{2.33}$$

The power required to pull one cable is, therefore, given as

$$P = T_1 V \cos \alpha \tag{2.34}$$

where

P = Power

V = Towing velocity

T_1 = Cable tension

CHAPTER 3

LITERATURE REVIEW

3.1 Mathematical Modeling of Fish Nets

The computation of drag force of a fish net by analytical approach is known as mathematical modeling of nets. An estimate of the magnitude of drag at a given speed determines the capability of a trawler to tow the net at that speed. Also, if the net is to be physically modeled and tested, an estimate of drag is necessary to design the force measuring instruments. However, published research papers dealing with the calculation of drag on fish net by mathematical models are scarce. The main features of one approach found in the literature are described below.

Giannotti (1973) assumes the total resistance of a fish net to a current to be equal to the sum of the individual resistances of the components of the net. This assumption neglects the effect of the interference between components. The fish net is divided into two major sections, namely, cod end and belly. The minor components include foot- and headropes and floats. The shape of cod end is assumed to be cylindrical and the drag acting on the cod end is computed by Equation (2.20).

Giannotti approximates the belly by a conical net with an elliptical mouth where the major axis of the ellipse is given by the wingspread 2a, and the minor axis by the headline height 2b. To compute the drag force acting on net panels, he conducted wind tunnel experiments on two net panels and presented an empirical formula on the form

$$F = \left(C_{D\ panel} \sin \alpha + 0.005\right)\left(\frac{\rho V^2}{2}\right)\left(A_{surface} \cdot S\right) \tag{3.1}$$

Applying Equation (3.1) to an elementary surface area of the elliptical cone and integrating it over the entire surface, the drag force acting on the belly is obtained.

$$F_{belly} = \left(\frac{\rho V^2}{2}\right)(S)\ \left[\left(C_{D\ panel}\ \pi ab\right) + 0.005\pi \times \sqrt{c^2ab + a^2b^2}\right] \tag{3.2}$$

where

F_{belly} = Drag force

c = Length of net

The second term in the radical of Equation (3.2) is very small compared to the first term. Therefore, this equation shows that the length of the net does not have any major effect on the drag force. Giannotti (1973, p. 56) also infers that "the flow essentially sees only a projected area as it passes through the cone, and the aspect ratio of the cone has no effect on the drag force." If the drag on

the belly is independent of the net length and depends only on the projected area of the net to a plane normal to the flow, it is to say then, that the shape of the net does not affect the drag force which is not true. Therefore, the basic equation (3.1) should not be applied to computing the drag force on the belly.

The angle of incidence of the flow in the belly varies from $\tan^{-1}$ (a/c) to $\tan^{-1}$ (b/c). For practical cases, the value lies in the range from 2° to 30°. As discussed in section 2.1.3 for this range, Equation (3.2) will predict low values of drag force because of the low prediction of projected solid areas. When a net panel is inclined at a small angle, α, Equation (3.1) estimates the projected solid area to be in the order of $(SA_{surface} \cdot \sin \alpha)$. But the actual value of the projected solid area is in the order of $(SA_{surface})$ since the projected area of an inclined cylindrical bar is in the same order of area of the cylindrical bars. Therefore, Equation (3.1) is not the proper form of equation in evaluating the magnitude of the drag force.

The resistance of minor components, footrope, headrope and floats has been calculated by equations given in section 2.2. The total resistance of the net is, therefore, the sum of the resistances of the cod end, belly, footrope, headrope and floats.

As Giannotti predicts very low values of drag force, his approach is not adequate. Hence, an adequate method of

finding the forces on and of testing fish nets is necessary. At present, physical model testing seems to be the only alternative and appropriate method of testing fish nets.

3.2 Physical Modeling of Nets and Trawls

Laws relating to the construction of hydraulic models and the interpretation of the results of model tests are described below.

3.2.1 Forces in a Fluid Flow

The forces acting on an element of fluid in a flow can be classified under active and reactive forces. Active forces include inertia, gravity, viscous, elastic, surface tension forces and, in rare cases, compressive forces. Reactive forces are the pressure forces.

Inertia force arises from the acceleration and deceleration of fluid mass. By Newton's second law of motion,

$$F_{inertia} = m'' \cdot \vec{a} \tag{3.3}$$

where

m'' = Mass

$\vec{a}$ = Acceleration

The gravity force if calculated by

$$F_{gravity} = m'' \cdot \vec{g} \tag{3.4}$$

where

$\vec{g}$ = Acceleration due to gravity

Viscous resistance to shear is the property of the fluid which varies directly with the velocity gradient normal to the direction of flow. Viscous forces, thus, depend on the motions in a system at an instant of time and feedback to modify the motions at succeeding instants of time.

Surface tension force exists at interfaces between fluids, whether liquid and liquid, or liquid and gas. The value of surface tension is the energy required to increase the surface area one unit.

Elastic forces in a fluid occur by virtue of change in volume. Reactive forces result from the active forces.

The equilibrium condition is, therefore (Fig. 3.1),

$$\vec{F}_{gravity} + \vec{F}_{viscous} + \vec{F}_{\substack{surface \\ tension}} + \vec{F}_{elastic} + \vec{F}_{pressure} + \vec{F}_{inertia} = 0 \qquad (3.5)$$

3.2.2 Similitude

To model a hydrodynamic flow system, the prototype and the model should satisfy the following three types of similarity.

Geometric similarity—Two objects are said to be geometrically similar if the ratios of all homologous

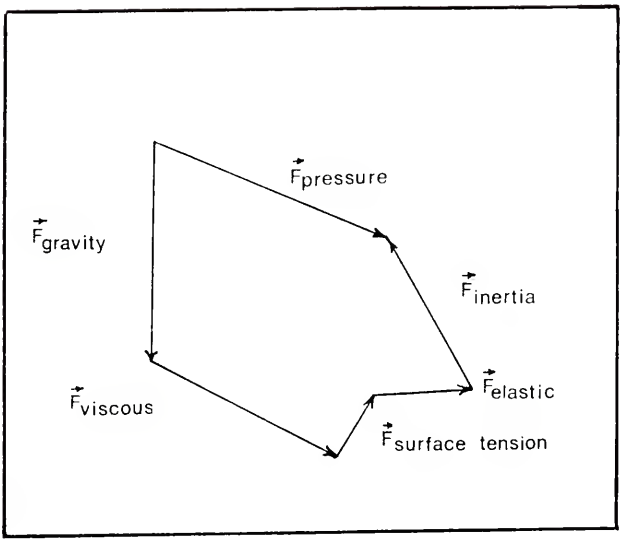

Figure 3.1. Force polygon of a fluid flow.

dimensions are equal. Thus, geometric similarity involves only similarity in form.

Kinematic similarity—Two flow motions are kinematically similar if the patterns or paths of motion are geometrically similar, and if the ratios of the velocities of the various homologous flow particles are equal.

Dynamic similarity—This is the similarity of forces. Therefore, the force polygon in the model must be geometrically similar to the force polygon in the prototype. This requires that the force scale must be the same for all forces.

3.2.3 Model Scales

The term model scale refers to a quantity in the prototype divided by the corresponding quantity in the model. Greek letters are used for the model scales while the subscripts p and m refer to the prototype and model, respectively.

The fundamental model scales are:

$$\text{Length scale} \qquad \lambda = \frac{L_p}{L_m} \tag{3.6}$$

$$\text{Time scale} \qquad \tau = \frac{T_p}{T_m} \tag{3.7}$$

$$\text{Force scale} \qquad \kappa = \frac{F_p}{F_m} \tag{3.8}$$

in which L, T and F stand for a characteristic length time

and force. All other model scales may be derived from the fundamental scales.

Velocity scale:

$$\frac{V_p}{V_m} = \frac{L_p/T_p}{L_m/T_m} = \frac{\lambda}{\tau} \tag{3.9}$$

Pressure scale:

$$\frac{P'_p}{P'_m} = \frac{F_p/L_p^2}{F_m/L_m^2} = \frac{\kappa}{\lambda^2} \tag{3.10}$$

Mass scale:

$$\frac{m''_p}{m''_p} = \left(\frac{F_p}{L_p/T_p^2}\right) \Big/ \left(\frac{F_m}{L_m/T_m^2}\right) = \frac{\kappa\tau^2}{\lambda} \tag{3.11}$$

Inertia force scale:

$$\kappa_{inertia} = \frac{\rho_p L_p^3 \cdot L_p/T_p^2}{\rho_m L_m^3 \cdot L_m/T_m^2} = \frac{\rho_p}{\rho_m} \cdot \frac{\lambda^4}{\tau^2} \tag{3.12}$$

Gravity force scale:

$$\kappa_{gravity} = \frac{\rho_p L_p^3 g_p}{\rho_m L_m^3 g_m} = \frac{\rho_p}{\rho_m} \cdot \lambda^3 \tag{3.13}$$

Viscous force scale:

$$\kappa_{viscous} = \frac{\left(\mu_p \frac{L_p}{T_p} \frac{1}{L_p}\right) L_p^2}{\left(\mu_m \frac{L_m}{T_m} \frac{1}{L_m}\right) L_m^2} = \frac{\mu_p}{\mu_m} \cdot \lambda^2 \tag{3.14}$$

Surface tension scale:

$$\kappa_{\substack{\text{surface}\\\text{tension}}} = \frac{O_p}{O_m} \cdot \frac{L_p}{L_m} = \frac{O_p}{O_m} \lambda \tag{3.15}$$

Elastic force scale:

$$\kappa_{\text{elastic}} = \frac{K_p}{K_m} \cdot \lambda^2 \tag{3.16}$$

where

μ = Dynamic viscosity of fluid

O = Surface tension

K = Bulk modulus of elasticity

Dynamic similarity condition requires that

$$\kappa = \kappa_{\text{inertia}} = \kappa_{\text{gravity}} = \kappa_{\text{viscous}} = \kappa_{\substack{\text{surface}\\\text{tension}}} = \kappa_{\text{elastic}} \tag{3.17}$$

From Equations (3.12) to (3.17),

$$\kappa = \frac{\rho_p}{\rho_m} \cdot \frac{\lambda^4}{\tau^2} = \frac{\rho_p}{\rho_m} \cdot \lambda^3 = \frac{\mu_p}{\mu_m} \cdot \frac{\lambda^2}{\tau} = \frac{k_m}{k_m} \cdot \lambda^2 \tag{3.18}$$

The length scale, λ, can be selected at will but all other unknown scales are to be solved as a function of λ. Equation (3.18) is actually three equations. They cannot be simultaneously solved for the unknown time scale, τ, unless a suitable fluid satisfying these equations is found

by chance. Therefore, the usual procedure is to neglect minor forces in the flow under consideration.

3.2.4 Model Laws

The ratio of the gravity force per unit mass to the inertia force per unit mass is $L\vec{g}/V^2$. The inverse of this ratio is called the Froude number. Therefore,

$$F_r = \frac{V}{\sqrt{gL}} = \left(\frac{\text{Inertia force}}{\text{Gravity force}}\right)^{\frac{1}{2}} \tag{3.19}$$

The Froude number is an important parameter whenever gravity is a factor which influences fluid motion. In such a case, the Froude number in the model and prototype must be the same.

The inverse of the ratio,

$$\frac{\text{Viscous force/mass}}{\text{Inertia force/mass}} = \frac{\mu V/\rho L^2}{V^2/L} = \frac{\mu}{\rho VL} \tag{3.20}$$

is the Reynolds number. It is important when viscous forces influence fluid motion. To model such fluid motion, the Reynolds number should be kept the same in the model and prototype.

The relationship between the inertia and pressure force defines Euler number E_u.

$$\frac{\text{Inertia force}}{\text{Pressure force}} = \frac{\rho L^3 \cdot L/T^2}{L^2 P'} = \frac{\rho V^2}{P'}$$

Therefore,

$$E_u = \frac{\rho V^2}{P'} \tag{3.21}$$

If the predominant forces are inertia and surface tension, the Weber number should be kept constant both in the model and the prototype. The Weber number W_n is defined as:

$$W_n = \frac{\text{Inertia force}}{\text{Capillary force}} = \frac{V^2/L}{O/\rho L^2}$$

$$W_n = \frac{\rho V^2 L}{O} \tag{3.22}$$

If similitude with respect to elastic force is to be insured, the Cauchy number or Mach number should be kept the same in the prototype and model. This is defined as:

$$\frac{\text{Inertia force}}{\text{Elastic force}} = \frac{\rho L^3 \cdot L/T^2}{L^2 E' \cdot L/L} = \frac{(L/T)^2}{E'/\rho}$$

$$C_a = M_a^2 = \frac{\rho V^2}{E'} \tag{3.23}$$

where

C_a = Cauchy number

M_a = Mach number

E' = Modulus of elasticity

In short, the predominant force scale ratios and the model laws are:

$$\kappa = \kappa_{inertia} = \kappa_{gravity} = \kappa_{viscous} = \kappa_{surface\ tension} = \kappa_{elastic} \tag{3.24}$$

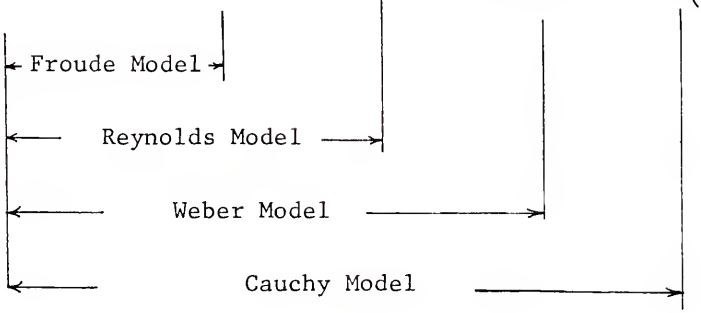

3.2.5 Derived Model Scales

In all the cases mentioned above, if the length scale, λ, is chosen, depending on the predominant forces, the time scale can be found from the model law. Then, the model scale ratio for any derived quantity can be solved.

For example, in the case of Froude's model law which considers the gravity and inertia forces as predominant forces, the inertia and gravity force scale ratio should be equal. From Equations (3.12) and (3.13), the time scale, τ, is:

$$\tau = \sqrt{\lambda} \tag{3.25}$$

When $\vec{g}_p = \vec{g}_m$, the corresponding velocity scale is:

$$\frac{V_p}{V_m} = \frac{\lambda}{\tau} = \sqrt{\lambda} \tag{3.26}$$

Similarly, the force scale ratio is obtained as:

$$\kappa = \frac{\rho_p}{\rho_m} \cdot \frac{\lambda^4}{\tau^2} = \frac{\rho_p}{\rho_m} \cdot \lambda^3 \qquad (3.27)$$

and so on.

Scales for derived quantities for different model laws can be obtained in a similar fashion. Table 3.1 summarizes the basic and derived scales for the model laws considered above (Christensen 1975a).

3.2.6 Limitations

In model studies, the following limitations are usually encountered.

Reproduction limit—As the size of the model decreases, the magnitude of the predominant forces in the model decreases significantly, such as, by the cube of the length scale in the case of Froude modeling. If the model is small, a surface tension force may become large enough to be of the same order of magnitude as that of the active forces since surface tension force is proportional to the first power of the length scale. In this case, extrapolation of model results to prototype conditions, where surface tension forces are not predominant, will be incorrect. However, this difficulty can be overcome by using the Weber model law in deriving the model scales, in which case, the Froude model law, of course, will be violated.

Cavitation limit—When atmospheric pressure is not reproduced in the model, cavitation phenomena in the prototype are not reproduced correctly in the model.

TABLE 3.1

BASIC AND DERIVED MODEL SCALES FOR HYDRAULIC MODELS

Magnitude	General Formula For Scale	Dimension in FPS Unit	Model Law			
			Froude $\frac{V}{\sqrt{gL}}$ = Constant	Reynolds $\frac{VL}{\nu}$ = Constant	Weber $\frac{V^2L}{O/\rho}$ = Constant	Cauchy $\frac{V}{\sqrt{K/\rho}}$ = Constant
Dimensionless Coefficient	-	-	1	1	1	1
Length	λ	ft	λ	λ	λ	λ
Area	λ^2	ft^2	λ^2	λ^2	λ^2	λ^2
Volume	λ^3	ft^3	λ^3	λ^3	λ^3	λ^3
Time	τ	sec	$\sqrt{\frac{g_m}{g_p}}\sqrt{\lambda}$	$\frac{\nu_m}{\nu_p}\lambda^2$	$\sqrt{\frac{O_m/\rho_m}{O_p/\rho_p}}\lambda^{3/2}$	$\sqrt{\frac{K_m/\rho_m}{K_p/\rho_p}}\lambda$
Force	κ	lb	$\frac{g_p\rho_p}{g_m\rho_m}\lambda^3$	$\frac{\rho_p}{\rho_m}\left(\frac{\nu_p}{\nu_m}\right)^2$	$\frac{O_p}{O_m}\lambda$	$\frac{K_p}{K_m}\lambda^2$

TABLE 3.1—Continued

Magnitude	General Formula For Scale	Dimension in FPS Unit	Model Law			
			Froude $\frac{V}{\sqrt{gL}}$ = Constant	Reynolds $\frac{VL}{\nu}$ = Constant	Weber $\frac{V^2L}{O/\rho}$ = Constant	Cauchy $\frac{V}{\sqrt{K/\rho}}$ = Constant
Mass	$\frac{\kappa\tau^2}{\lambda}$	$\frac{\text{lb sec}^2}{\text{ft}}$	$\frac{\rho_p}{\rho_m}\lambda^3$	$\frac{\rho_p}{\rho_m}\lambda^3$	$\frac{\rho_p}{\rho_m}\lambda^3$	$\frac{\rho_p}{\rho_m}\lambda^3$
Frequency	$\frac{1}{\tau}$	$\frac{1}{\text{sec}}$	$\sqrt{\frac{g_p}{g_m}}\ \frac{1}{\sqrt{\lambda}}$	$\frac{\nu_p}{\nu_m}\ \frac{1}{\lambda^2}$	$\sqrt{\frac{O_p/\rho_p}{O_m/\rho_m}}\ \frac{1}{\lambda^{3/2}}$	$\sqrt{\frac{K_p/\rho_p}{K_m/\rho_m}}\ \frac{1}{\lambda}$
Velocity	$\frac{\lambda}{\tau}$	ft/sec	$\sqrt{\frac{g_p}{g_m}}\ \sqrt{\lambda}$	$\frac{\nu_p}{\nu_m}\ \frac{1}{\lambda}$	$\sqrt{\frac{O_p/\rho_p}{O_m/\rho_m}}\ \frac{1}{\sqrt{\lambda}}$	$\sqrt{\frac{K_p/\rho_p}{K_m/\rho_m}}$
Discharge	$\frac{\lambda^3}{\tau}$	ft^3/sec	$\sqrt{\frac{g_p}{g_m}}\ \lambda^{5/2}$	$\frac{\nu_p}{\nu_m}\ \lambda$	$\sqrt{\frac{O_p/\rho_p}{O_m/\rho_m}}\ \lambda^{3/2}$	$\sqrt{\frac{K_m/\rho_p}{K_m/\rho_m}}\ \lambda^2$
Discharge per Unit Width	$\frac{\lambda^2}{\tau}$	ft^2/sec	$\sqrt{\frac{g_p}{g_m}}\ \lambda^{3/2}$	$\frac{\nu_p}{\nu_m}$	$\sqrt{\frac{O_p/\rho_p}{O_m/\rho_m}}\ \lambda^{1/2}$	$\sqrt{\frac{K_p/\rho_p}{K_m/\rho_m}}\ \lambda$
Acceleration	$\frac{\lambda}{\tau^2}$	ft/sec^2	$\frac{g_p}{g_m}$	$\left(\frac{\nu_p}{\nu_m}\right)^2\ \frac{1}{\lambda^3}$	$\frac{O_p/\rho_p}{O_m/\rho_m}\ \frac{1}{\lambda^2}$	$\frac{K_p/\rho_p}{K_m/\rho_m}\ \frac{1}{\lambda}$

TABLE 3.1—Continued

Magnitude	General Formula For Scale	Dimension in FPS Unit	Model Law			
			Froude $\frac{V}{\sqrt{gL}}$ = Constant	Reynolds $\frac{VL}{\nu}$ = Constant	Weber $\frac{V^2L}{O/\rho}$ = Constant	Cauchy $\frac{V}{\sqrt{K/\rho}}$ = Constant
Stress	$\frac{\kappa}{\lambda^2}$	$\frac{\text{lbs}}{\text{ft}^2}$	$\frac{g_p \rho_p}{g_m \rho_m} \lambda$	$\frac{\rho_p}{\rho_m} \left(\frac{\nu_p}{\nu_m}\right)^2 \frac{1}{\lambda^2}$	$\frac{O_p}{\rho_m} \frac{1}{\lambda}$	$\frac{K_p}{K_m}$
Moment, Work or Energy	$\kappa\lambda$	lb ft	$\frac{g_p \rho_p}{g_m \rho_m} \lambda^4$	$\left(\frac{\rho_p}{\rho_m}\right)\left(\frac{\nu_p}{\nu_m}\right)^2 \lambda$	$\frac{O_p}{O_m} \lambda^2$	$\frac{K_p}{K_m} \lambda^3$
Power	$\frac{\kappa\lambda}{\tau}$	$\frac{\text{lb ft}}{\text{sec}}$	$\left(\frac{g_p}{g_m}\right)^{3/2} \frac{\rho_p}{\rho_m} \lambda^{7/2}$	$\left(\frac{\rho_p}{\rho_m}\right)\left(\frac{\nu_p}{\nu_m}\right)^3 \frac{1}{\lambda}$	$\left(\frac{O_p}{O_m}\right)^{3/2} \sqrt{\frac{\rho_p}{\rho_m}} \lambda$	$\left(\frac{K_p}{K_m}\right)^{3/2} \sqrt{\frac{\rho_p}{\rho_m}} \lambda^2$
Momentum	$\kappa\tau$	lb sec	$\sqrt{\frac{g_p}{g_m}} \frac{\rho_p}{\rho_m} \lambda^{7/2}$	$\frac{\rho_p}{\rho_m} \frac{\nu_p}{\nu_m} \lambda^2$	$\sqrt{\frac{O_p \rho_p}{O_m \rho_m}} \lambda^{5/2}$	$\sqrt{\frac{K_p \rho_p}{K_m \rho_m}} \lambda^3$
Moment of Mementum	$\kappa\tau\lambda$	lb sec ft	$\sqrt{\frac{g_p}{g_m}} \frac{\rho_p}{\rho_m} \lambda^{9/2}$	$\frac{\rho_p}{\rho_m} \frac{\nu_p}{\nu_m} \lambda^3$	$\sqrt{\frac{O_p \rho_p}{O_m \rho_m}} \lambda^{7/2}$	$\sqrt{\frac{K_p \rho_p}{K_m \rho_m}} \lambda^4$

Wave limit—If waves are to be reproduced correctly in the model, wave velocities in the model should be greater than 0.755 ft/sec corresponding to the minimum capillary wave velocity.

Laminar-turbulent limit—The model should not be so small that the flow in the model becomes laminar while the corresponding prototype flow is turbulent. By obeying Reynolds' model law, this limit can be avoided.

Subcritical and supercritical limit—Sometimes it is necessary to use a different scale for the vertical dimension than for that of the horizontal dimension. This is known as vertical distortion. Where subcritical and supercritical flows of the prototype are to be reproduced properly, the Froude model law should be used.

Sediment transport limit—If a sediment transport phenomenon is to be modeled, the sediments cannot usually be scaled down to the length or depth scale. E.g., if normal sand is the prototype bed material and if it is to be scaled down to a realistic scale, say, $\lambda = 50$, then clay or silt should be used in the model. But clay and silt behave differently than sand due to their cohesive properties. Therefore, special model laws are usually needed for these types of models (Christensen 1975b).

Roughness limit—Small wall and bed roughness in the prototype cannot be reproduced correctly in a small model. Christensen and Snyder (1975) present a procedure to model the roughness elements by distortion.

3.2.7 Model Laws Applied to Fish Net

Tauti (1934) has applied the hydraulic model laws to fishing nets by assuming: (1) that the elongation of the netting twine is negligible, (2) that the netting twines are flexible, (3) that Newton's law of hydrodynamic resistance is valid for every portion of the net irrespective of its Reynolds number and (4) that any change in the form of the net occurs so slowly that the external forces acting on each element of the net can be considered to be in quasi-equilibrium. Considering an element of the net with area, A, and circumference, S' (Fig. 3.2), he examines the forces acting on it under equilibrium conditions. From assumptions (1) and (4), the forces are gravity, drag and webbing tensile forces.

The gravity force is the apparent weight of the elemental area of the net and is expressed as:

$$w = f_1(\phi)\left(\rho_s - \rho_w\right) D \cdot \left(\frac{D}{M} + c_1 \left(\frac{D}{M}\right)^2\right) \qquad (3.28)$$

where

$f_1(\phi) = \frac{\pi p'}{2 \sin 2\phi}$ = Function depending on degree of slackness of netting

$c_1 = \frac{M_k}{2D_k} \sqrt{p'/p'_*}$ = Constant which depends on type of knot and its tightness

w = Apparent weight of net per unit surface area

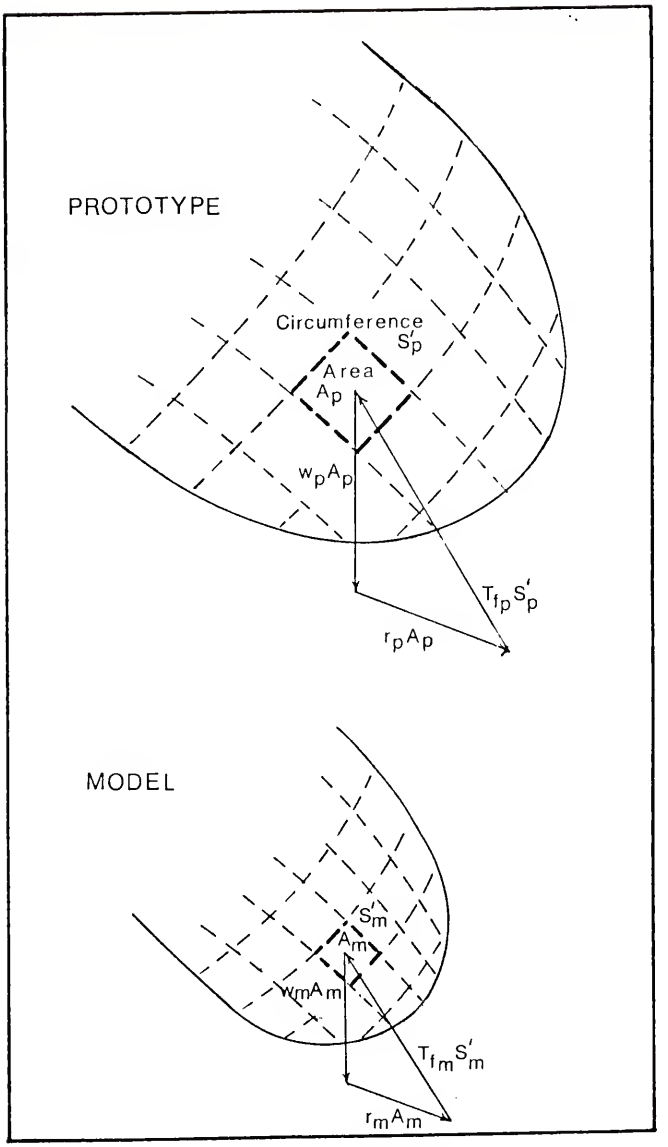

Figure 3.2. Force polygon in the model and full-scale net.

The resistance r acting on a unit area of the webbing is expressed by

$$r = f_2(\phi) \left[\frac{D}{M} + C_2 \left(\frac{D}{M} \right)^2 \right] V^2 \tag{3.29}$$

where

$f_2(\phi)$ = Function which depends on incident angle of the current and half of the angle between two adjacent bars

Geometric similarity requires that α an ϕ should be the same in the model and the prototype and dynamic similarity yields:

$$\frac{w_p A_p}{w_m A_m} = \frac{r_p A_p}{r_m A_m} = \frac{T_{f_p} S'_p}{T_{f_m} S'_m} = \frac{F_p}{F_m} = \kappa \tag{3.30}$$

where

T_f = Tension per unit length

F = Total force acting on net

Tauti sets the twine diameter scale to be equal to the bar length scale.

$$\frac{D_p}{D_m} = \frac{M_p}{M_m} \Longrightarrow \lambda_D = \lambda_M \tag{3.31}$$

He gives the scales of the area and the circumference to be equal to the square of the length scale and the length scale, respectively. From Equations (3.28) to (3.31), Tauti gets:

$$\lambda^2 \lambda_D \left(\frac{\rho_{s_p} - \rho_{w_p}}{\rho_{s_m} - \rho_{w_m}} \right) = \lambda^2 \left(\frac{V_p}{V_m} \right)^2 = \lambda \quad \frac{T_{f_p}}{T_{f_m}} = \frac{F_p}{F_m} \tag{3.32}$$

Equating the first and second terms in Equation (3.32), the scale ratio for velocity is obtained as:

$$\frac{V_p}{V_m} = \sqrt{\frac{\rho_{s_p} - \rho_{w_p}}{\rho_{s_m} - \rho_{s_m}} \cdot \lambda_D} \tag{3.33}$$

From Equation (3.33), it is seen that the velocity scale depends on the mesh scale λ_D, rather than the length scale ratio λ.

From the third and second terms, the scale for the tension per unit length is:

$$\frac{T_{f_p}}{T_{f_m}} = \lambda \left(\frac{V_p}{V_m} \right)^2 \tag{3.34}$$

and, the second and fourth terms give:

$$\frac{F_p}{F_m} = \lambda^2 \left(\frac{V_p}{V_m} \right)^2 \tag{3.35}$$

Summary points of Tauti's model laws for fishing nets: The linear length scale λ is chosen arbitrarily; the mesh length scale is distorted and chosen arbitrarily; the velocity scale depends on the mesh scale rather than the linear scale and the force scale is given by Equation (3.35) which is in agreement with Froude's law.

Using the dynamic similarity concept, Dickson (1959) argues that the velocity scale ratio should be dependent on the linear scale λ instead of the mesh length ratio. Neglecting the small density difference between the prototype and the model fluid, he presents:

$$\frac{V_p}{V_m} = \sqrt{\lambda} \tag{3.36}$$

Fridman (1973) considers the diameter of the bar as the characteristic linear dimension and reasons that the drag coefficient for the net is independent of the linear length of the net. Therefore, he supports the model laws developed by Tauti.

Kawakami (1959) extends the results of Tauti to model ropes, floats and sinkers. He considers two cases of modeling of ropes. In the first case, the rope is used as the main part of the net, the reduction ratio is equal to that of the main body of the net, i.e.,

$$\frac{\ell_{r_p}}{\ell_{r_m}} = \lambda \tag{3.37}$$

In the second case, the rope length is independent of the size of the main body of the net, as in the case of the towing warp of a trawl.

In both cases, Kawakami (1959) considers the three forces acting on a rope: The hydrodynamic force, the apparent weight of the rope, and the tension in the rope.

He also assumes the elongation of the rope to be negligible. He expresses the hydrodynamic resistance r_r acting per unit length of the rope as:

$$r_r = r_{r_0} \sin^2 \alpha \cdot H_r \cdot V^2 \tag{3.38}$$

where

r_{r_0} = A constant
H_r = Diameter of rope
α = Angle between rope and current

The apparent weight of the rope per unit length w_r is given by

$$w_r = \frac{\pi H_r^2}{4} (\gamma_r - \gamma_w) \tag{3.39}$$

in which

γ_r = Specific weight of rope

The force ratios must be equal in order to satisfy the dynamic similarity. From Equation (3.35),

$$\frac{\ell_{r_p} w_{r_p}}{\ell_{r_m} w_{r_m}} = \frac{\ell_{r_p} r_{r_p}}{\ell_{r_m} r_{r_m}} = \frac{T_{r_p}}{T_{r_m}} = \lambda^2 \left(\frac{V_p}{V_m}\right)^2 \tag{3.40}$$

where

ℓ_r = Length of rope
T_r = Tension in rope

For the first case, where the rope is used as a main body of the net,

$$\frac{\ell_{r_p}}{\ell_{r_m}} = \lambda$$

Substitution of Equations (3.38) and (3.39) in (3.40), yields:

$$\frac{H_{r_p}}{H_{r_m}} = \lambda$$

and

$$\frac{\gamma_{r_p} - \gamma_{w_p}}{\gamma_{r_m} - \gamma_{w_m}} = \frac{(V_p/V_m)^2}{\lambda} \tag{3.41}$$

For the second case where the rope length is independent of the size of the net,

$$\frac{\ell_{r_p}}{\ell_{r_m}} = \lambda_r \neq \lambda \tag{3.42}$$

Kawakami gives:

$$\frac{H_{r_p}}{H_{r_m}} = \frac{\lambda^2}{\lambda_r}$$

and

$$\frac{\gamma_{r_p} - \gamma_{w_p}}{\gamma_{r_m} - \gamma_{w_m}} = \left(\frac{V_p}{V_m}\right)^2 \cdot \frac{\lambda_r}{\lambda^2} \tag{3.43}$$

Therefore, the diameter and density of the rope in the model should be chosen to satisfy Equations (3.41) or Equations (3.43).

To model floats and sinkers, Kawakami (1959) analyzes the forces acting on them which are the apparent weight and the hydrodynamic resistance. Denoting the number of floats or sinkers per unit length of rope by n, the apparent weight w, per unit length, is calculated by

$$w = k_1 E^3 \left(\gamma_s' - \gamma_w\right) n \tag{3.44}$$

where

k_1 = A constant depending on the shape of float or sinker

E = Diameter

γ_s' = Specific weight of material

The hydrodynamic resistance is expressed in the form,

$$r_a = k_2 E^2 V^2 n \tag{3.45}$$

where

r_a = Hydrodynamic resistance per unit length of rope

k_2 = A constant

From the dynamic similarity condition and from Equations (3.35), (3.44) and (3.45),

$$\frac{\gamma'_{s_p} - \gamma_{w_p}}{\gamma'_{s_m} - \gamma_{w_m}} = \left(\frac{V_p}{V_m}\right)^2 \sqrt{\frac{n_p}{n_m}\,\frac{1}{\lambda}}$$

and

$$\frac{E_p}{E_m} = \sqrt{\lambda\,\frac{n_m}{n_p}} \tag{3.46}$$

Therefore, the floats and sinkers of the model should satisfy Equation (3.46). In cases where Equation (3.46) cannot be satisfied, an approximation should be made in considering the forces acting on floats or sinkers. Neglecting the hydrodynamic resistance force compared to the apparent weight, the similarity condition yields:

$$\left(\frac{E_p}{E_m}\right)^3 \left(\frac{\gamma'_{s_p} - \gamma_{w_p}}{\gamma'_{s_m} - \gamma_{w_m}}\right) = \left(\frac{V_p}{V_m}\right)^2 \lambda\,\frac{n_m}{n_p} \tag{3.47}$$

A bibliography on development of model laws is given in Appendix B.

3.2.8 Dimensional Analysis

The variables that can influence the profile of a net characterized by a linear dimension S' are: (1) series of linear dimensions defining the boundaries L, M, D (2) kinematic and dynamic quantities such as mean velocity V and force F and (3) the physical properties of the fluid

and of the net such as density ρ, viscosity μ, specific weight of twine γ_s and elastic properties. These variables and the functional relation can be expressed in the form:

$$S' = f\left(\rho,\ L,\ V,\ \mu,\ t,\ M,\ D,\ F,\ \xi,\ \varepsilon,\ u_1,\ u_2,\ \gamma^*\right) \qquad (3.48)$$

Using Buckingham's π theorem, Fridman (1973) derives the following dimensional numbers:

$$\frac{S'}{L} = f\left(\frac{D}{L},\ \frac{M}{L},\ \frac{Vt}{L},\ \frac{\rho V^2}{\gamma^* L},\ \frac{\rho VL}{\mu},\ \frac{F}{\rho V^2 L^2},\ \xi,\ u_1,\ u_2,\ \varepsilon\right) \qquad (3.49)$$

where

ξ = Elastic displacement

u_1, u_2 = Hanging coefficients

ε = Unit elongation of the twine

Therefore, for the complete similarity condition, the following terms should be the same for the model and for the prototype:

1. M/L and
2. D/L or these terms can be grouped into single one term, D/M
3. Vt/L which is the Strouhal number
4. $\frac{\gamma V^2}{\gamma^* gL}$, a modified Froude number
5. VL/ν, the Reynolds number
6. $\frac{F}{\rho V^2 L^2}$
7. ξ, u_1, u_2, ε (geometry of the net)

Fridman (1973) analyzes each term in detail and determines whether it is possible to keep the term constant both in model and prototype. He derives the model laws and scales considering only the major forces acting on the net, which vary from case to case.

3.2.9 Model Experiments

Model experiments are conducted in hydraulic flumes generally by two different methods. In the first method, the water is at rest and the net is towed by a carriage moving on rails. In this case, the length of the flume must be sufficient to allow enough time to conduct the tests while not accelerating or decelerating. If the behavior of the net is to be visually observed and photographed, the sides of the flume should be transparent. Few such tanks are available in the U.S.A. for testing of nets.

In the second method, the net is stationary and the water flows through it. This facilitates visual observation of a conveniently stationary net. In this case, the water velocity varies from zero, at the bottom of the flume, to a particular value at the top of the water surface. The mean velocity of water in the flume is found by the Froude model law. However, the variation of velocity with depth follows a logarithmic law (Nikuradse 1933):

$$\frac{v}{V_f} = 8.48 + 2.5 \ln \left(\frac{y}{k}\right) \qquad (3.50)$$

where

V_f = Friction velocity

y = Depth from bottom

k = Equivalent sand roughness

v = Velocity at distance y from the bed

Literature on model experiments (Appendix C) indicates that most of the tests on fixed nets are conducted in flume where the velocity distribution of water follows Equation (3.50). But in the prototype, the net is pulled through stagnant water which means that the profile of water velocity with respect to the trawl is uniform. Therefore, the relative velocity has the same value at all distances from the bed. To satisfy similarity conditions, the same velocity distribution should be obtained also in the model. The uniform velocity distribution can be achieved by constructing a movable bed which can be moved at a velocity probably equal to the spatial mean velocity.

The Chamber of Commerce at Boulogne-sur-Mer, France, owns and operates a flume in which such a movable bed is constructed. The details of the flume are reported by World Fishing (1972). However, this flume was used as a simple observation tank rather than a testing tank. Therefore, in the literature, quantitative test results of model experiments of fish net, using a uniform velocity distribution from the bed to water level, are not found, so far.

3.3 Prototype Experiments

Any model law should, of course, be verified both by model and field (prototype) experiments. Reports on field tests of fishing gear detail the parameters measured and the instrumentation used in the tests. A substantial list of such reports is found in Appendix D. The parameters measured in the field tests can be grouped under the following headings: (1) Linear dimensions, such as net spread and height; (2) Angles, such as angle or attack, tilt, etc.; (3) Forces, warp tensile force and (4) Velocity, such as towing speed and current velocity.

The instruments to measure these parameters can be grouped under two divisions: (1) Decktype instruments and (2) Underwater instruments. Decktype instruments that are used on the ship deck include warp tensile load cells, warp declination and divergence meters, and ship's speed log. Underwater instruments are generally batterypowered and self-recording. Some of the underwater instruments are load cells that measure door spread, tensile force on head- and footropes, net height, etc.

de Boer (1959) used a differential manometer to measure the net opening. Motte et al. (1973) describes an accoustical transducer to measure the linear dimension of door spread and net height.

The forces in the footrope and headrope can be measured by a self-recording load cell. One such load cell

is described by Nicholls (1964). He also gives a method of finding the loads acting on netting twines. The principle of this method is the same as the Brinnell Hardness test, a hardened steel used to give an indentation in a relatively soft metal plate.

The angles measured in a full-scale field test are the angle of attack, the pitch, and the heel of the doors. If a rod is attached to a door and suspended to move in horizontal and vertical directions, the free end sliding over the ground will adopt the towing direction of the door. This is the principle underlying the angle of attack meter used by de Boer (1959) and Nicholls (1964). The warp divergence and dip angles can be measured by a protractor and indicator arrangement as described by Motte et al. (1973).

The towing speeds of the trawler, with respect to the water and with respect to the bottom, can be obtained by a conventional ship's taffrail log and navigational instrumentation.

3.4 Pitfalls in Existing Physical Model Laws

The existing model laws described in section 3.2.7 do not consider the effect of elongation of the netting twine under load. If the geometric similitude is to be satisfied, the strain of the twine in the model and in the prototype should be the same. However, if the same netting

twine material is used, both in the model and in the prototype, strain cannot be the same because of the high change in the order of magnitude of forces in the two cases. Therefore, the geometric similarity will not be satisfied in this case and predictions of prototype linear dimension from the model results will be erroneous. Thus, adequate model laws that take the elongation of twine into consideration should be developed.

These model laws should be verified both by field and model data. While conducting the model experiments, it is emphasized that the velocity of water should have the same distribution from top to bottom as in the field experiments, i.e., in most cases, be constant. It will not be adequate to set the mean velocity of water in the flume as the desired velocity. Because the mean velocity occurs at a point whose distance is 0.368 times the depth of flow from the bed if a logarithmic velocity distribution is assumed. This means that the water velocity below that point will be less than the required velocity. This distance is crucial for model tests of bottom trawl since the major portion of the model lies in that region. Therefore, the model drag forces will probably be less than the actual forces. Consequently, the projection of model test results to prototype conditions may not be correct.

In short, the model laws which take the elongation of netting twine into consideration should be verified by

tests in the flume where the velocity distribution is uniform from top to bottom as in the case of field experiments. Such tests are conducted and will be explained in subsequent chapters.

CHAPTER 4

DEVELOPMENT OF MODEL LAWS

4.1 Froude Modeling

To model a flow through and around a trawl, the predominant forces acting on it must be considered. The predominant forces are due to gravity, inertia and the viscosity of the water. The viscous forces will have the least influence on the model if its twine is not thin. Therefore, it is assumed that this type of force has negligible effect on the trawl and that the predominant forces are due only to gravity and inertia. As discussed in section 3.2.4 to model such a flow field, the Froude model law is required.

Equating the inertia and gravity force scales, the time scale ratio is obtained as given by Equation (3.25). The model scale ratios for other derived quantities can then be expressed in terms of the fundamental model scales (Table 3.1).

4.2 Mesh-Twine Distortion

While the principal dimensions of the prototype trawl (length and width of the net) are reduced by the

length scale λ, it is not advisable to reduce the twine size by the same length scale. Such a reduction will, in most cases, result in such low values of the model Reynolds number, which is based on twine diameter, that viscous forces may predominate in the model but not in the prototype. This may happen in spite of the fact that the length scale used in net and trawl models is usually approximately one order of magnitude smaller than the length scales usually used in models of rigid hydraulic structures. The problem may be overcome by using a larger twine size and compensating for the twine distortion by also distorting the mesh size in such a way that the hydrodynamic drag forces acting on any section of the prototype trawl and the corresponding section of the model have the correct force scale.

Figure 4.1 shows a prototype section of a net and its corresponding model section. The drag force acting on a section due to the flow velocity V, relative to the trawl, is computed by calculating the drag force acting on the bars and on the knots. The drag force acting on a twine may be written:

$$F_{bar} = C_{Db} \frac{\rho V^2}{2} MD \tag{4.1}$$

Similarly, the drag force acting on a knot is given by

$$F_{knot} = C_{Dk} \frac{\rho V^2}{2} \left[\frac{\pi D_k^2}{4}\right] \tag{4.2}$$

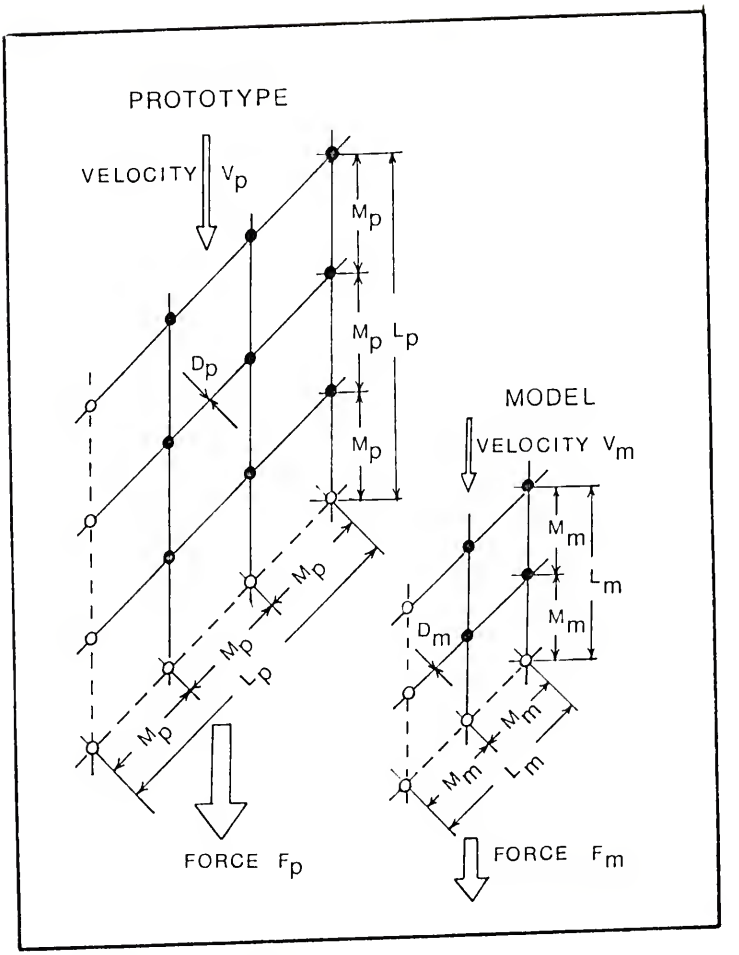

Figure 4.1. Idealized mesh and twine in prototype and model.

where

D_k = Diameter of knot

It is assumed that the diameter of the knot is proportional to the diameter of the twine. The total solid areas of the bars and the knots on which the drag force is acting may be written:

$$A_b = \left(\frac{L}{M}\right)(LD) \tag{4.3}$$

and

$$A_k = \left(\frac{L}{M}\right)^2 \left(\frac{\pi}{4} D_k^2\right) \tag{4.4}$$

From Equations (4.1) to (4.4), the total drag force F, acting on the prototype section, is computed from

$$F_p = c_1 \left(\frac{L_p}{M_p}\right) L_p D_p \rho_p V_p^2 + c_2 \left(\frac{L_p}{M_p}\right)^2 D_p^2 \rho_p V_p^2 \tag{4.5}$$

where

c_1 and c_2 = Constants of twine and knot, respectively

If the Reynolds number based on the twine diameter is not small, both in the model and in the prototype, then the drag coefficients will have the same value in the model and in the prototype. Therefore, the constants c_1 and c_2 also remain the same for the model. The drag force in the model is expressed as:

$$F_m = c_1 \left(\frac{L_m}{M_m}\right) L_m D_m \rho_m V_m^2 + c_2 \left(\frac{L_m}{M_m}\right)^2 D_m^2 \rho_m V_m^2 \tag{4.6}$$

Therefore, the drag force scale ratio is:

$$\frac{F_p}{F_m} = \frac{\dfrac{c_1 L_p^2 D_p}{M_p} + c_2 L_p^2 \dfrac{D_p^2}{M_p^2}}{c_1 L_m^2 \dfrac{D_m}{M_m} + c_2 L_m^2 \dfrac{D_m^2}{M_m^2}} \cdot \frac{\rho_p}{\rho_m} \left(\frac{V_p}{V_m}\right)^2 \tag{4.7}$$

But, the drag force and gravity force scales must be equal to satisfy the dynamic similarity condition. Therefore, from Equations (3.26), (3.27) and (4.7),

$$\frac{\dfrac{D_p}{M_p}\left(c + \dfrac{D_p}{M_p}\right)}{\dfrac{D_m}{M_m}\left(c + \dfrac{D_m}{D_m}\right)} = 1 \tag{4.8}$$

where

$c = c_1/c_2$ = A constant

The mesh scale, λ_M, and twine scale, λ_D, are defined as:

$$\lambda_M = \frac{M_p}{M_m} \tag{4.9}$$

and

$$\lambda_D = \frac{D_p}{D_m} \tag{4.10}$$

Substitution of Equations (4.9) and (4.10) into (4.8), yields:

$$\left(\frac{\lambda_D}{\lambda_M}\right)^2 - \frac{c}{c + \frac{D_p}{M_p}} \frac{\lambda_D}{\lambda_M} - \frac{\frac{D_p}{M_p}}{c + \frac{D_p}{M_p}} = 0 \qquad (4.11)$$

The solution of $\frac{\lambda_D}{\lambda_M}$ is:

$$\frac{\lambda_D}{\lambda_M} = 1 \qquad (4.12)$$

or,

$$\frac{\lambda_D}{\lambda_M} = - \frac{\frac{D_p}{M_p}}{c + \frac{D_p}{D_p}} \qquad (4.13)$$

Equation (4.13) gives a negative value for $\frac{\lambda_D}{\lambda_M}$ which is not possible. Therefore, the only solution of Equation (4.11) is given by Equation (4.12), i.e.,

$$\lambda_D = \lambda_M \qquad (4.14)$$

which is independent of the constant c.

Tauti (1934) has applied Equation (4.14) in deriving the model laws, but he has chosen the result as an arbitrary value instead of a necessary condition. Equation (4.14) is also consistent with the findings of Fridman (1973) who derives the condition from dimensional analysis. A special

case of Equation (4.14) occurs where both scales are equal to one indicating that the same twine and mesh size may be used in both model and prototype. However, the model twine size is determined from the elastic properties of the prototype twine material.

4.3 Elongation of Twine

As discussed in section 2.2.1, the stress-strain relationship of netting twines is expressed in the form:

$$\sigma = A\varepsilon^{B} \tag{4.15}$$

in which

σ = Stress corresponding to the strain ε

A and B = Constants which are properties of the considered twine

The stress-scale is, therefore, obtained:

$$\frac{\sigma_p}{\sigma_m} = \frac{A_p}{A_m} \frac{\varepsilon_p^{B_p}}{\varepsilon_m^{B_m}} \tag{4.16}$$

Geometric similarity requires that the strain in the model, ε_m, is equal to the corresponding strain in the prototype, ε_p.

Equation (4.15) is valid within the strain ranges normally encountered in nets and trawls, and the dimensionless exponent B is nearly the same in most net and trawl materials (Fig. 4.2). A representative value is B = 0.9.

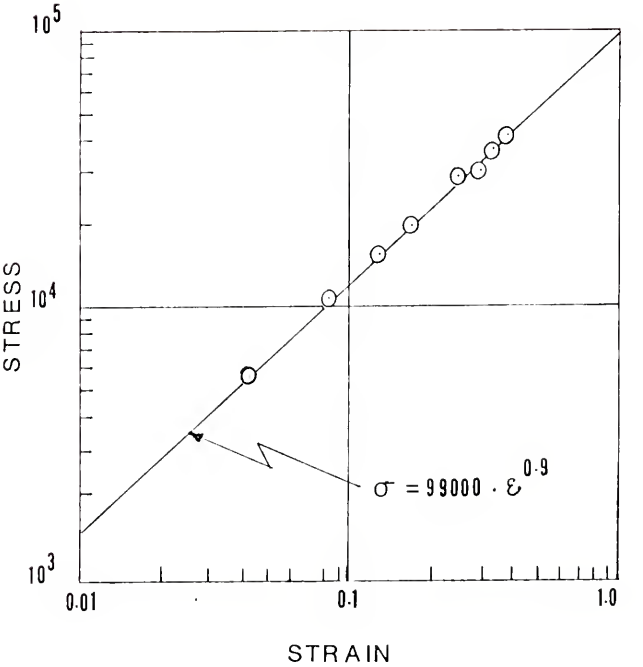

Figure 4.2. Typical stress-strain curve for polyamide twine.

The dimensional constant A varies substantially from material to material. Therefore, Equation (4.16) reduces to:

$$\frac{\sigma_p}{\sigma_m} = \frac{A_p}{A_m} \tag{4.17}$$

The average stress on a twine oriented in the direction of flow may be evaluated by considering the number of twines existing in a prototype length L (Fig. 4.3). The total area on which the total drag force F acts is calculated to be $\frac{L}{M} c_3 D^2$, where c_3 is a constant. Therefore, the average stress is obtained as:

$$\sigma = \frac{F}{\left(\frac{L}{M}\right) c_3 D^2} \tag{4.18}$$

and, hence, the stress scale is:

$$\frac{\sigma_p}{\sigma_m} = \frac{\frac{F_p}{F_m}}{\frac{L_p}{L_m} \frac{l}{\frac{M_p}{M_m}} \frac{c_{3_p}}{c_{3_m}} \left(\frac{D_p}{D_m}\right)^2} \tag{4.19}$$

Because of the requirement of geometric similitude c_{3_m} and c_{3_p} must have the same value. Therefore, Equation (4.19) becomes:

$$\frac{\sigma_p}{\sigma_m} = \frac{\frac{F_p}{F_m}}{\frac{\lambda \cdot \lambda_D^2}{\lambda_M}} \tag{4.20}$$

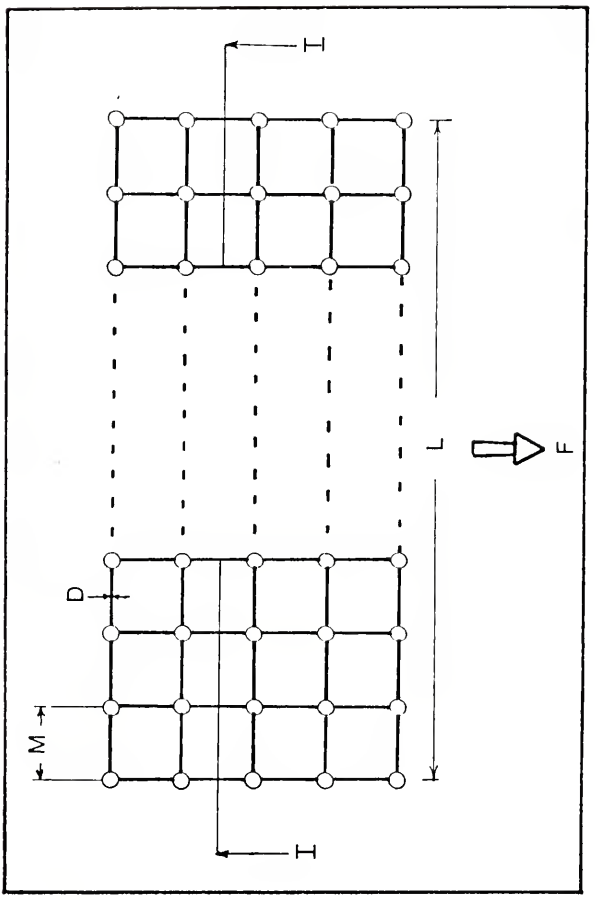

Figure 4.3. Evaluation of average stress in a twine.

The substitution of Equation (3.27) and (4.14) into (4.20), yields:

$$\frac{\sigma_p}{\sigma_m} = \frac{\rho_p}{\rho_m} \cdot \frac{\lambda^2}{\lambda_M} \tag{4.21}$$

From Equations (4.17) and (4.21),

$$\lambda = \sqrt{\frac{A_p}{A_m} \cdot \frac{\rho_m}{\rho_p} \cdot \lambda_M} \tag{4.22}$$

from which the basic length scale λ is to be determined.

Equation (4.22) shows that the length scale cannot be chosen arbitrarily. Once λ_D and the material for the prototype and model are chosen, the model dimension is fixed by them. From Equation (4.22), the corresponding mesh number scale:

$$\eta = \frac{N_p}{N_m} = \frac{\frac{L_p}{M_p}}{\frac{L_m}{M_m}} = \frac{\lambda}{\lambda_M} \tag{4.23}$$

where

N = Number of meshes in a given length, L

4.4 Modeling of Ropes

Ropes (such as headrope, footrope, etc.) are to be considered. The active forces on such ropes may be classified in three categories: (a) forces transferred from the webbing due to the hydrodynamic drag on the

webbing and the catch contained in the trawl, (b) gravity and buoyancy forces acting directly on the rope itself not including such forces on floats or sinkers directly attached to the rope and (c) hydrodynamic drag on the rope itself not including the drag on any floats or sinkers which may be attached directly to the rope. Categories (b) and (c) are usually of a smaller order of magnitude than A which must follow the general force scale given by Equations (3.27).

Consider for instance a headrope with diameter H in which the tensile force is F (Fig. 4.4).

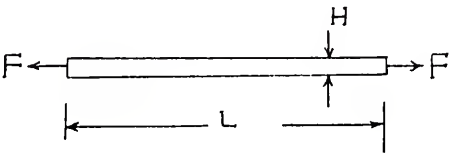

Figure 4.4. Headrope.

The corresponding stress in the rope is:

$$\sigma_p = \frac{F_p}{c_4 H_p^2} \tag{4.24}$$

and

$$\sigma_m = \frac{F_m}{c_4 H_m^2} \tag{4.25}$$

in prototype and model, respectively. The constant, c_4, is

a shape factor assumed to have the same value in prototype and model because of the geometrical similitude.

The combination of Equations (4.2), (4.17), (4.24) and (4.25) yields the rope size scale:

$$\lambda_H = \frac{H_p}{H_m} = \sqrt{\frac{\rho_p}{\rho_m} \cdot \frac{A_m}{A_p}} \quad \lambda^{3/2} \tag{4.26}$$

In cases where the elastic deformations of the ropes are small, compared to the deformations of the webbing (that is, when steel ropes or ropes with steel cores are applied), the requirement $\varepsilon_m = \varepsilon_p$ may be neglected and normal scaling (i.e., application of the λ scale for the rope sizes) may be used.

4.5 Modeling of Floats and Sinkers

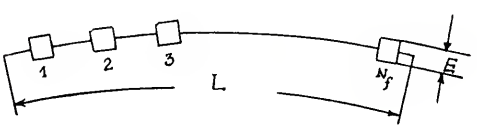

Figure 4.5. Attachments in a rope.

Let N_f floats of diameter E be attached to the length L of the headrope (Fig. 4.5). The buoyant force acting on these floats is:

$$B_b = N_f c_5 E^3 \left(\gamma_s' - \gamma\right) \tag{4.27}$$

where

c_5 = Another constant shape factor

γ_s' = Unit weight of dry float material

γ = Unit weight of water

The corresponding hydrodynamic drag force acting on these N_f floats may be expressed as:

$$F = N_f c_6 E^2 \rho V^2 \tag{4.28}$$

where

c_6 = A constant

The force scale of these two forces must be the same, that is,

$$\frac{B_{b_p}}{B_{b_m}} = \frac{F_p}{F_m} \tag{4.29}$$

given together with Equation (3.25) for the time scale:

$$\lambda_E = \left(\frac{\gamma'_{s\cdot m} - \gamma_m}{\gamma'_{s\cdot p} - \gamma_p}\right) \cdot \left(\frac{\gamma_p}{\gamma_m}\right) \quad \lambda = \lambda \left(\frac{\frac{\gamma'_{s\cdot m}}{\gamma_m} - 1}{\frac{\gamma'_{s\cdot p}}{\gamma_p} - 1}\right) \tag{4.30}$$

where

$\lambda_E = E_p/E_m$ = Float (or sinker) diameter scale

The two force scales in Equation (4.29) must also be equal to the general force scale given by Equation (3.27). This requirement results in the formula:

$$N_{f_m} = N_{f_p}\left(\frac{\lambda_E}{\lambda}\right)^2 \tag{4.31}$$

from which the number of floats in the model may be determined when the float diameter scale is found from Equation (4.20). Equations (4.30) and (4.31) may also be used for sinkers.

4.6 Modeling of Doors

The major dimensions of the door such as length and weight should be reduced by the basic length scale λ. Sometimes it is not possible to reduce the thickness of the boards exactly to a scale of λ. In such cases, the thickness of the shoe in the door should be chosen to satisfy the weight scale ratio given by Equation (3.27).

The bracing and its connection arrangement should be modeled properly to the length scale. Care should be taken that the center of gravity of the model door is in correspondence with the center of gravity of the prototype door.

The model laws developed in the preceding discussion are verified by force and stress measurements, by observation of model behavior in the flume, and by comparison with measurements and observations from divers in the ocean of the corresponding prototype trawl.

CHAPTER 5

PROTOTYPE FIELD TESTS

5.1 Parameters Measured

When embarking on the verification of any hydrodynamic model law, it is necessary to decide what parameters should be measured and compared in the field and in the model experiments. These parameters should be representative of the functional behavior of the model system. Two major parameters representing the geometry of the net are, in this case, the vertical opening and the horizontal spread of the net and doors. In general, the greater the vertical opening means the smaller the horizontal spread. In some cases, a large horizontal spread is desired to cover more fishing ground for such species as lobster, flounder and shrimp. In other cases, a large opening may be required to catch higher swimming fish such as butterfish.

Another important parameter is the total drag acting on the gear. Drag increases as the towing velocity of the net increases. It consists of: (1) drag due to the net (hydrodynamic), (2) drag due to the doors (hydrodynamic and bottom friction and (3) drag due to towing cables (hydrodynamic). The magnitude of the total drag may be measured as the tensile force in the towing cable.

Also, in order to evaluate the distribution of load from the net to the footrope and headrope, it is necessary to measure the load in these ropes at strategic points. It is also desirable to observe the load in the twine itself so that an idea of the magnitude of stresses and strains in the twine may be obtained.

The relative velocities of the vessel with respect to the water and the bottom are important parameters because the behavior of the net depends on the speed at which it is being dragged. Because of currents caused by wind or tidal action, the speed, relative to the water, may not be equal to the speed of vessel and net with respect to the ocean bottom. It is, therefore, necessary to conduct the field experiments in such a way that the influence of this speed discrepancy is eliminated.

5.2 Net and Towing Site

The basic net chosen for the test was manufactured by the Burbank Net Shop, Fernandina Beach, Florida. This is a trawl widely used by the Florida shrimp fleet. This net was towed by the twin trawler Captain Gene, belonging to the University of Georgia Marine Extension Center. The specifications of the net are given in Table 5.1. The corresponding net and door diagram are shown in Figures 5.1 and 5.2, respectively. Because of the clearness of the water near Shell Island in the Gulf of Mexico, the towing site was done in that area (Fig. 5.3).

TABLE 5.1

SPECIFICATIONS OF BURBANK FLAT NET

Item	Dimension	Material	Remarks
Hanging line	1/2" diameter	Stainless steel combination net rope	Hang 3 meshes on 4-1/4 " ties. Double selvedge all hanging meshes
Hanging twine	# 36 thread	Spun-tex	--
Brail line	5/16" diameter	--	5 meshes on 4" ties
Chains	10 loops of 1/4" diameter	Galvanized steel chain	--
	10 loops of 3/16" diameter		--
Doors	7' × 3' (see Fig. 5.2)	# 1, C pine	with 3/8" chain total weight = 528 lbs
Towing warp	1/2" diameter	Steel wire	Length = 300'
Floats	0.431 lbs and 137.30 $inch^3$ volume	Foam	Ellipsoid in shape, 21 numbers

5.3 Instrumentation

The locations of the instrumentation needed to measure the previously discussed parameters are shown in Figure 5.4. Description of the instruments used in the field study are given in the following paragraphs.

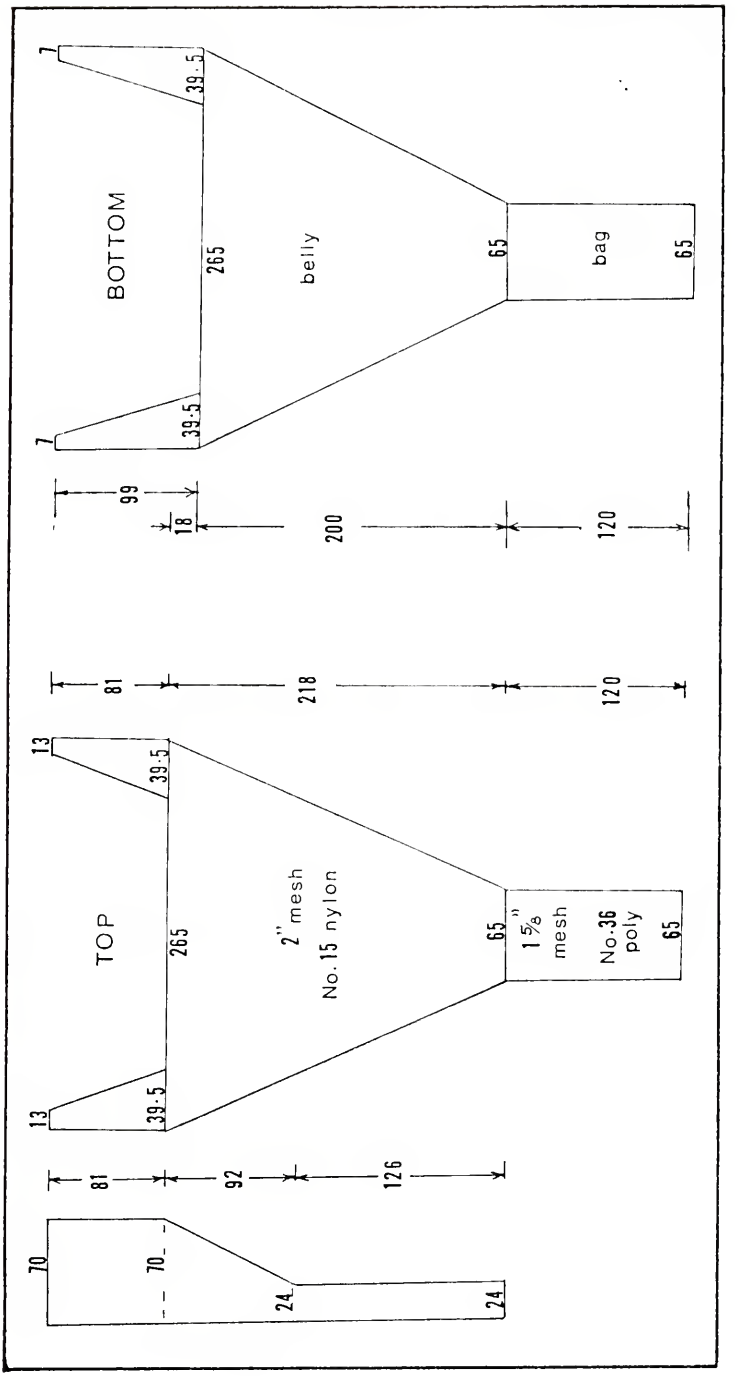

Figure 5.1. Net diagram of Burbank flat net.

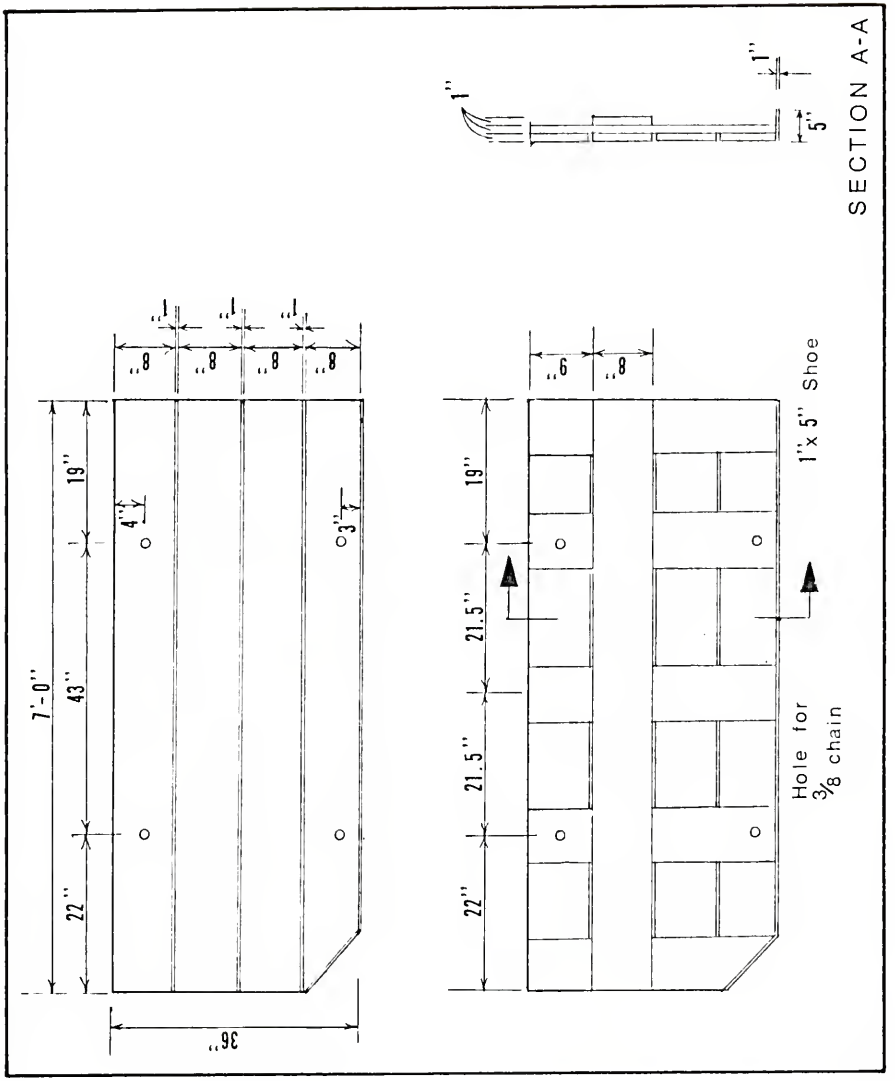

Figure 5.2. Dimensions of door.

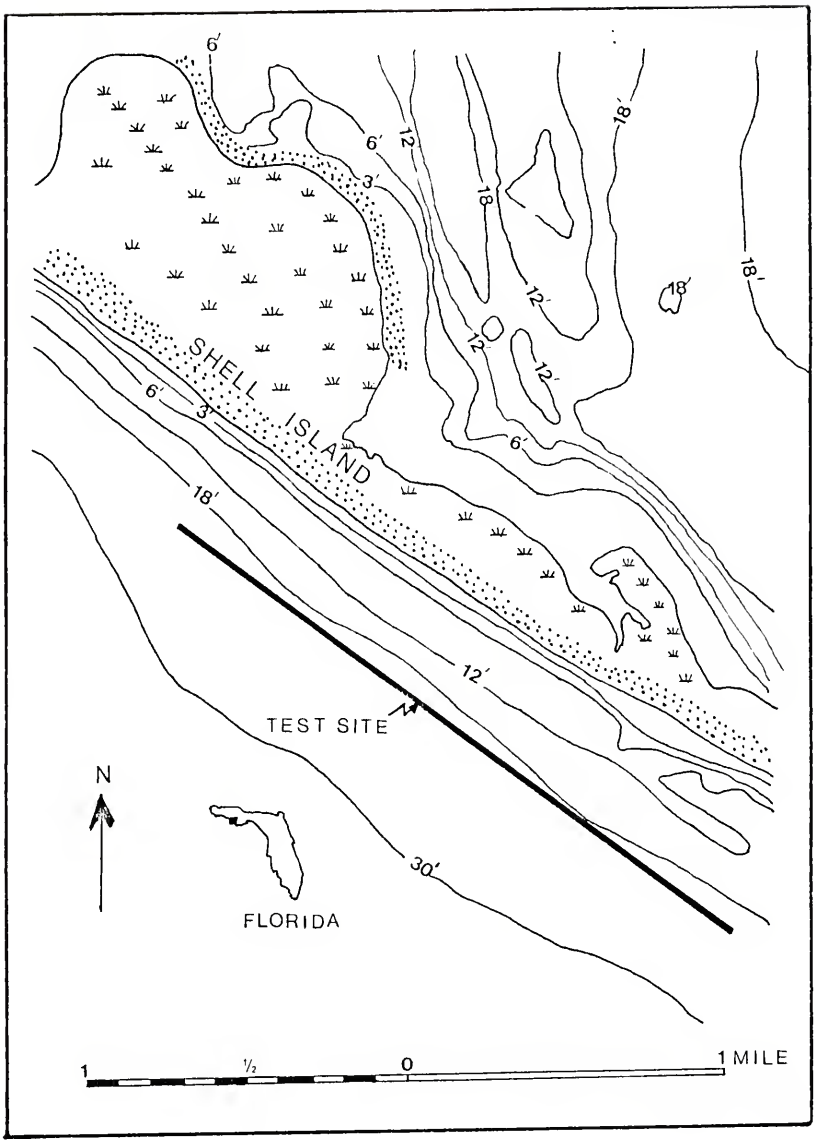

Figure 5.3. Site of prototype field study.

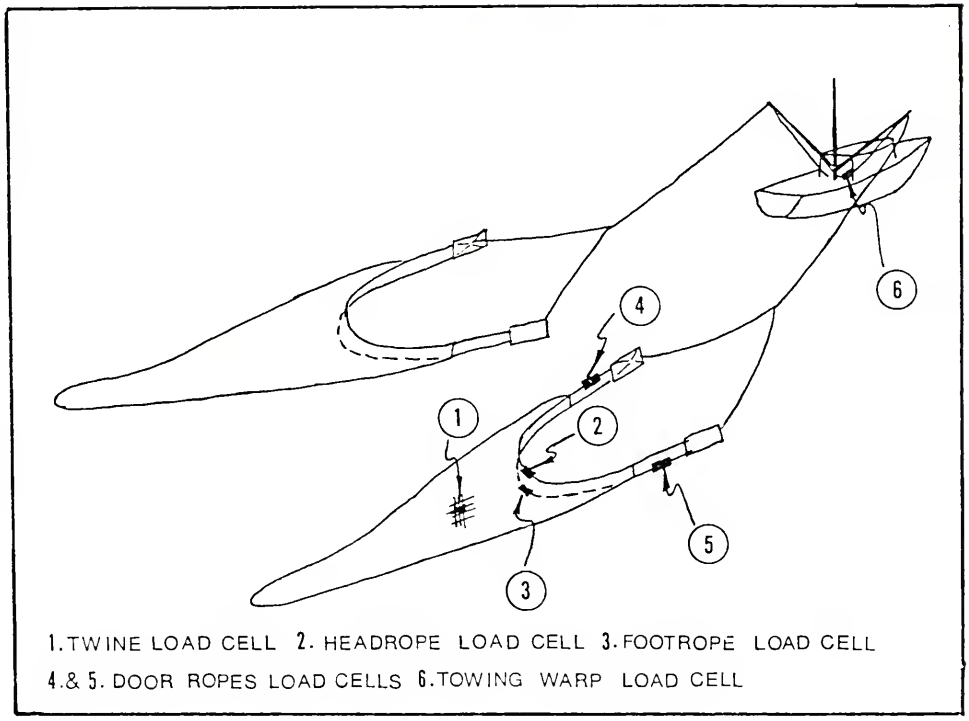

Figure 5.4. Instrumentation of prototype net.

5.3.1 Warp Tension Measurement

The tension in the towing cables (warps) was measured by a strain gage embedded in a steel bolt. The maximum capacity of the load that could be measured by this bolt was 20 tons. A strain indicator with two channels of input and output (for strip recording) was built and calibrated up to 3 tons by means of static loading. This bolt was attached to the rail block on one end and clamped to the towing cable between the rail block and the towing block on the other end (Fig. 5.5).

As the net is being dragged through the water, eddies created by the turbulent flow of water around the towing cables and doors induce vibrations in the cable. Since it is the time-mean values of the observed parameters which are of interest, it is desirable to record continuously the load in the cables in a strip chart recorder. The recorder used was a Hewlett-Packard Strip Chart Recorder Model 7100B. It has two channels and two independent pen drives. The speed of the chart may be varied in twelve steps ranging from 1 in/hr to 2 in/sec. Figure 5.6 shows the bolt, the attachments and the recorder.

Ideally, the tension in both the warps towing the two doors should be measured. However, since the vessel used was a twin-type trawler, attempts to tow only one net with each warp on starboard and port side of the vessel created navigational problems. Therefore, the tension was measured in

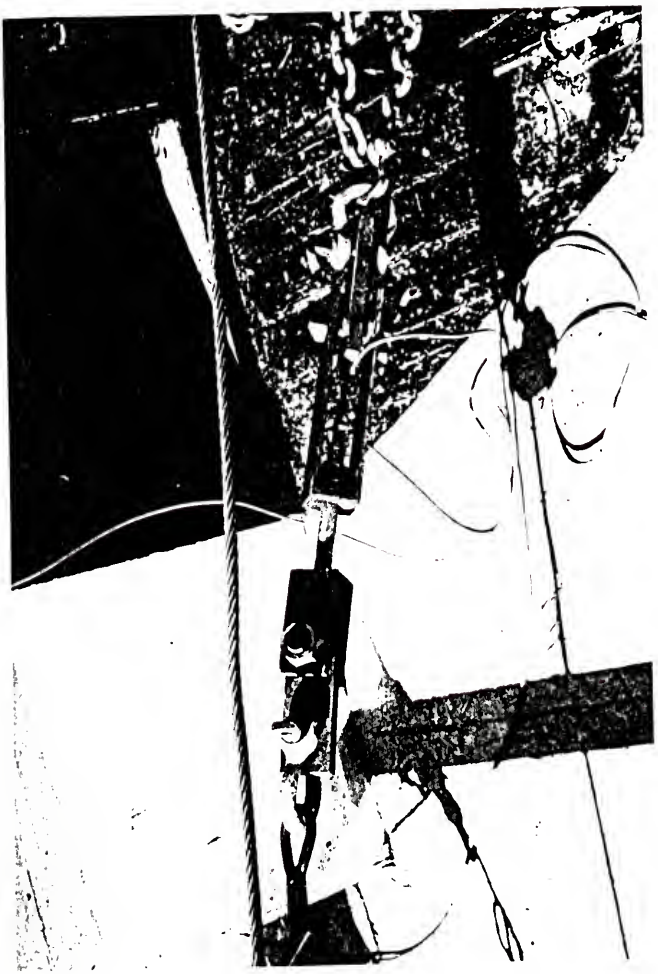

Figure 5.5. Attachment of bolt to the cable.

only one combined cable of the two warps as shown in Figure 5.4.

5.3.2 Underwater Load Cell

Two types of load cells were used underwater, one with a 0-1500-lb range and the other with a 0-2400-lb range. The load cells are battery powered and waterproofed. Each cell is housed in aluminum tube canisters, sealed by o-rings, and with a hook on each side for attachment. This load cell has a Rustrak recorder. The chart speed is slow enough to use this load cell for more than 3 hours without reloading. A view of the load cell with its power source and recorder is shown in Figure 5.7.

Two, 1500-lb load cells were attached to the footrope and headrope at the midsection of the rope (Fig. 5.8). One, 2400-lb load cell was installed between the top of one door and the headrope by means of shackles. The other 2400-lb load cell was attached to the bottom end of the other door and the footrope. These locations are shown in Figure 5.4. Figure 5.9 shows the connection of the load cells to the doors.

5.3.3 Twine Load Cells

The twine load cell is a very small diameter, thin walled tube. The tube is slipped over the twine and bonded to it by a special high-temperature adhesive (epoxy). The dimensions of the load cell are small enough to permit installing one into a bar of the prototype mesh (Fig. 5.10).

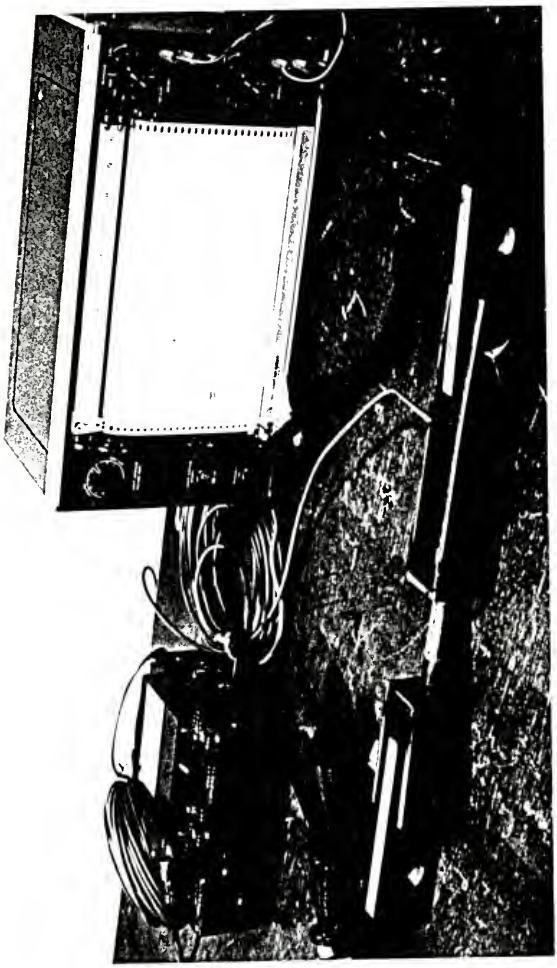

Figure 5.6. Bolt load cell, its attachments and the recorder.

Figure 5.7. Underwater load cell.

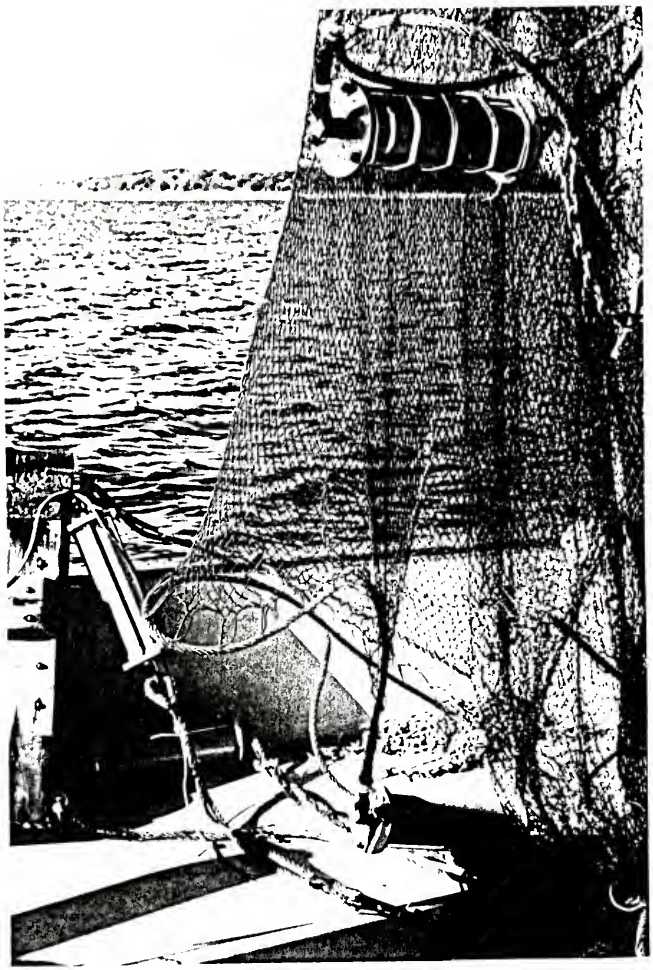

Figure 5.8. Attachment of underwater load cell to the footrope and headrope.

Figure 5.9. Attachment of underwater load cell to the door.

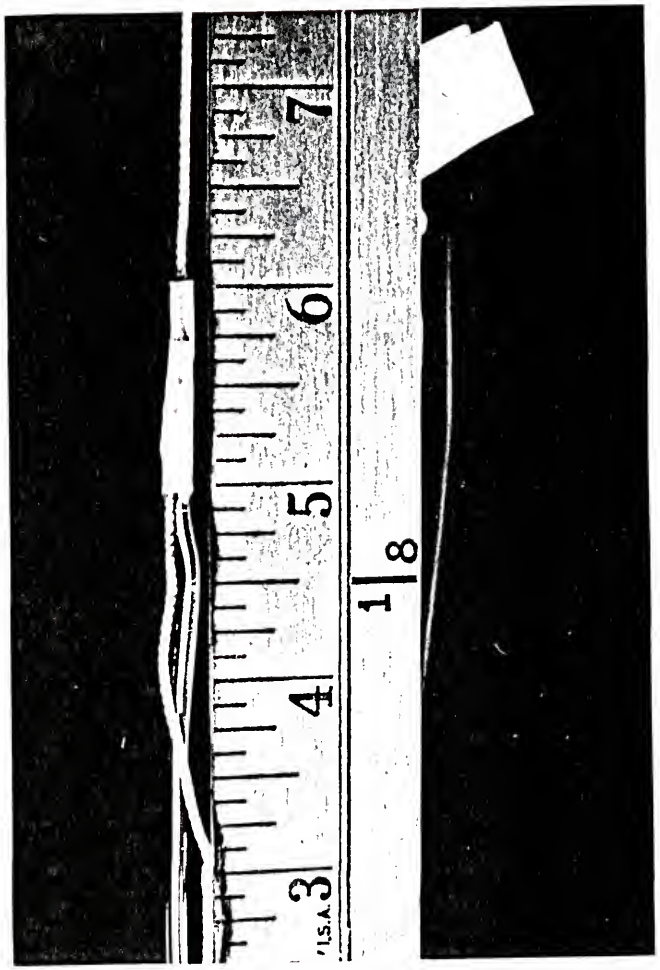

Figure 5.10. Twine load cell.

Three sizes of this type of load cells are available; 2-lb range, 10-lb range and 20-lb range. Two-lb range load cells were used. Four load cells of this type formed four meshes (Fig. 5.11).

The leads from these load cells were connected to the terminals of a multichannel cable. These connections were waterproofed. The multichannel cable was, in turn, attached to a nylon rope to avoid damage to the cable during towing. The other end of the cable was connected to a channel selector switch placed on the vessel. The load could be read from a calibrated strain indicator meter. These instruments are shown in Figure 5.12.

5.3.4 Trawler Speed

The trawler speed was measured in three different manners. In the first method, a Lionel Taffrail Log was used. This log gives the distance traveled in nautical miles and from the time taken to travel that distance, the trawler's speed with respect to the water was calculated. In the other two methods, propeller meters were used. One propeller meter was the conventional precision Ott micro-current meter widely used in the laboratory. The other propeller meter was the more crude direct reading field type manufactured by General Oceanics (Model 2030).

In each run, velocity measurements were taken while the trawler was traveling with and against the current. The average of these two velocity measurements would give

Figure 5.11. Twine load cells in the net.

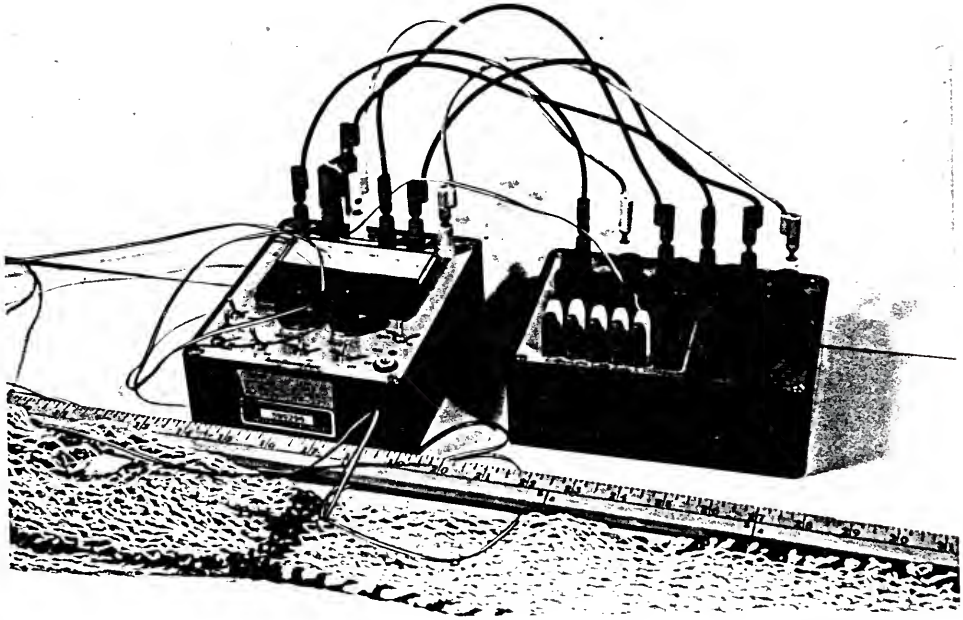

Figure 5.12. Channel selector switch and strain indicator for the twine load cells.

the velocity of the trawler thereby, eliminating the influence of the current with respect to the ocean bottom. This is, of course, only correct when it is assumed that the current, with respect to the ocean bottom, does not change during the two runs. Due to the short time needed for making the two runs, this assumption must be considered valid, in this case.

5.3.5 Net Dimensions

The vertical opening and the horizontal spread of the net were measured by divers by means of a nylon line held between the doors and between the footrope and headrope. This method proved successful at low speeds but was impractical at higher speeds because of difficulties in positioning the diving sled at these speeds.

Two buoys were attached to the doors. The horizontal distance between these buoys, measured during trawling, represents the horizontal opening of the net. The location of each float was determined by triangulation from the deck.

In order to observe the net profile, a 14-ft boat equipped with an echo sounder (Benmar), traveled over the net taking soundings. The difference in the readings between the ocean bottom and the top of the net would then give the vertical opening of the net.

5.4 Test Procedure

A course line was set parallel to the beach by means of three buoys. The distance between the end buoys was

determined by triangulation from the beach. The net was towed in a straight line defined by these buoys in all runs. The distance between the outer buoys was found to be 2.4 miles.

Two series of tests were conducted. In the first series, the net was not fitted with floats on the headline except for one attached above the load cell to compensate for the weight of this instrument. In the second series of the test, twenty-one floats were attached to the headline. Each series of tests consisted of three runs. In each run, the net was towed at a constant velocity or speed of the vessel with respect to the water obtained by a fixed engine rps). The rpm chosen for the runs were 1100, 1300 and 1500.

The vessel was set along the course line defined by the buoys. Time was noted at the beginning and end of each run. During the run, angle measurements were taken from two points of the deck to the floats attached to the doors. The net profile was observed by the echo sounder on the small boat which was riding at the top of the net. The readings of the ship log, Ott meter, and the other propeller meter were taken. The output from the bolt load cell attached to the towing cables was recorded automatically on the recorder. The time of start and finish of each run were marked on the chart paper.

Difficulties were encountered with the twine load-cell readings. It was suspected that the electric system of the trawler's engine interacted with the electronic

systems of this strain indicator. Therefore, reliable readings from these load cells could not be taken.

The length of warp set out in each run remained a constant 300 ft. And, at the end of each series, the weight of catch was estimated to be 100 lb. Underwater pictures and movies were taken by the divers. At the end of each series, the chart papers were taken out from the underwater load cells and the start and end of each run were marked on the chart paper.

During each run, the following parameters were measured: (1) the speed of the vessel, (2) the total drag on the towing cable, (3) the drag due to the net alone, (4) the force in the footrope, (5) the force in the headrope, (6) the vertical opening of the net and (7) the horizontal spread of the net. Furthermore, the general shape of the net was observed by the divers and recorded on 16 mm color film.

5.5 Test Results

Table 5.2 summarizes the results of Series 1 and Series 2. The velocity of the trawler was used to compute the Reynolds number, R_{eD}, of the flow around the twines of the fish net. By definition,

$$R_{eD} = \frac{VD}{\nu} \tag{5.1}$$

where

TABLE 5.2

RESULTS OF FIELD TESTS

Quantity	Headrope Without Floats			Headrope With Floats		
Run number	1	2	3	4	5	6
Engine (rpm)	1100	1300	1500	1100	1300	1500
Velocity (fps)	2.75	3.59	3.74	2.41	3.06	3.69
Door spread (ft)	26.66	27.73	28.80	23.00	25.00	27.00
Mouth opening (ft)	4.50	3.50	2.50	12.58	10.33	8.08
Warp tensile force (lb)	795	1266	1488	968	1361	1785
Force in ropes—Top between door and net (lb)	100	150	250	100	225	350
Bottom	125	250	400	200	325	450
Force in footrope at center (lb)	30	30	30	60	60	60
Force in headrope at center (lb)	10	20	20	10	10	10
Reynolds number	1217	1589	1655	1066	1354	1633

V = Velocity of trawler

D = Diameter of twine

ν = Kinematic viscosity of seawater at 65°F

The values of the coefficient of drag for the net panel corresponding to these Reynolds numbers were found in Figure 2.9 (Fridman,1973) and they were all equal to 1.3

indicating that the flow was in the turbulent range before the boundary layer transition from laminar to turbulent.

The magnitude of warp tension was plotted against the speed of the trawler (Fig. 5.13). The relationship between the warp tension and the speed of the ship was found to be:

$$T_1 = 282\ V^{1.414} \quad \text{with floats} \tag{5.2}$$

$$T_1 = 118\ V^{1.908} \quad \text{without floats} \tag{5.3}$$

where

T_1 = Warp tension in lb

V = Speed of trawler in fps

From Equations (5.2) and (5.3), it can be seen that drag increases as the velocity of the trawler increases. However, for a given engine rpm, the speed of the trawler decreases as the drag is increased by attaching additional floats to the net. Also, Table 5.2 shows that the headline height reduces as the wingspread increases.

These observations will be compared with the data obtained from the model testing.

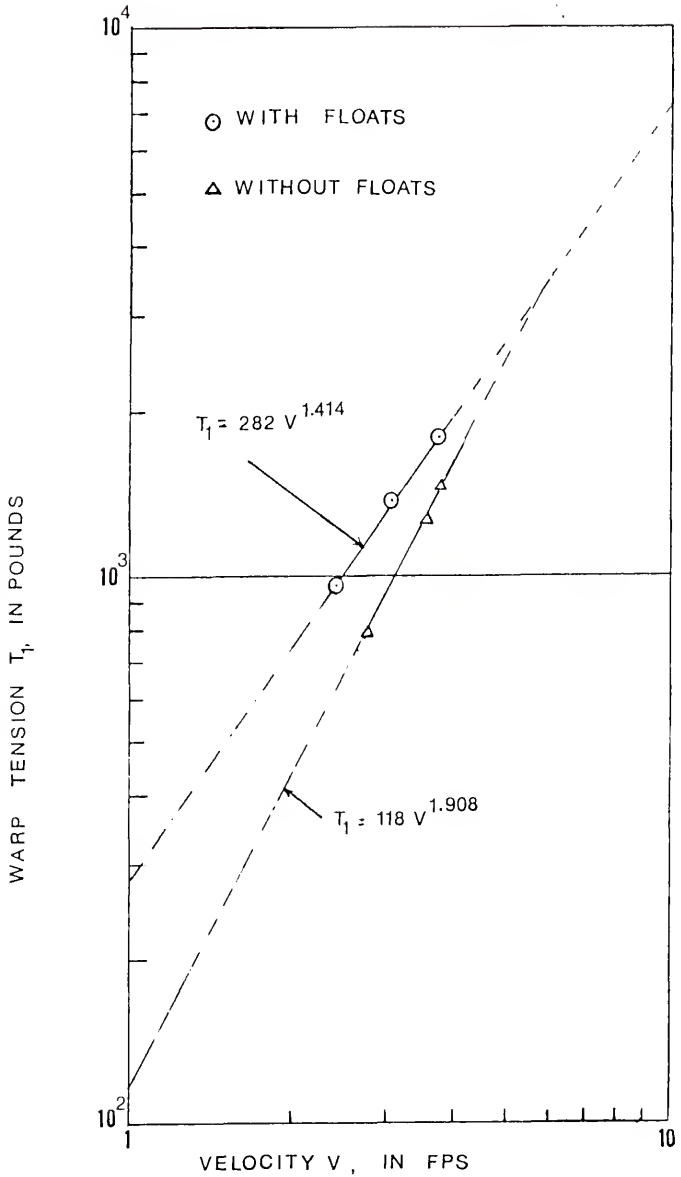

Figure 5.13. Relationship between warp tension and trawler speed.

CHAPTER 6

MODEL EXPERIMENTS

6.1 Selection of Scale Ratios

6.1.1 Model Net

The prototype net is made of nylon twine of diameter $D_p = 0.06$ in and with a 2 in stretched mesh (M_p). A suitable model twine and mesh corresponding to this prototype are commercially available and satisfy Equation (4.14), $(\lambda_D = \lambda_M)$. Ace Net Company in Wisconsin manufactures cotton webbing with 1 in stretched mesh (M_m) and with a No. 9 cotton twine which has a diameter of 0.03 in (D_m). This twine was chosen as the model twine, and the twine diameter and mesh scale ratios are:

$$\lambda_M = \lambda_D = 2 \tag{6.1}$$

The basic length scale λ can now be calculated from Equation (4.22).

$$\lambda = \sqrt{\frac{A_p}{A_m} \cdot \frac{\rho_m}{\rho_p} \cdot \lambda_M}$$

if the elastic constants of the model and prototype materials A_m and A_p are known. To find these constants, the stress-

strain curves of the materials should be known. These curves were obtained by testing the twines in a Tinius Olsen Tension Testing Machine (Fig. 6.1). During testing, it was noted that if the twine was secured between two grips (normal procedure), there is a substantial bend in the twine. When subjected to the tensile force, this bend causes stress concentration in the grips and gives unreliable results. Therefore, a special set of grips was designed to eliminate this difficulty (Fig. 6.2). The length of the twine was fixed at 12 in. The twine was soaked in water for 24 hours before testing. Using a strain rate of 0.8 percent per second, the twine was tested until the breaking point. The testing procedure conforms to the standard procedure for testing twines as outlined by von Brandt and Carrothers (1964).

The stress and strain of the twines were plotted in a logarithmic paper and straight lines were fitted by method of least squares (Fig. 6.3). The stress-strain relationship is expressed by:

$$\sigma_p = 99000\ \varepsilon^{0.9} \tag{6.2}$$

$$\sigma_m = 840\ \varepsilon^{0.9} \tag{6.3}$$

from which

$$A_p = 99000$$

and

$$A_m = 840 \tag{6.4}$$

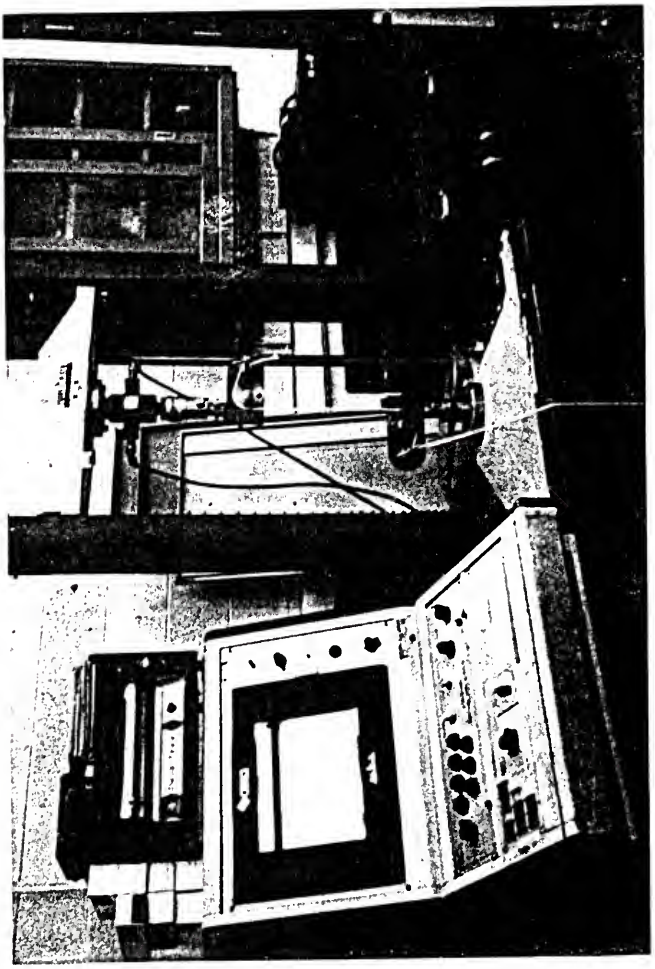

Figure 6.1. Tension testing of twines.

Figure 6.2. Grip for testing of twines.

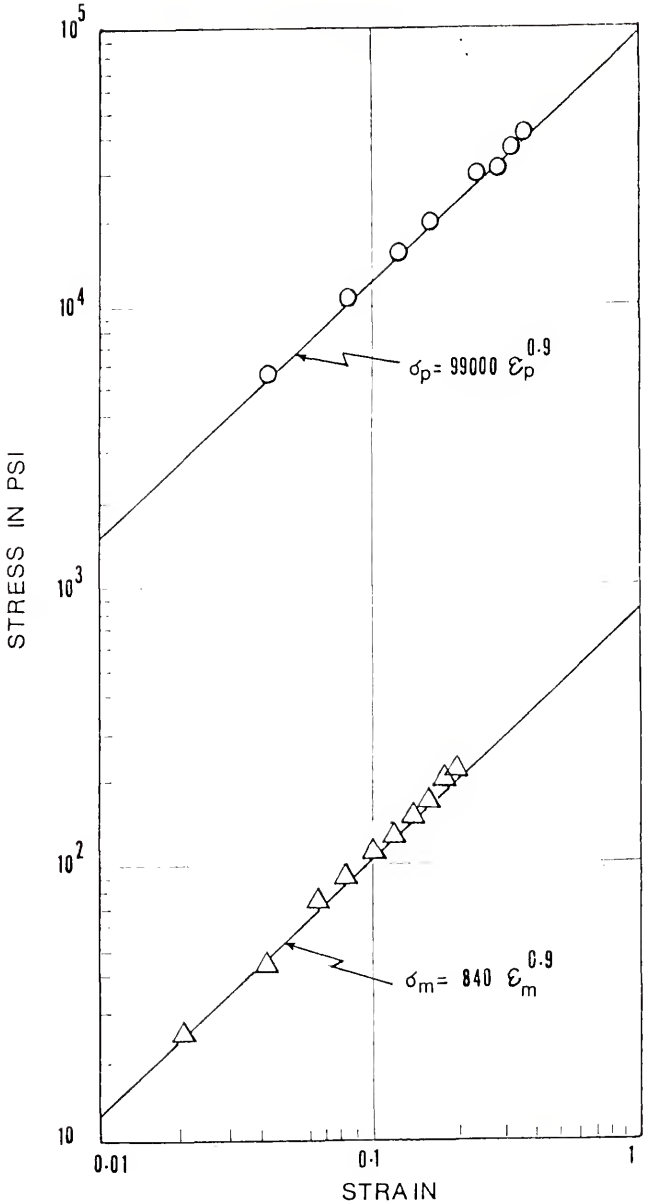

Figure 6.3. Elastic characteristics of twines.

By substituting the values of the density for the seawater at 65°F and for the freshwater at 81°F, the basic length scale λ is obtained:

$$\lambda = \sqrt{\frac{99000}{840} \cdot \left(\frac{1.933}{1.989}\right) \cdot 2} = 15.2 \qquad (6.5)$$

The flume can easily accommodate a model net built to this length scale. With this length scale ratio, the scale for the number of meshes in the net becomes:

$$\eta = \frac{\lambda}{\lambda_D} = 7.6 \qquad (6.6)$$

Therefore, all meshes in the prototype net should be divided by η to obtain the model net meshes. The model net corresponding to the field net (Fig. 5.1) is illustrated in Figure 6.4.

6.1.2 Float Scale

The floats used in the field tests are ellipsoid in shape. The weight and volume of each float are 0.431 lb and 137 in^3, respectively. The commercial market does not offer model floats of the same shape and density; however, spherical cork floats are readily available in different sizes. The specific weight of these cork floats is 12.36 lb/ft^3. Therefore, the float scale λ_E is found from Equation (4.30).

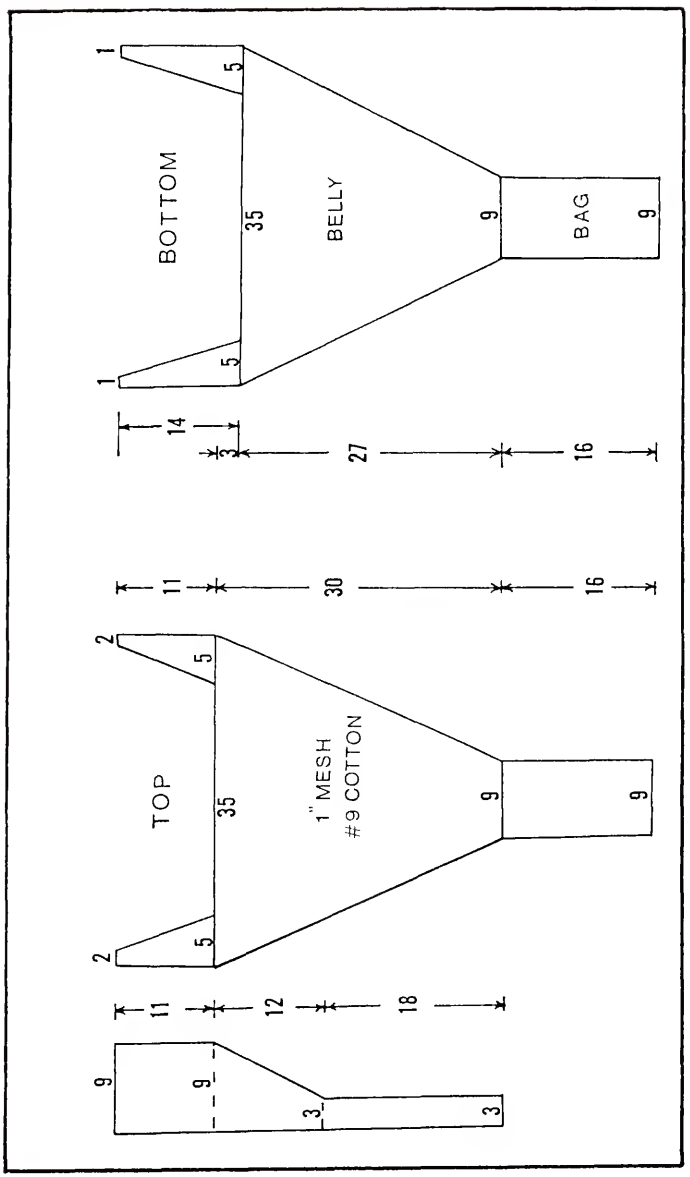

Figure 6.4. Model net diagram.

$$\lambda_E = \frac{\frac{\gamma'_{s\cdot m}}{\gamma_m} - 1}{\frac{\gamma'_{s\cdot p}}{\gamma_m} - 1} \cdot \lambda = \frac{\left(\frac{12.36}{62.4}\right) - 1}{\left(\frac{5.42}{64}\right) - 1} \cdot (15.2) = 13.31 \tag{6.7}$$

An equivalent diameter of spherical float which has the same value of the ellipsoid float is calculated from the expression:

$$\text{volume} = \frac{\pi E_p^3}{6} = 137.3$$

from which

$$E_p = 6.4 \text{ in} \tag{6.8}$$

It is shown here that the buoyancy which is proportional to E^3, which is predominant in this case when compared to the drag force is, of course, proportional to E^2. From Equations (6.7) and (6.8), the diameter of the model float E_m, is computed:

$$E_m = 0.481 \text{ in}$$

Using a commercially available float, the number of floats in the model is determined from Equation (4.31).

$$n_m = n_p \left(\frac{\lambda_E}{\lambda}\right)^2 = 21 \left(\frac{12.8}{15.2}\right)^2$$

$$n_m = 14.89 \tag{6.9}$$

Therefore, the number of model floats is 15.

The weight of sinkers attached in the footrope is obtained from the weight scale given by Equation (3.27):

$$\kappa_{gravity} = \frac{\rho_p}{\rho_m} \cdot \lambda^3 = 3613.5 \qquad (6.10)$$

Therefore, the weight of sinkers in the model is equal to the weight of sinkers in the prototype divided by $\kappa_{gravity}$, that is $= \frac{(13.8)(16)}{(3613.5)} = 0.06$ oz.

6.1.3 Rope Scale

From the field tests, it is seen that the predominant force in the rope is the tension. Therefore, the model rope size should be determined taking the elastic deformation into consideration. Tension tests were made with the prototype and model ropes. The stress-strain relationship of the materials are (Fig. 6.5):

$$\sigma_p = (2.4)(10^5)\ \varepsilon_p \qquad (6.11)$$

and

$$\sigma_m = 1000\ \varepsilon_m \qquad (6.12)$$

From Equations (4.26), (6.11) and (6.12), the scale for rope diameter is:

$$\frac{H_p}{H_m} = \sqrt{\frac{\rho_p}{\rho_m} \cdot \frac{A_m}{A_p}} \cdot \lambda^{3/2} = 3.88 \qquad (6.13)$$

Therefore, the diameter of the model cotton rope is:

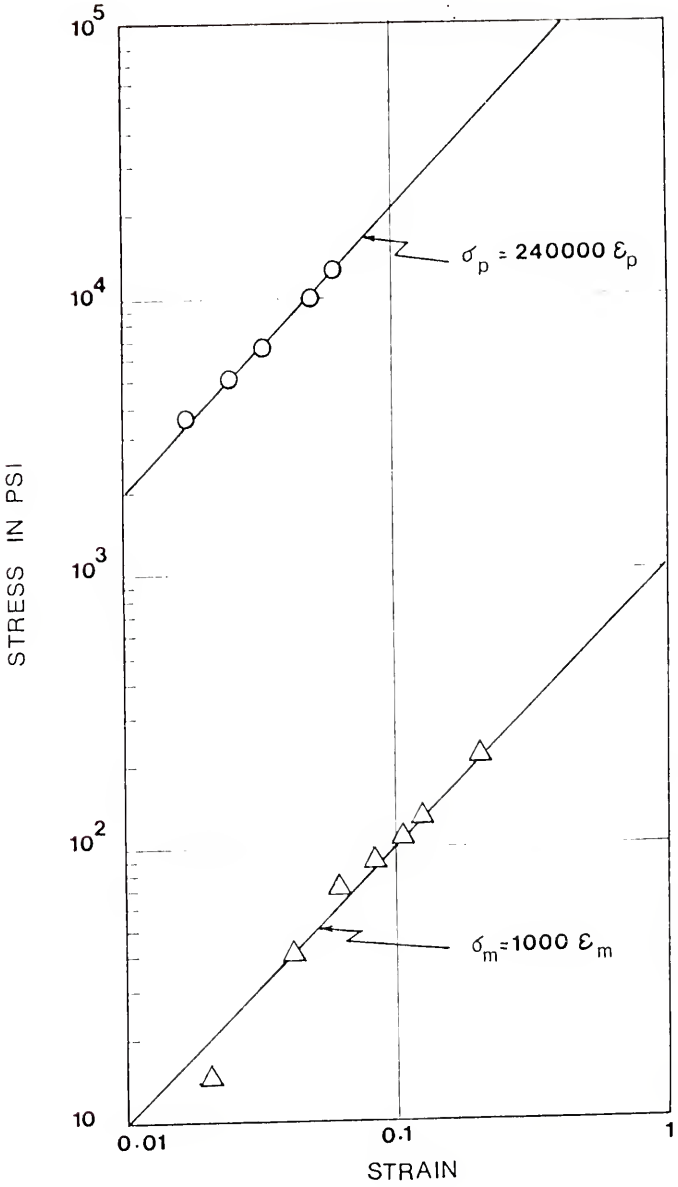

Figure 6.5. Elastic characteristics of ropes.

$$H_m = \frac{H_p}{\frac{H_p}{H_m}} = \frac{0.50}{3.88} = 0.129 \text{ in} \qquad (6.14)$$

The model net is hung on 0.125 in cotton rope.

In the towing warp, the strain is negligible because this rope is a steel rope with a very high modulus of elasticity compared to normal nonmetallic ropes. Therefore, in this case, normal scaling (λ scale) is used.

6.1.4 Model Door

The dimensions of the model door are obtained from the basic length-scale ratio. The weights of the shoe and the door are computed from the gravity force ratio. The bracings for the doors are hooked in accordance with the bracings of the prototype. The center of gravity of the model door must also be modeled correctly. The dimensions of the model door are given in Figure 6.6 and Figure 6.7 gives a general view of the door.

All scale ratios derived from the model law are summarized in Table 6.1. The model net is built to this specification and is shown in Figure 6.8

6.2 Instrumentation of Model Net

The tensile load in the model trawl was measured at different locations by small range load cells. These locations correspond to the locations in the trawl in the field tests (Fig. 5.4). The ranges of the underwater load

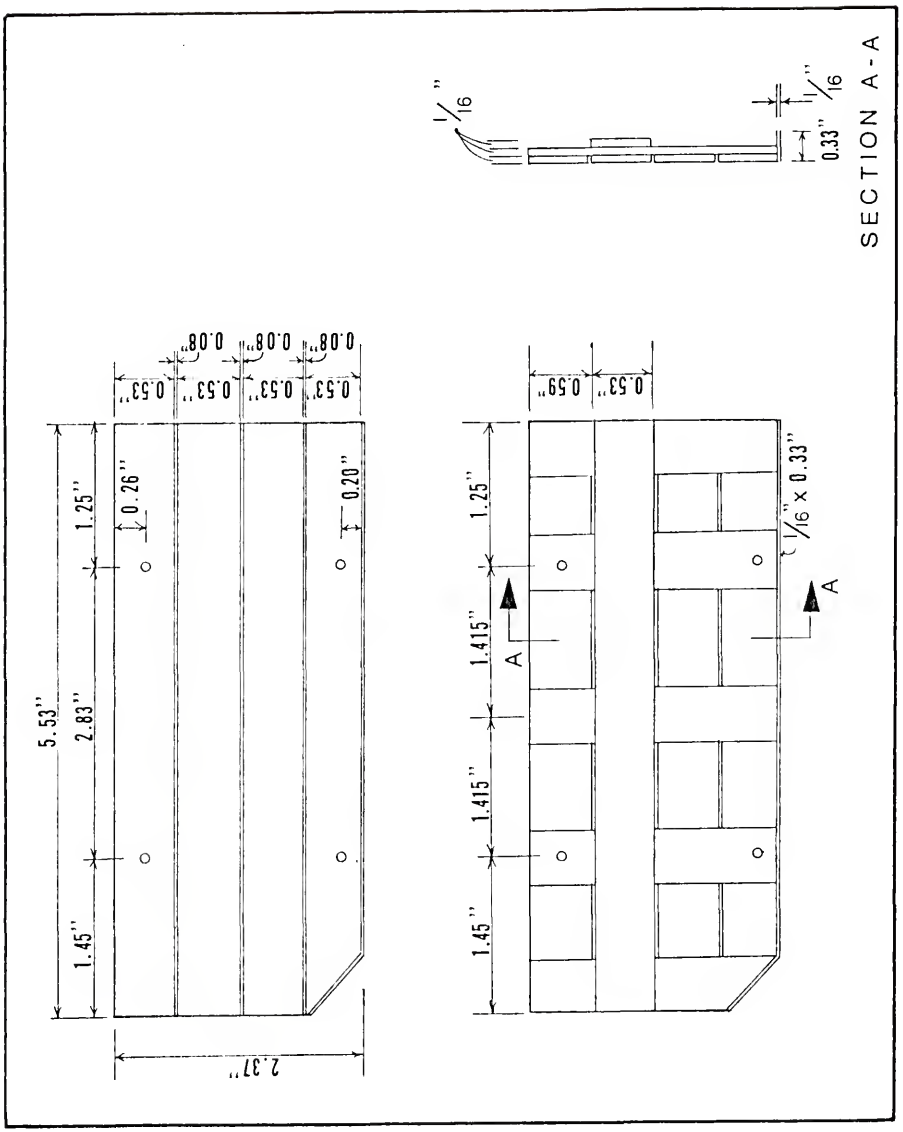

Figure 6.6. Dimensions of model door.

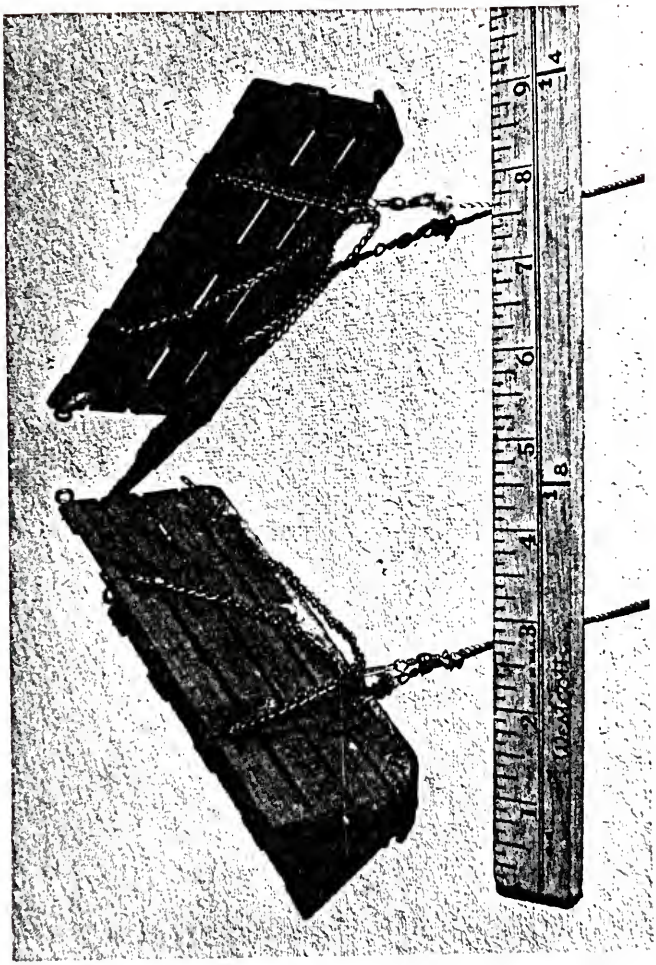

Figure 6.7. Model doors.

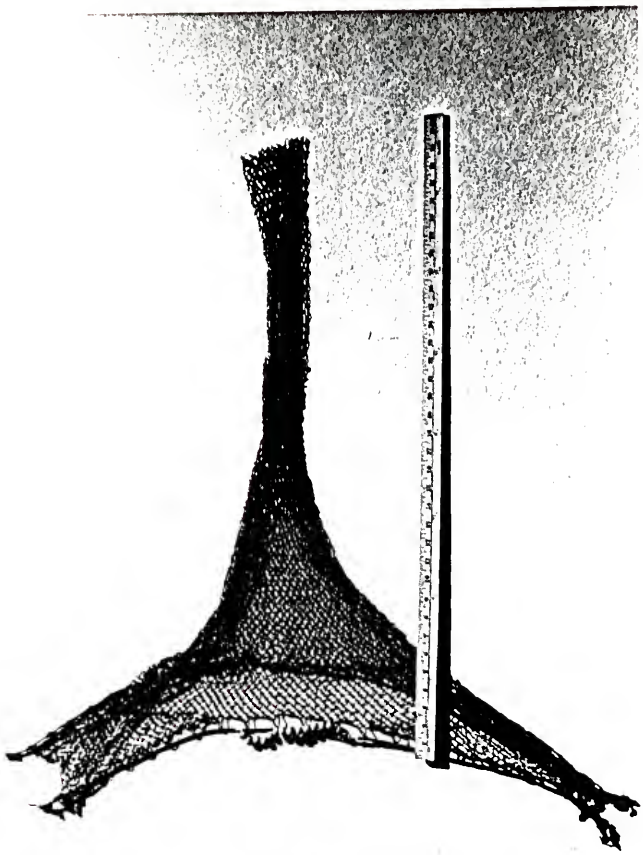

Figure 6.8. Model net.

TABLE 6.1

SUMMARY OF SCALE RATIO

Quantity	Value
Mesh bar and twine diameter	2
Linear length	15.2
Number of mesh	7.6
Float diameter	12.8
Rope diameter	4
Warp diameter	15.2
Weight ratio	3613.5

cells are 0-300 and 0-5 grams. The tension in the towing warp was measured by the 300-gram range load cell. This load cell was attached to the warp by means of a swivel arrangement (Fig. 6.9). The same load cell was also used to measure the tension in the rope between the net and the door (Fig. 6.10).

To measure the tension in the midsection of the head- and footrope, a small portion of the rope was cut and the 5-gram load cell was attached in its place. Because of the small dimensions of the load cell, its influence on the drag measurement is small. Figure 6.11 shows the load cell attached at the midsection of the headrope. A strip-chart recorder was used to record continuously all readings in the rope.

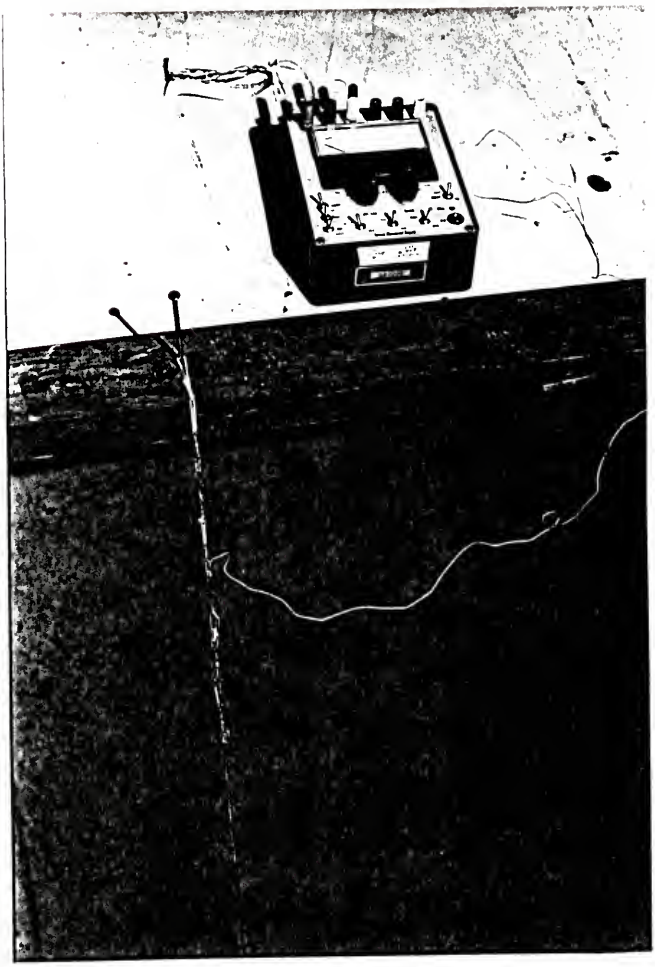

Figure 6.9. Load cell to measure warp tensile force.

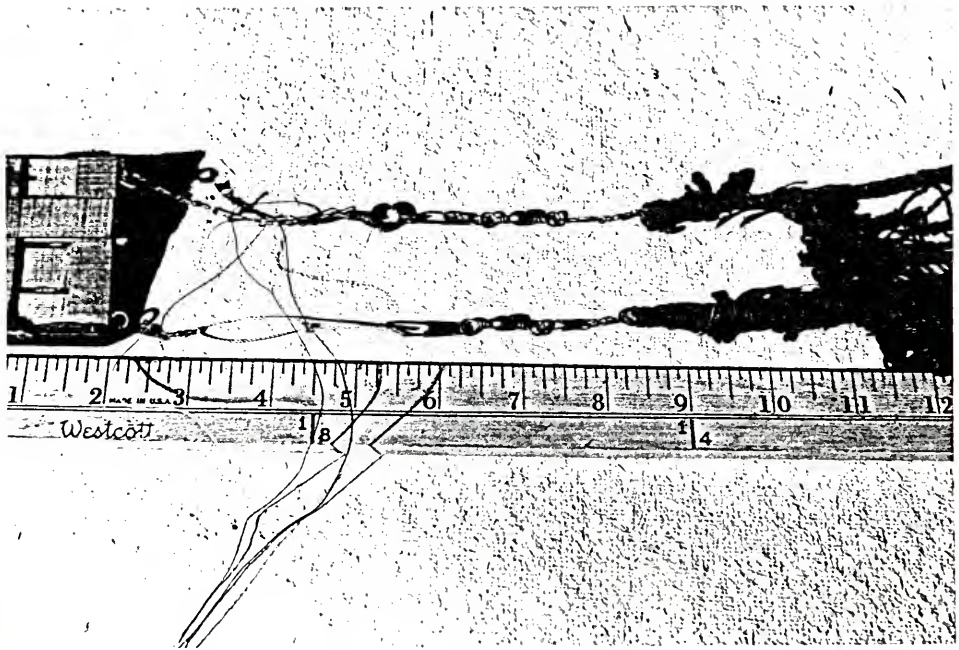

Figure 6.10. Load cell to measure the tensile force in the rope between door and net.

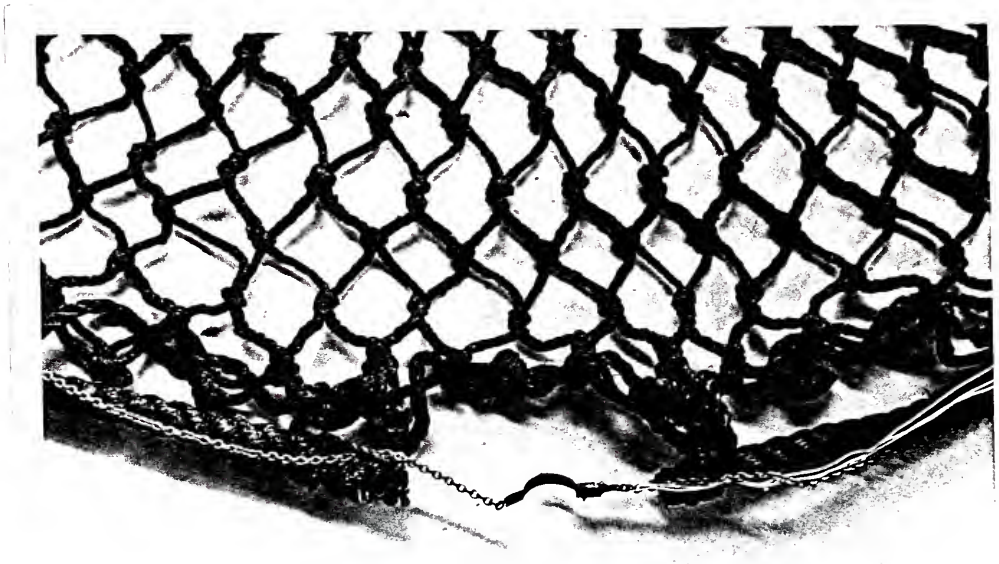

Figure 6.11. Load cell to measure tensile force of the midsection of headrope.

6.3 Description of Experimental Apparatus

6.3.1 Flume

The model tests were conducted in a recirculating hydraulic flume. The flume consists of two portions: the main flume which is 120 ft long and a return flume of 140 ft length. The main flume is 8 ft wide and 2.5 ft deep. The width and depth of the return flume are 4 ft and 3.5 ft, respectively. The depth of water in the flume can be controlled by a gate (Fig. 6.12) at the downstream end of the main flume. The gate can be raised or lowered by an electrically operated gear motor.

Water is pumped from a storage tank to the main flume by a 70 hp and 12-ft head pump. The pumping capacity is from 0 to 40 cfs and the flow is regulated by a 30-in gate valve and a 20-in bypass gate valve. Figure 6.13 shows the view of the storage tank, the pump and the bypass pipe. Flow from the pump is determined by a calibrated Poncelet weir. The head on this weir and the discharge are related by the curve shown in Figure 6.14. The head on the weir is measured by electric point gauges as shown in Figure 6.15. The flow passes through a series of honeycomb structured baffles which dissipate the energy uniformly. By a combination of wooden strips placed in front of the baffles, a uniform velocity distribution across the width of the main flume can be obtained. The baffles and the weir are shown in Figure 6.16.

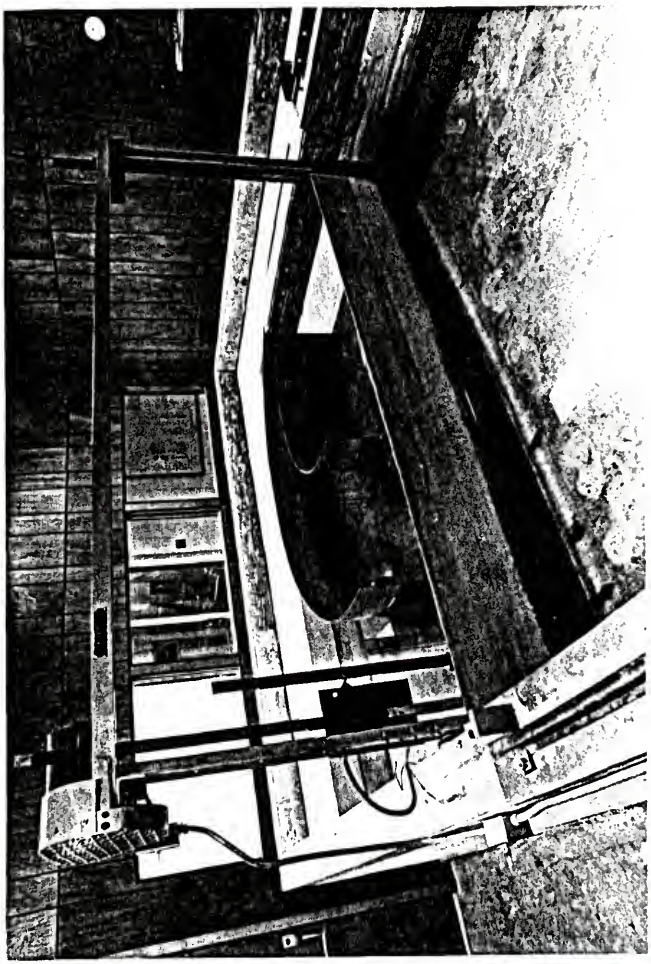

Figure 6.12. Gate, main and return flumes.

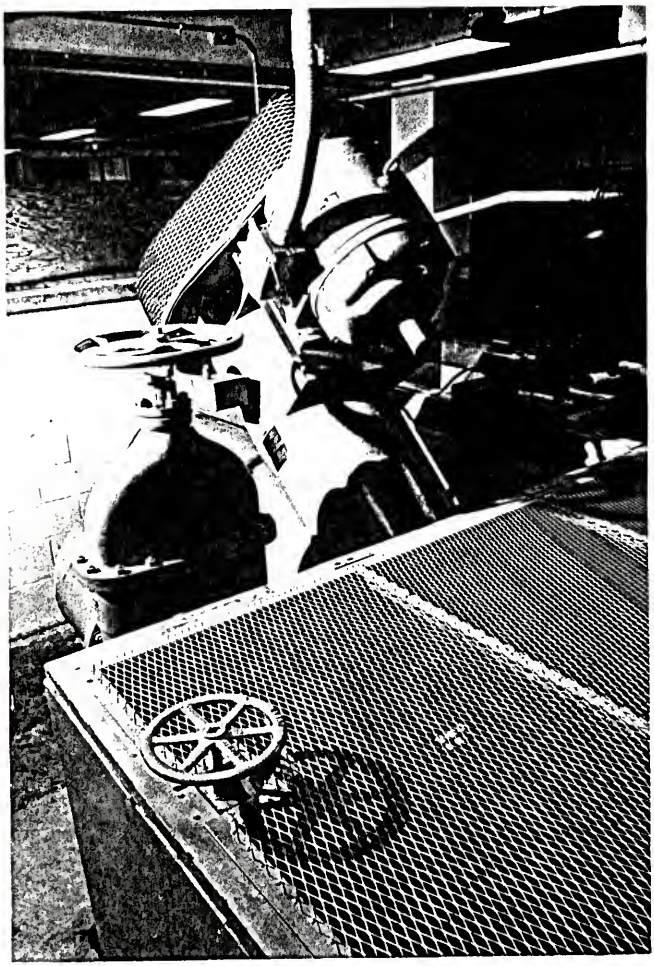

Figure 6.13. Storage tank, pump and bypass pipe.

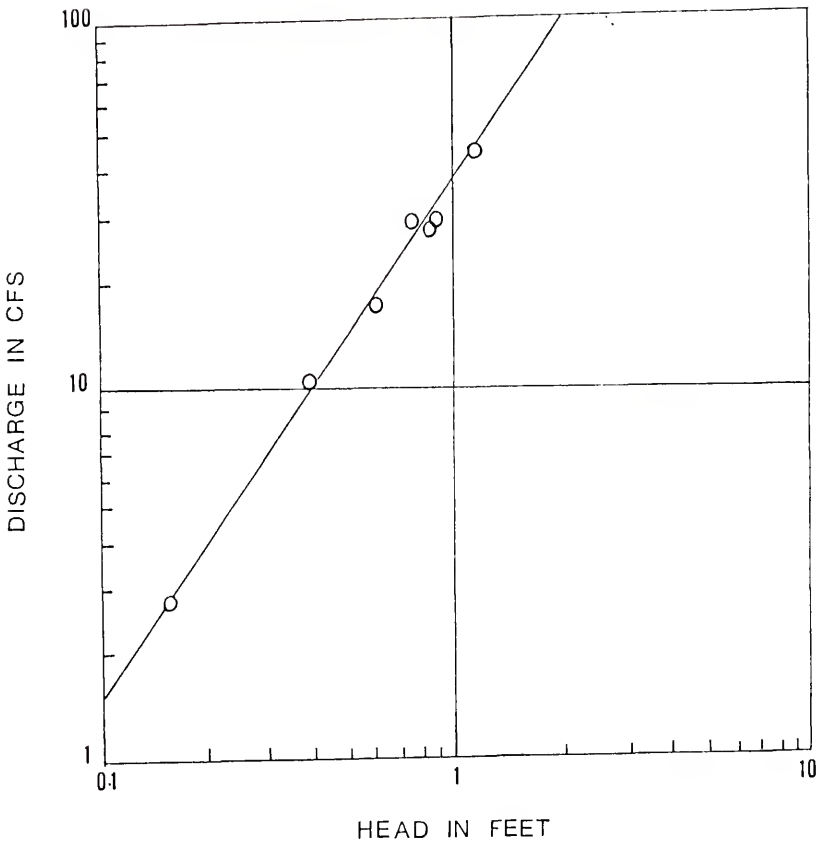

Figure 6.14. Relationship between weir head and flume discharge.

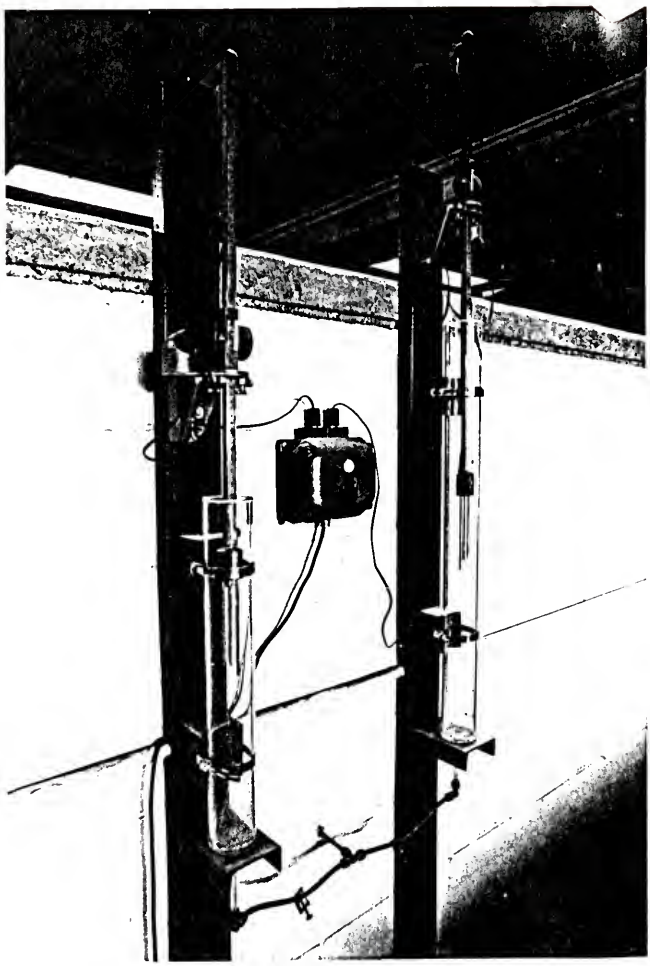

Figure 6.15. Electric point gauges for measurement of the head on the weir.

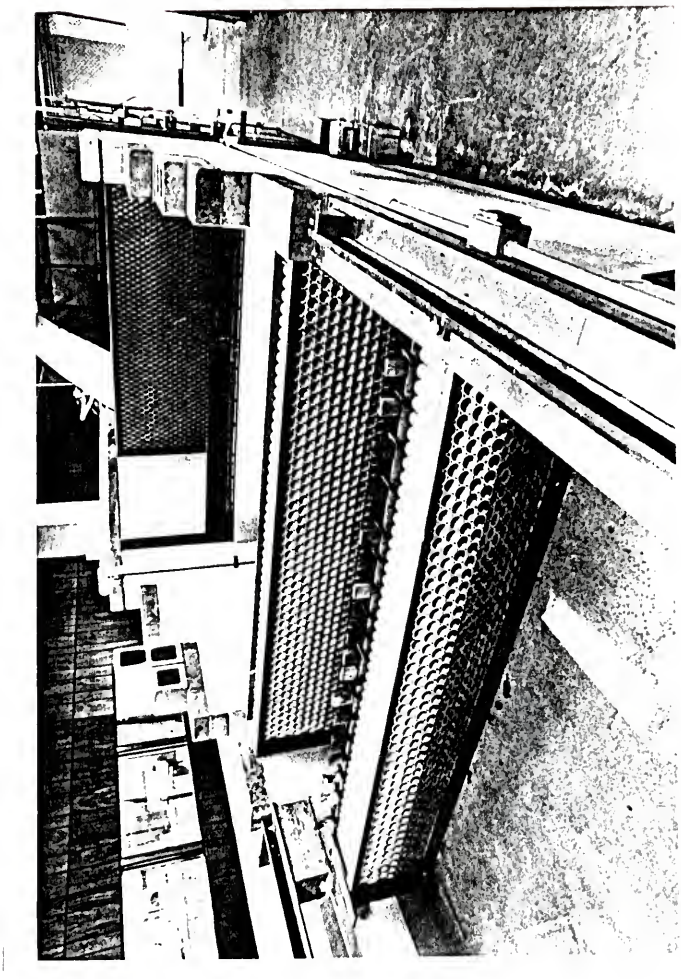

Figure 6.16. Weir and flow straighteners.

The flume is equipped with a trolley operated on horizontal rails by a variable speed DC motor. The maximum trolley speed is 2 fps. There is also a carriage in the trolley which moves across the width of the main flume. With the combination of the trolley and the carriage, the position of any point in the flume can, therefore, be located. Provision is also made on this carriage to support current meters, point gauges or similar instrumentation.

The test section of the flume is located in the middle of the main flume. It is 20 ft long, 8 ft wide and 3.3 ft deep. One side of the test section is fitted with glass panels for visual observation and for photography. Water in the flume is cleaned periodically by a sand filter (Fig. 6.17).

6.3.2 Movable Bed

The movable bed consists of two parallel conveyor belts driven by a 3/4 hp, 110 V DC motor. The rpm of the motor and, hence, the speed of the belts may be regulated by a SCR control. The shaft of the motor is connected to a high torque 5:1 gear reducer. The power from the gear reducer is transmitted to a driving shaft by means of worm gears and a drive belt. Figure 6.18 illustrates the mounting of the motor, the gear reducer and the speed control.

The conveyor belt is made of 36 oz orange woven dacron with a width of 42 in. Each belt moves on an 8 in diameter pulley drum on either side of the test section.

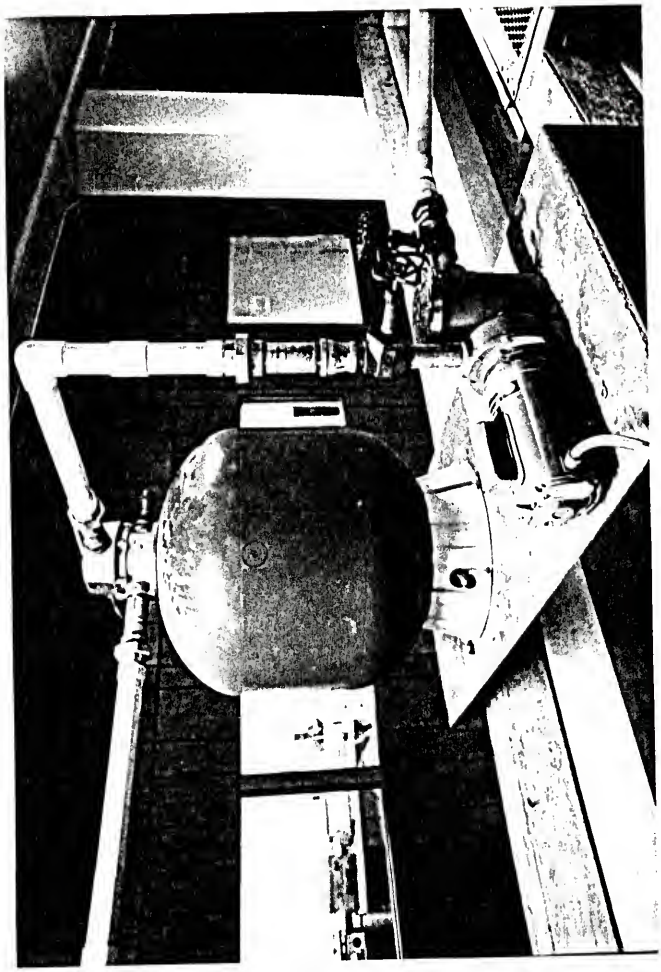

Figure 6.17. Sand filter for the flume.

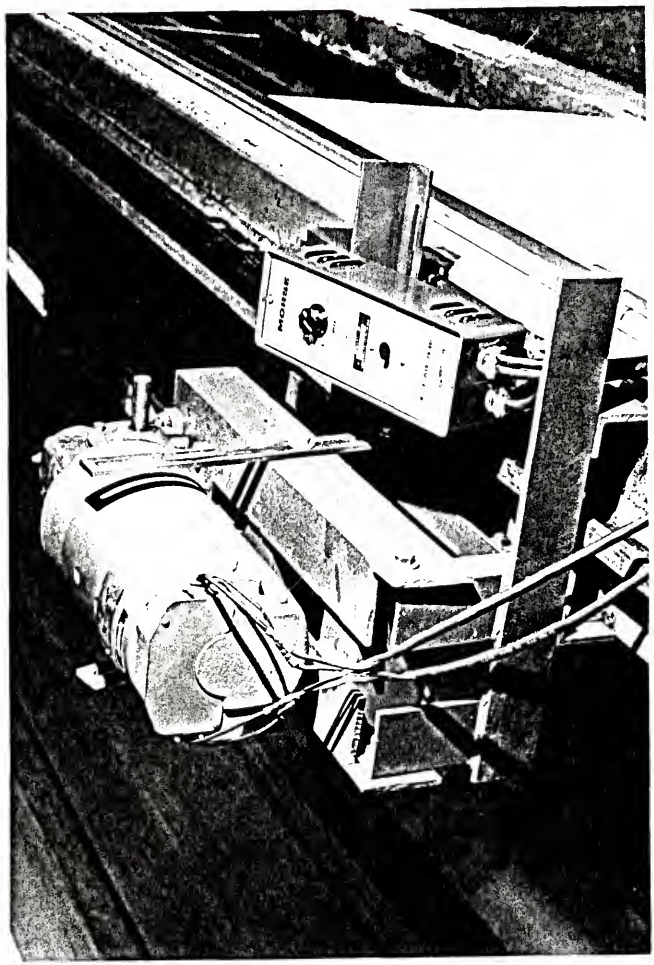

Figure 6.18. Mounting of motor and regulator for the movable belt.

The drive shaft on the motor side of the test section is common for both drums (Fig. 6.19). While on the other side, the drums run on two independent idler shafts. In this manner, the tension in each belt can be adjusted independently. The shafts are all rotating in ball bearings attached to the frame.

The pulley drum has a larger diameter in the middle than in the sides to keep the belts on the drum. The belts are supported by fiberglass sheets placed between the drums so that there will be no sagging in the belt.

6.4 Test Procedure

6.4.1 Velocity Measurements

Initial experiments were conducted to determine the effect of the belts on the velocity distribution. The velocity of the belts was fixed initially at the mean velocity of the flow. The velocity profile in a vertical was taken at the midsection of one of the belts, i.e., 15.5 in away from the center of the cross section. A conventional laboratory Ott meter was used to measure the velocity. Velocity measurements were also made at zero belt speed while maintaining the same discharge and depth of flow. An example of such profiles is shown in Figure 6.20.

The movable belts give a better uniform distribution of velocity across the depth compared to the one without moving belts (Fig. 6.20). The belts act like a pump moving

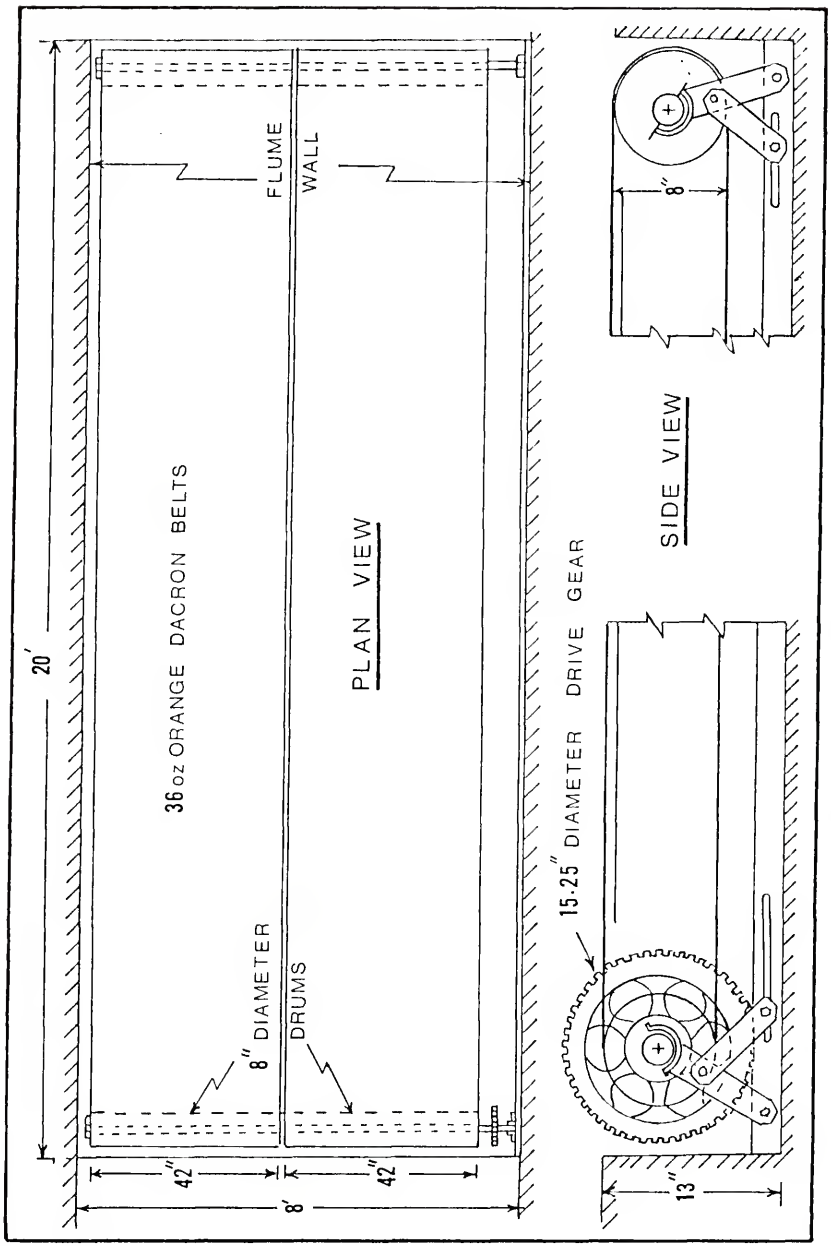

Figure 6.19. Movable bed.

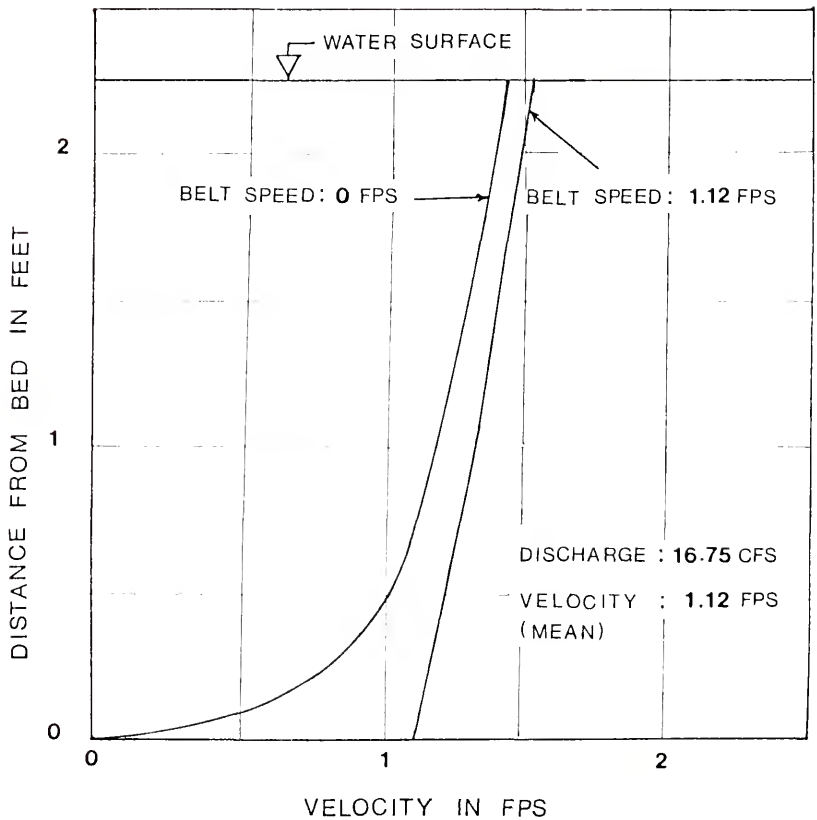

Figure 6.20. Velocity distribution at center section of right belt.

water from the bottom to top of the belts through the spaces between the walls of the test section and the rotating drums. Efforts were made to cover the empty spaces with aluminum sheets in the upstream and downstream of the belts in order to avoid this effect. However, the velocity profiles do not improve significantly and the belts proved to be unstable on the drums when these sheets were installed. Therefore, in order to achieve a uniform velocity distribution, initial trials were made to run the belts at a slightly higher velocity than the mean velocity of the flow. By trial and error, the correct belt speed for a velocity profile approximating uniform velocity distribution is obtained. The wooden strips on the baffles were adjusted for the uniform velocity distribution across the width of the flume. Isovels for the required model discharges are shown in Figures 6.21 to 6.26.

6.4.2 Experiments on Nets

For every run, the discharge and the belt speed were set to get the correct velocity distribution. The height of the net was found by measuring with a point gauge the differences in level between the top of the headrope and the belt (Fig. 6.27). The door spread was measured directly. Typical net profiles during the tests are shown in Figures 6.28 through 6.31.

The tensile force in the warp was measured with the 300 gram range load cell. The calibration of the load cell was checked both before and after a reading. Because of the

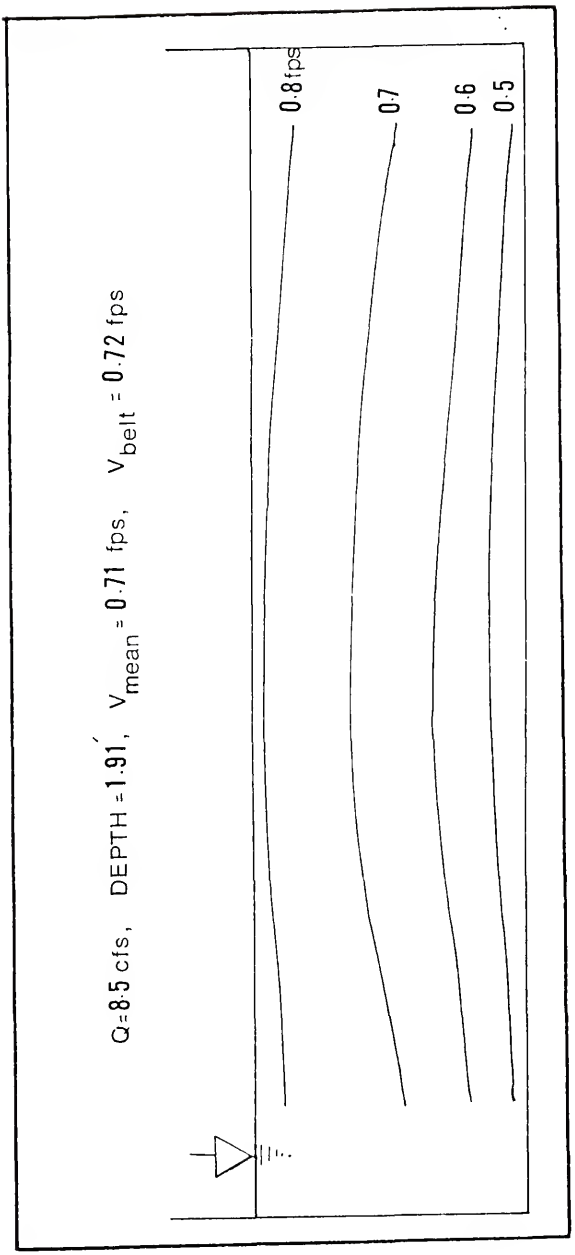

Figure 6.21. Isovels for run 1.

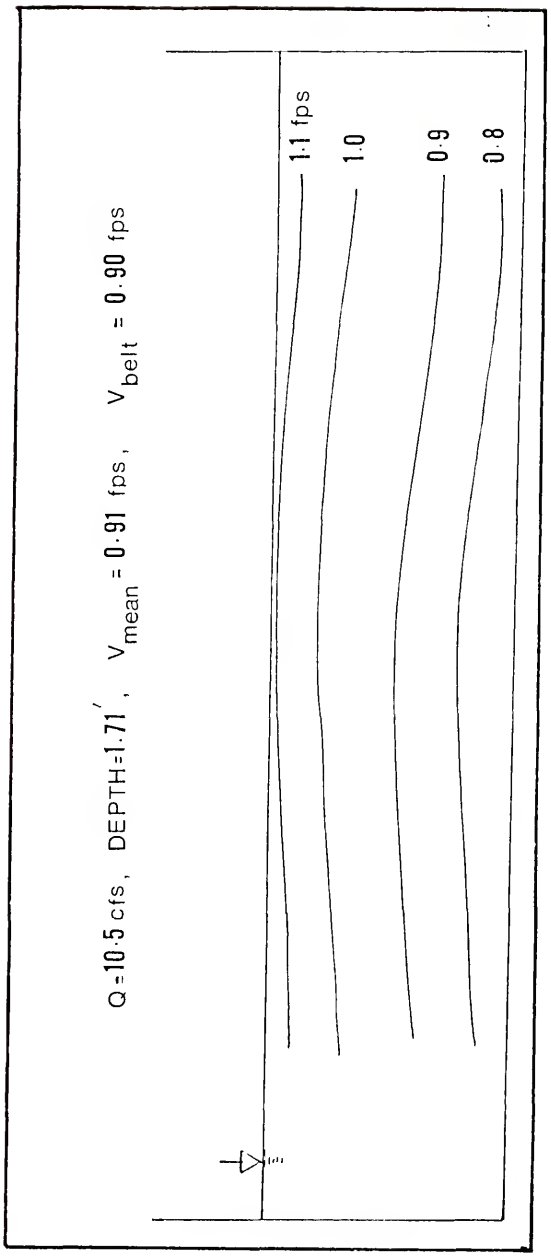

Figure 6.22. Isovels for run 2.

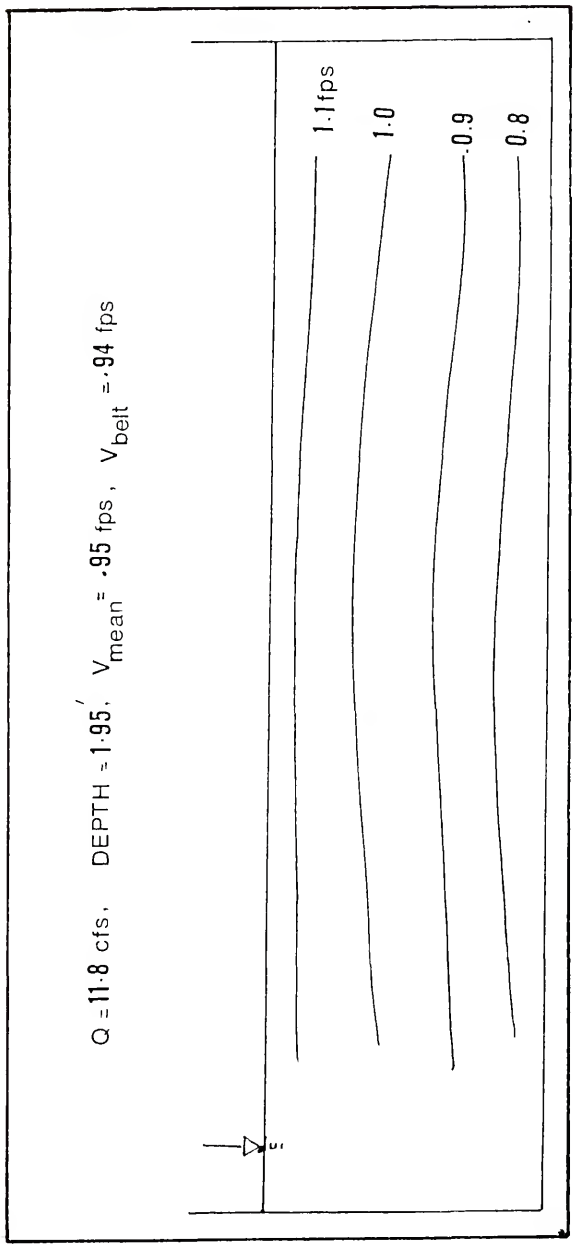

Figure 6.23. Isovels for run 3.

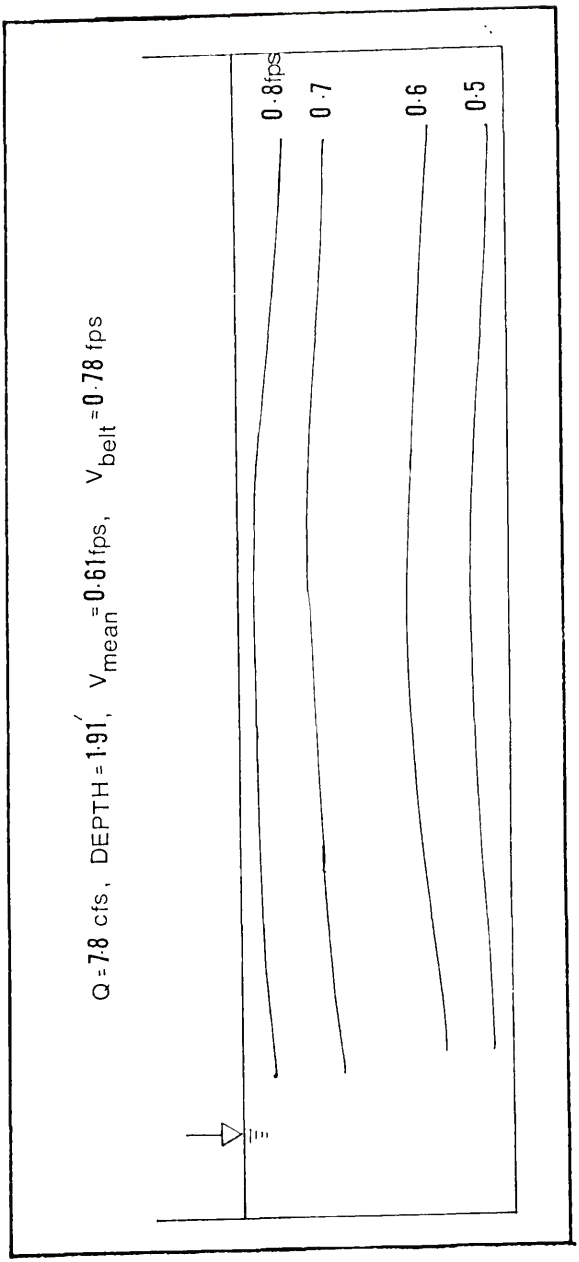

Figure 6.24. Isovels for run 4.

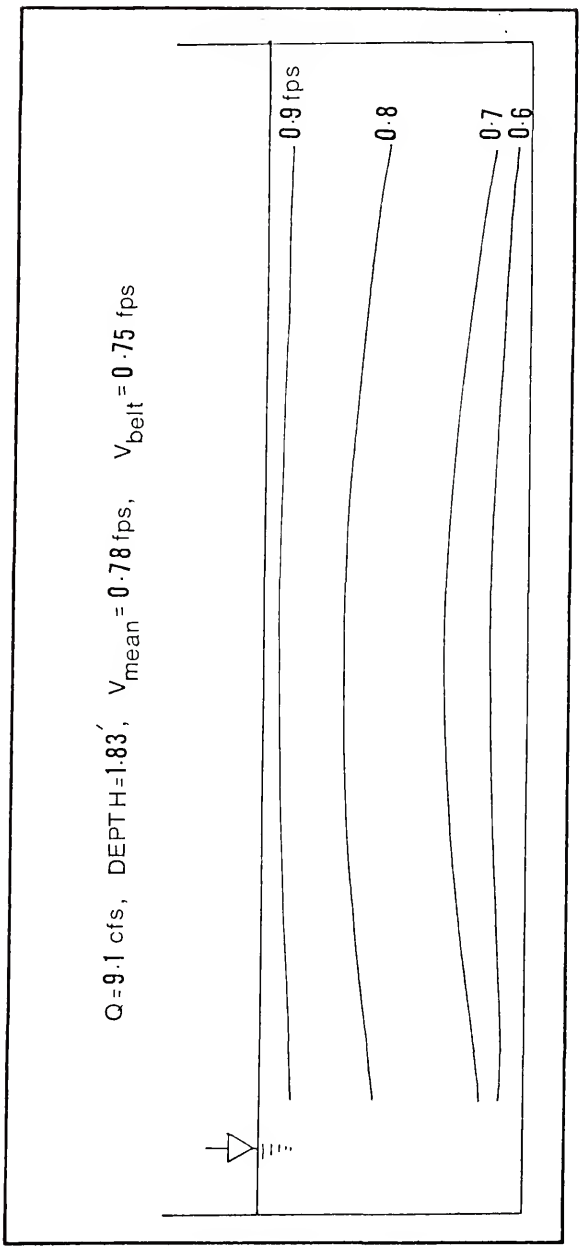

Figure 6.25. Isovels for run 5.

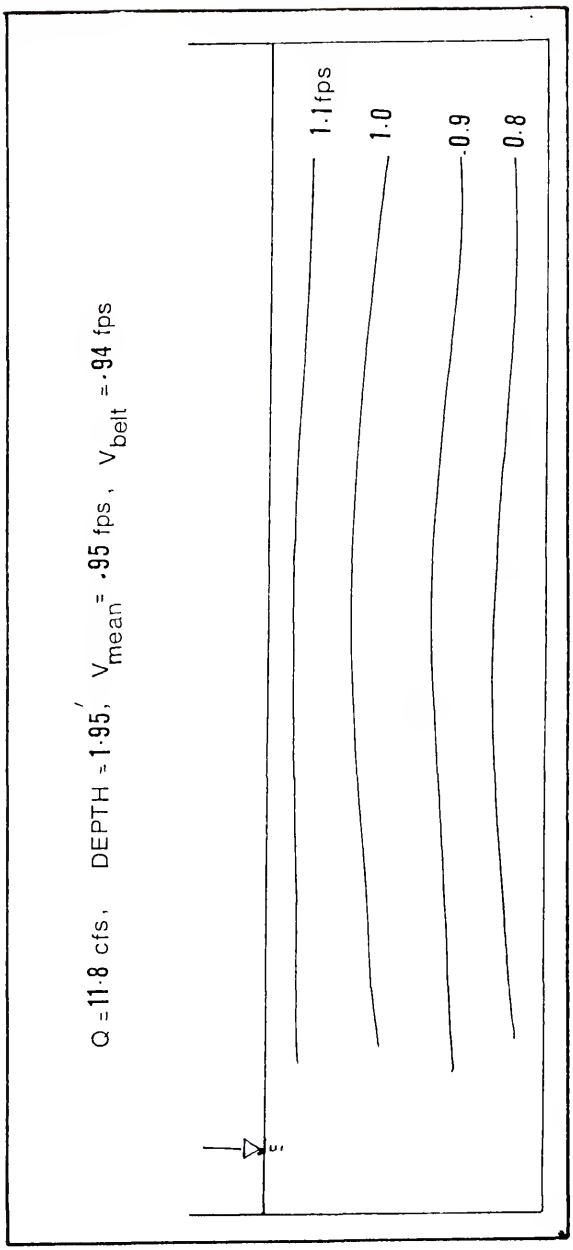

Figure 6.26. Isovels for run 6.

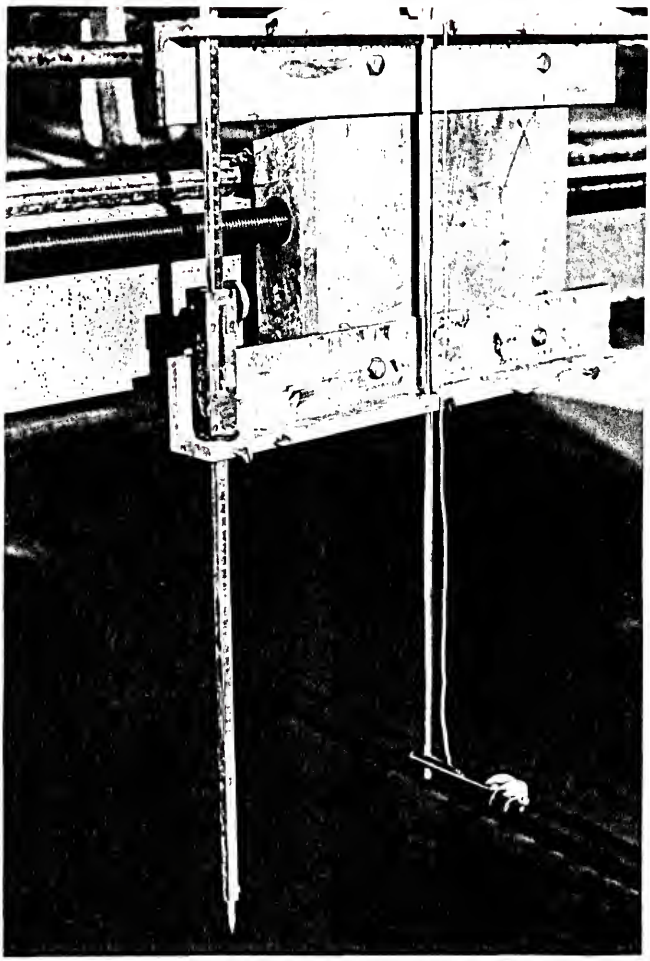

Figure 6.27. Point gauge and Ott current propeller.

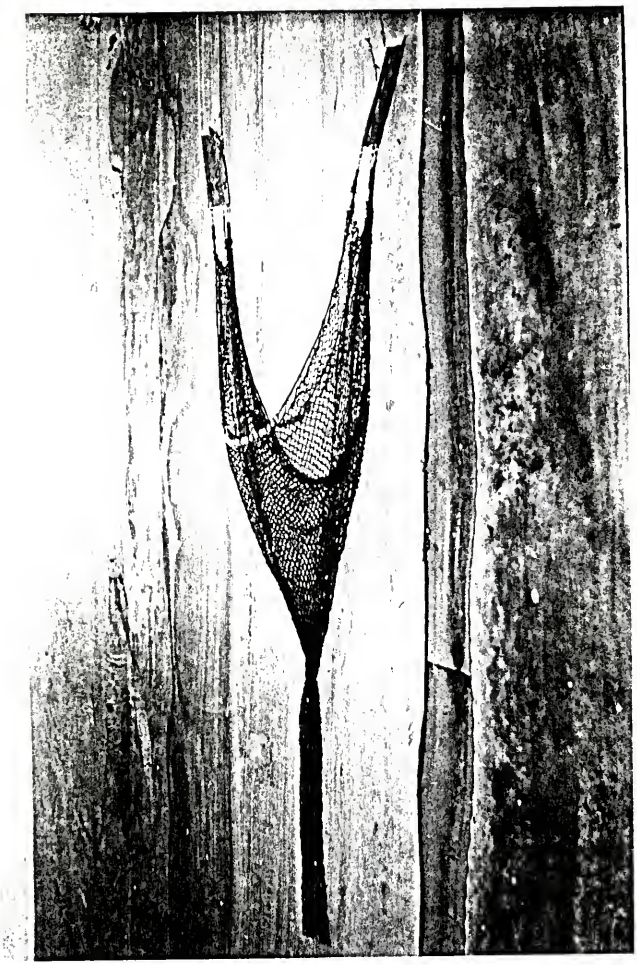

Figure 6.28. Net profile during testing.

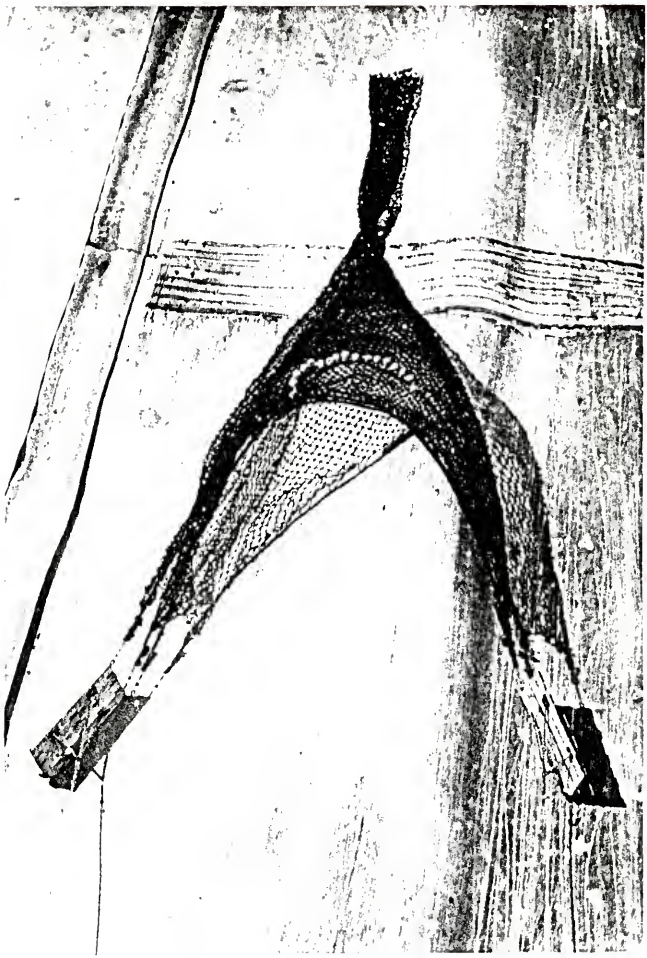

Figure 6.29. Plan view of net during testing.

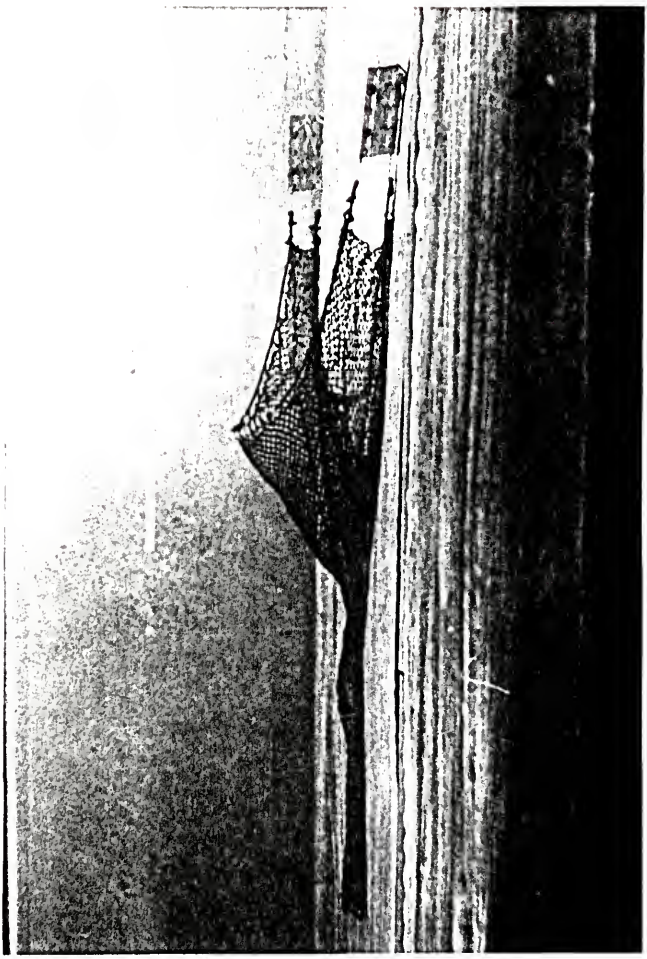

Figure 6.30. Side view of net during testing.

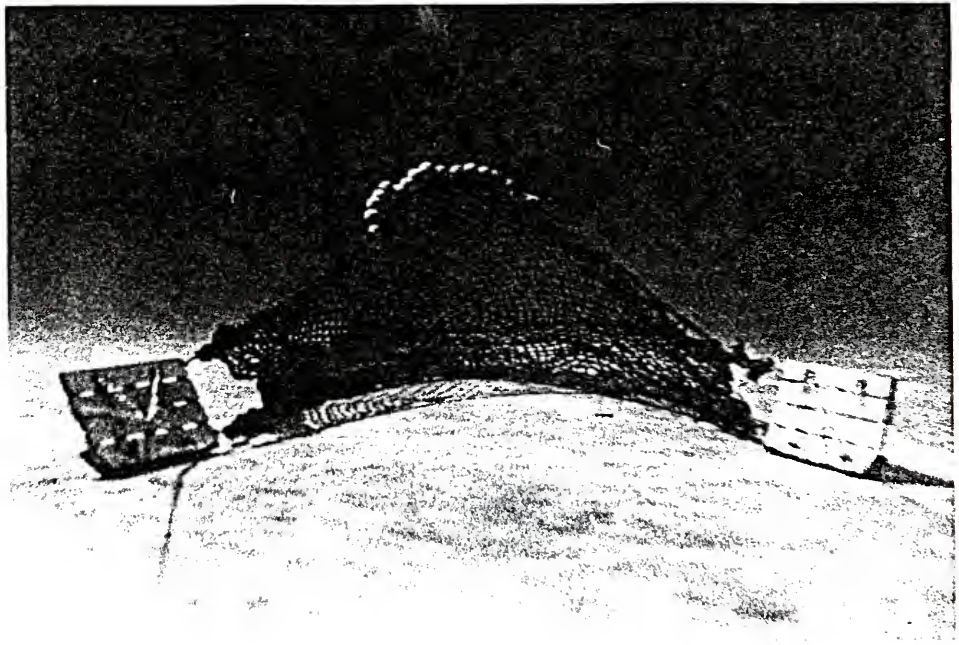

Figure 6.31. Front view of net during testing (underwater photograph).

repetitious nature of the force measurements, the steel wire (towing warp) was replaced for easier handling by a nylon twine of the same diameter. The differences in the force measurements with the steel wire and the nylon twine were negligible. The readings during the test were steady except when the moving belt seam hit the doors. Therefore, these readings were not recorded.

The tensile force in the legs (rope between the net and the door) was measured in the same manner as described above, and the calibration was checked each time. Figure 6.32 shows the view of the door during a typical test.

A portion of the rope at the midsection of the headrope was cut and the 5 gram range load cell was attached in order to measure the tensile force. Because of the rather substantial fluctuations of the readings, these force measurements were recorded on the strip chart recorder, and the average reading was found by planimetering the area of the chart and dividing the area by the time of the record. The same procedure was adopted to find the tensile force in the midsection of the footrope. Table 6.2 summarizes the model test results with the movable belts.

To compare the effects of movable belts on the performance of the model trawl, a second set of tests was conducted. In this set, the belts remained stationary. The mean velocity of the cross section was set at the

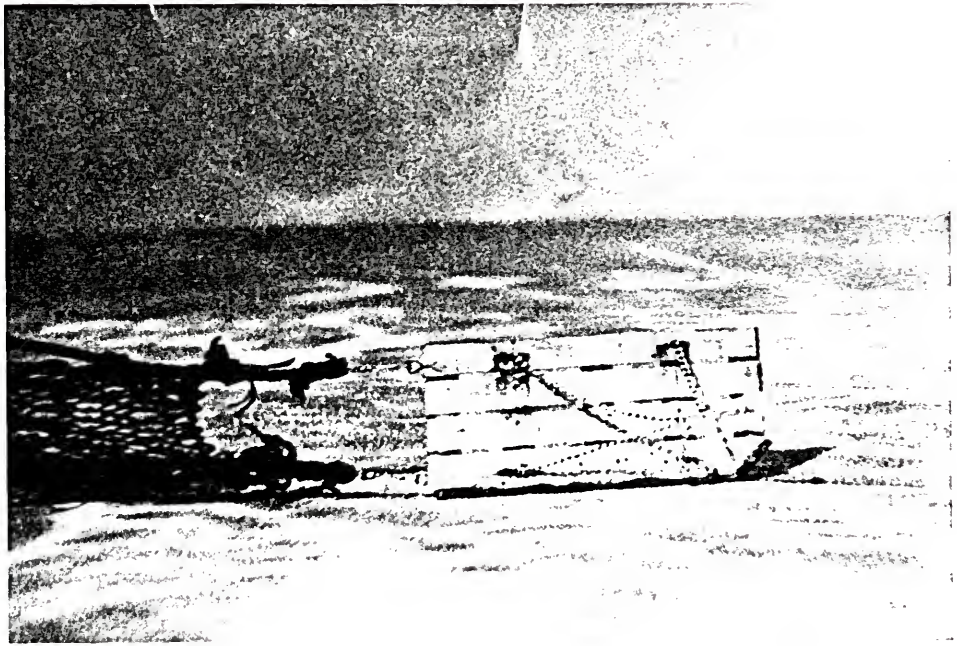

Figure 6.32. Side view of door during testing (underwater photograph).

TABLE 6.2

MODEL RESULTS WITH MOVABLE BEDS

Quantity	Headrope Without Floats			Headrope with Floats		
Run number	1	2	3	4	5	6
Velocity (fps)	0.71	0.91	0.95	0.61	0.78	0.95
Door spread (in)	21.0	22.0	22.5	18.0	20.0	21.5
Mouth opening (in)	3.50	2.50	2.00	9.55	8.25	6.95
Warp tensile force (gf)	102.1	178.9	193.7	117.9	174.5	225.0
Force in ropes — Top between door and net (gf)	12.76	18.94	31.60	12.50	27.40	45.30
Bottom	17.02	33.68	52.60	26.30	42.10	57.90
Force in footrope at center (gf)	4.00	4.00	4.00	8.42	7.38	6.95
Force in headrope at center (gf)	1.30	2.98	2.98	1.30	1.30	1.30
Reynolds number	193	247	258	166	212	258
Coefficient of drag	1.50	1.41	1.51	1.53	1.50	1.41

required velocity found from the Froude model law. The experimental procedure described above was repeated and the same model data were taken. These data are given in Table 6.3.

TABLE 6.3

MODEL RESULTS WITHOUT MOVABLE BEDS

Quantity	Headrope Without Floats			Headrope with Floats		
Run number	1	2	3	4	5	6
Velocity (fps)	0.707	0.915	0.959	0.618	0.780	0.941
Door spread (in)	19	21	22	17	19	20
Mouth opening (in)	4.0	3.0	2.5	11.0	10.0	8.0
Warp tensile force (gf)	80.0	101.1	152.0	89.6	117.9	153.6
Force in ropes — Top between door and net (gf)	8.42	12.63	16.80	14.58	23.15	31.60
Bottom	12.63	18.95	21.10	10.42	27.36	33.70
Force in footrope at center (gf)	4.00	4.00	4.00	8.42	7.38	6.95
Force in headrope at center (gf)	1.30	2.98	2.98	1.30	1.30	1.30
Reynolds number	193	249	261	168	212	256
Coefficient of drag	1.50	1.41	1.40	1.52	1.41	1.41

CHAPTER 7

DISCUSSION OF RESULTS

7.1 Validity of Model Laws

The Reynolds number $R_{eD} = \frac{VD}{\nu}$ for each run in the model experiments are calculated and given in Tables 6.2 and 6.3. The corresponding drag coefficients C_D for the net panels are found in Figure 2.9 and, also, tabulated with the values of the Reynolds numbers. The variation in the values of C_D is negligible and they are considered to be equal, indicating that the flow in the model tests is in the turbulent range. Therefore, the assumption that the viscous forces in the model trawl may be neglected is a valid one.

7.1.2 Comparison Between Model and Field Test Results

The results of model tests are converted to prototype data by using the proper scale ratios given in Table 6.1. For example, the predicted forces in the prototype experiments are obtained by multiplying the values of the forces in the model experiments by the gravity force scale ratio κ gravity. The percentage of error between the predicted values and the measured values is computed by the expression:

$$\text{Percentage of error} = \left(\frac{\text{Measured Value} - \text{Predicted Value}}{\text{Measured Value}}\right)(100) \quad (7.1)$$

The predicted data of the prototype experiments and the values of the percentage of error are tabulated in Table 7.1.

The velocities in the model tests were obtained within 1.2 percent of the required velocity calculated from the Froude model law. The mean value of the velocity in the model experiments was computed from the velocity traverse. Ideally, it is desirable to have a complete uniform velocity distribution across the depth. Though the present arrangement of the movable belts works satisfactorily, improvements are desired to achieve the above objective.

All the door spread values are predicted within a margin of error of 1.3 percent. However, the errors in the prediction of mouth opening in Runs 2 and 6 are higher than the other values. These are due to the fluctuations of the model headrope in the depth plane. But the trend of decrease in the headline height with the increase of doorspread is to be noted in the prediction, as observed in the prototype testings.

The predicted values of warp tensile force agree with the measured values with an error of 3 percent except for the value in Run 2. Contrary to expectations, the former values are noticeably higher than the latter ones. In the field experiments, the trawl encountered additional ocean bottom frictional resistance from discrete roughness element not

TABLE 7.1

PROJECTED FIELD DATA FROM THE RESULTS OF MODEL EXPERIMENTS WITH MOVABLE BEDS

Quantity		Headrope Without Floats			Headrope with Floats		
Run number		1	2	3	4	5	6
Velocity	(fps)	2.77	3.55	3.70	2.38	3.04	3.70
	(% error)	(-0.7)	(+1.1)	(+1.1)	(+1.2)	(+0.7)	(-0.3)
Door spread	(ft)	26.60	27.87	28.50	22.80	25.33	27.23
	(% error)	(+0.4)	(-0.6)	(+1.0)	(+0.9)	(-1.3)	(-0.9)
Mouth opening	(ft)	4.43	3.17	2.53	12.10	10.45	8.80
	(% error)	(+1.6)	(+9.4)	(-1.2)	(+4.0)	(+1.5)	(-8.6)
Warp tensile force	(lb)	813	1424	1542	938	1389	1791
	(% error)	(-2.3)	(-12.5)	(-3.6)	(+3.1)	(-2.1)	(-0.3)
Force in rope between net and door	Top	102	151	252	100	218	361
	(% error)	(-2.0)	(-0.7)	(-0.8)	(0)	(+3.1)	(-3.1)
	Bottom	136	268	419	209	335	461
	(% error)	(-8.8)	(-7.2)	(-4.8)	(-4.5)	(-3.1)	(-2.4)
Force in foot-rope at center	(lb)	32	32	32	67	59	55
	(% error)	(-6.7)	(-6.7)	(-6.7)	(-11.7)	(1.7)	(8.3)
Force in head-rope at center	(lb)	10	22.8	23.8	10	10	10
	(% error)	(0)	(+19.0)	(+19.0)	(0)	(0)	(0)

reproduced in the model and also additional resistance due to a small catch (estimated to be about 100 lb). The model trawl was not subjected to these resistances in the experiments. It may be fortuitous that the resistance of the movable belts to the model trawl may have corresponded to the resistance of the ocean bottom to the prototype trawl at the test site.

One other explanation for this discrepancy is the effect of the friction of the towing block on the towing cable. In the field tests, the tensile force in the towing cable was measured in a small length of cable near the drum. Because of the friction between the tow cable and block, the magnitude of the force in the cable drumside of the towing block will be smaller than the magnitude of the force in the cable netside of the block. However, in the model experiments, the warp tensile force was measured without using a towing block. This absence of the frictional resistance in the model tests may have counteracted the absence of the ocean bottom frictional force in the field tests, giving the correct values of the magnitude of tension in the towing cable.

The predicted results of the force in the footrope agree with the measured ones, within a reasonable margin of error. However, the error in the predicted force in the headrope is the highest in the whole prediction in Runs 2 and 3. This is due to instrumentation difficulty.

Observations from the underwater movie during the field studies show that the load cell got tangled in the webbing near the headrope, hence giving incorrect readings of the force. The underwater load cell in the footrope must also have had the effect of bottom friction, as the paintings from the cover of the load cell had been worn off during the testings. Therefore, the effors in the forces of both the head and footropes are attributed to the measurement techniques rather than to the model laws.

7.2 Effect of the Movable Belts

The data of the model experiments conducted without the movable belts have been projected onto the field data by using the scale ratios given in Table 6.1. These predicted values and the corresponding percentage errors are tabulated in Table 7.2. The values of the Reynolds numbers and the coefficients of drag tabulated in Table 6.3 show that in this set of experiments as well as in the first set, the flow in all the runs was in the turbulent range. Therefore, the influence of viscous forces on the model trawl is fairly negligible.

The values of door spread in the experiments conducted without movable belts are less than those with movable belts. This is due to the lack of higher velocity of the water particles near the bed to provide the necessary drag to open up the net, as in the experiments with movable belts.

TABLE 7.2

PROJECTED FIELD DATA FROM THE RESULTS OF MODEL EXPERIMENTS WITHOUT MOVABLE BEDS

Quantity		Headrope Without Floats			Headrope with Floats		
Run number		1	2	3	4	5	6
Velocity	(fps)	2.76	3.57	3.74	2.41	3.04	3.67
	(% error)	(-0.4)	(+0.6)	(0)	(0)	(0.7)	(0.6)
Door spread	(ft)	24.07	26.60	27.87	21.53	24.07	25.33
	(% error)	(+9.7)	(+4.1)	(+3.3)	(+6.4)	(+3.7)	(+6.6)
Mouth opening	(ft)	5.07	3.80	3.17	13.93	12.67	10.13
	(% error)	(-12.7)	(-8.6)	(-26.8)	(-10.7)	(-22.7)	(-25.4)
Warp tensile force	(lb)	637	805	1211	714	939	1224
	(% error)	(+19.8)	(+36.4)	(+18.6)	(+26.3)	(+31.0)	(+31.4)
Force in rope between net and door	Top	67	101	134	116	184	252
	(% error)	(+33.0)	(+32.7)	(46.4)	(-16.0)	(+18.2)	(28.0)
	Bottom	101	151	168	83	218	268
	(% error)	(+19.2)	(+39.6)	(+58.0)	(+58.5)	(+32.9)	(+40.4)
Force in foot-rope at center	(lb)	32	32	32	67	59	55
	(% error)	(-6.7)	(-6.7)	(-6.7)	(-11.7)	(+1.7)	(+8.3)
Force in head-rope at center	(lb)	10	23.8	23.8	10	10	10
	(% error)	(0)	(+19.0)	(+19.0)	(0)	(0)	(0)

Because of the lower values of the door spread the percentage error is large, implying the necessity of the correct velocity distribution in the model experiments. The predicted values of the net height in this case are higher than the observed values, confirming the inverse relationship between the door spread and the net height. Therefore, the higher the door spread, the lower the net mouth opening.

Correspondingly, the predicted values of the warp tensile force are lower than the measured values, giving a very high percentage of error. The predicted tensile forces in these two cases are compared in Figure 7.1. The predicted values of the force in the legs follow the same trend as above (Fig. 7.2).

7.3 Comparison Between Physical and Mathematical Models

Kowalski and Giannotti (1974) give a numerical method of predicting the warp tensile force in a trawl. They point out that the main source of error in predicting the force is the interaction between the sea-bottom and door. However, as outlined in section 3.3, in addition to the frictional effect, the error also lies in the prediction of the drag of the net. In their development, the basic form of equation in computing the drag net is incorrect. The observed field data (Table 5.3) are used to determine the validity of this argument.

Numerically, the drag force acting on the net is calculated by adding the drag of the individual components given by the formulas that are outlined in section 3.1

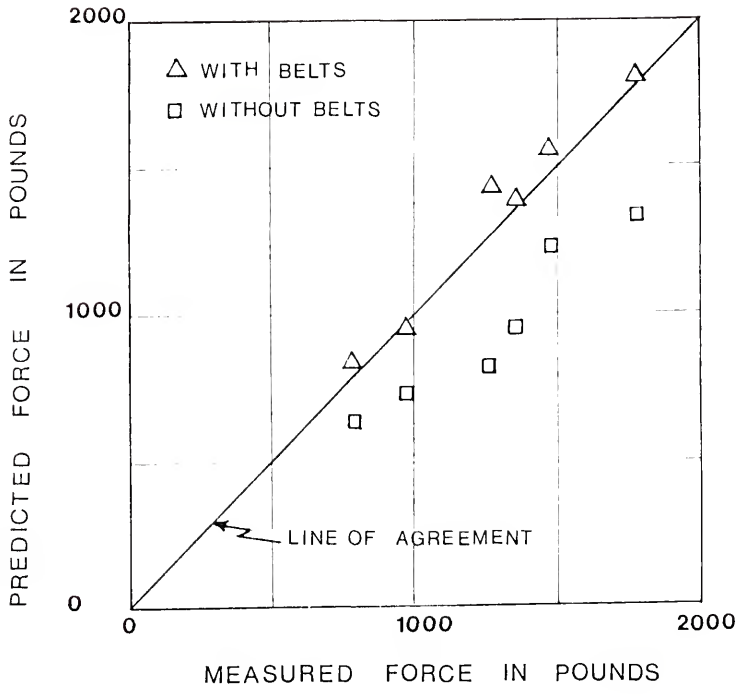

Figure 7.1. Prediction of warp tensile force from model results.

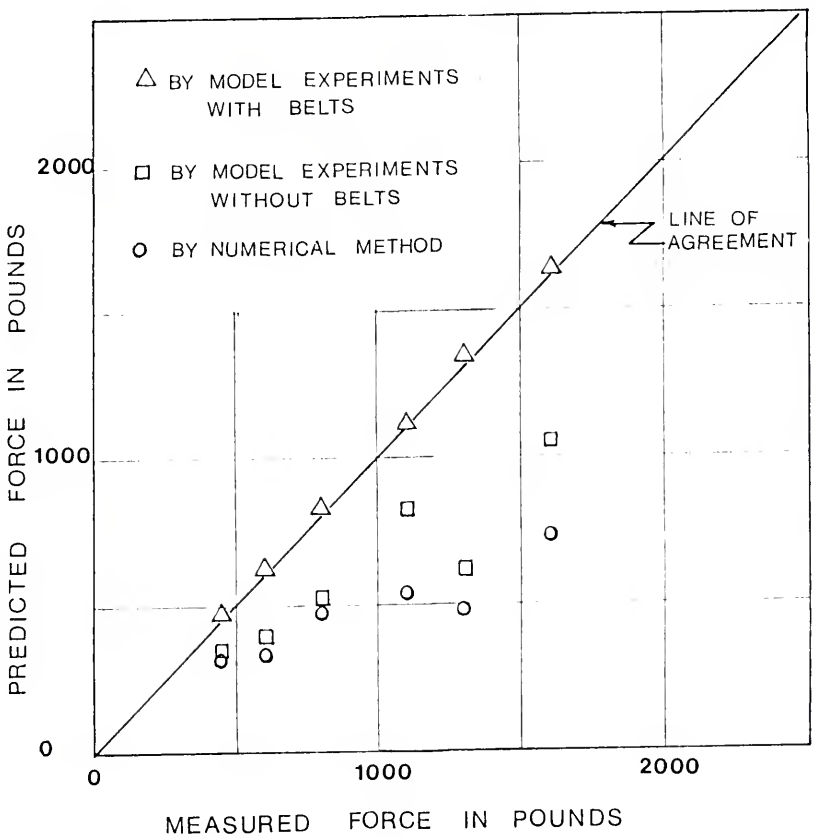

Figure 7.2. Prediction of drag force acting on a net.

$$F_{net} = F_{cone} + F_{cod\ end} + F_{lines} + F_{ropes} + F_{floats} \quad (7.2)$$

The calculations of F_{net} for each velocity observed in the field tests are given in Appendix E.

The corresponding observed values of F_{net} are obtained from the measured values of the tensile forces in the ropes between door and net.

$$F_{net} = 2 \left(F_{top} + F_{bottom} \right) \quad (7.3)$$

where

F_{net} = Measured drage force of net

F_{top} and F_{bottom} = Measured tensile forces in top and bottom rope between door and net

The predicted and measured values of the drag of the net are tabulated in Table 7.3. The corresponding percentage of error for each run is also given in Table 7.3.

Table 7.3 shows that the numerical method estimates very low values of drags. This is due to the improper form of equation used in calculating the drag of the belly. As mentioned earlier in section 3.3, further work is necessary in deriving the proper form of equation to estimate the drag of the belly.

The values of F_{net} measured in the field experiments are plotted in Figure 7.2 with the predicted values of F_{net}, (1) by model experiments conducted with movable belts,

TABLE 7.3

COMPARISON BETWEEN PREDICTED VALUE OF NET DRAG BY NUMERICAL METHOD AND MEASURED VALUE IN THE FIELD TEST

Run Number	1	2	3	4	5	6
Predicted value (lb)	306	473	477	341	529	726
Measured value (lb)	450	800	1300	600	1100	1600
% Error	32	40.8	63.3	43.2	51.9	54.6

(2) by model experiments without movable belts and (3) by numerical method. It is seen that only the prediction by model experiments with movable belts agreeswell with the measured values. Therefore, at present, model experiments seem to be the only reliable method of testing the fish nets.

CHAPTER 8

APPLICATION OF MODEL APPROACH IN DESIGNING A BEAM TRAWL

8.1 Introduction

The development of model laws and verification of these laws by both model and field tests have provided a tool to test and modify the existing trawls. The model approach can also be used in developing new trawls. Currently, inshore shrimping along the Florida coast is limited only to a particular season. In order to provide a year-round opportunity of employment for fishermen, it is proposed to harvest and market the deep-water species, "Royal Red Shrimp." However, the existing conventional otter door trawls are not adequate for shrimping in deep water. For, when pulled on muddy and soft bottoms, the doors tend to dig into the soft bottom and it is difficult to break the doors loose from the ocean bottom once they become stuck. They may also collapse while running on soft bottoms at a lower speed.

In order to overcome these difficulties, a beam trawl, which provides a constant net spread, is proposed. A description and design of a beam trawl for this application

and an evaluation of its efficiency by the model approach are presented in the following.

8.2 Description of the Beam Trawl

The beam trawl (Fig. 8.1) consists of a beam, a pair of heads and a net comprised of wings, belly and cod end. The beam gives a constant spread while the heads give stability to the trawl. The length of the beam depends on the size of the vessel and type of fish to be caught. The beam is made of tube sections in three parts. The outer parts have a lesser diameter than the middle part and they can be telescoped into the middle section. In this way, the beam can be stored easily on the deck of the boat. The middle section of the beam has an eye for the towing warp.

The trawl head height is fixed by the type of fish to be caught. The head is made of a circular plate (Fig. 8.2) with an iron shoe attached along its lower edge. The width of the shoe depends on the type of bottom; the softer the bottom, the broader the shoe. The towing warp is attached to the front of the trawl head, and provision is made to change the point of attachment. There are different pad eyes in the trawl head for the footrope, lazyline and tickler chains.

Because of the constant spread, a beam trawl has the following advantages: the length of warp has much less influence on the beam trawl than on the otter door trawl;

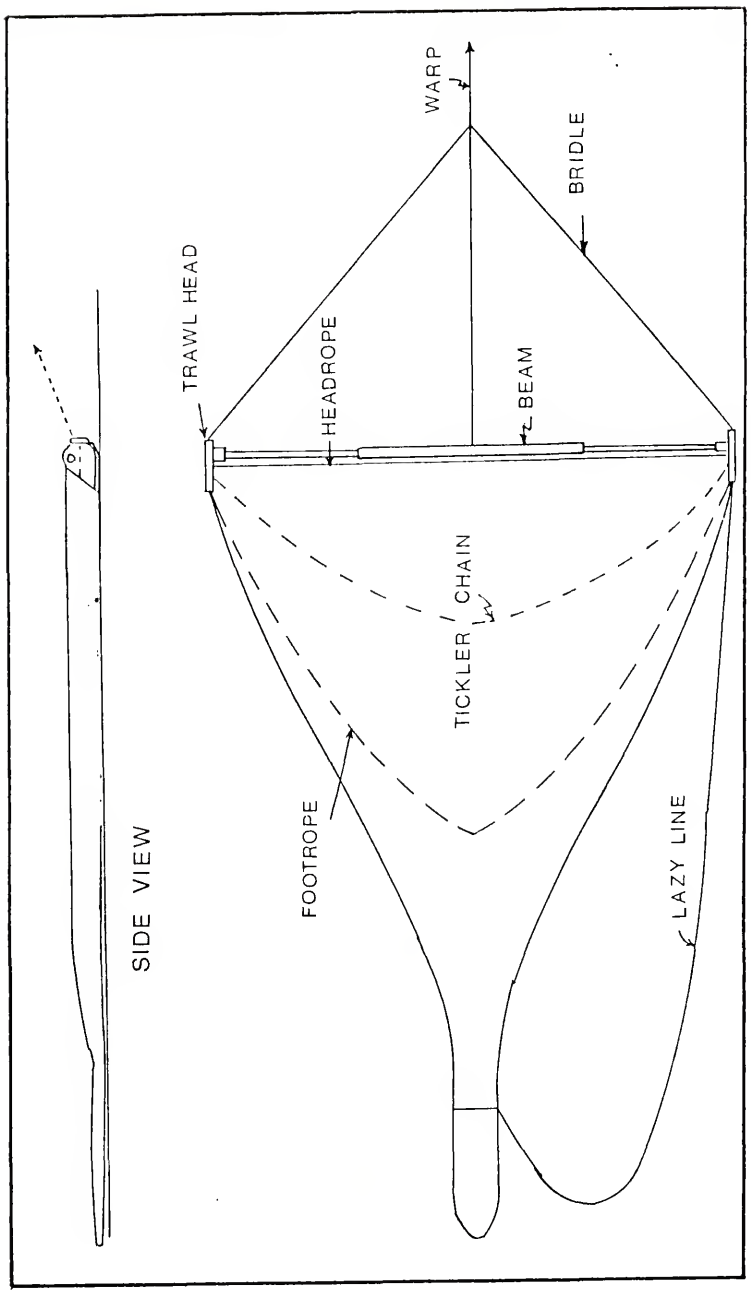

Figure 8.1. Beam trawl.

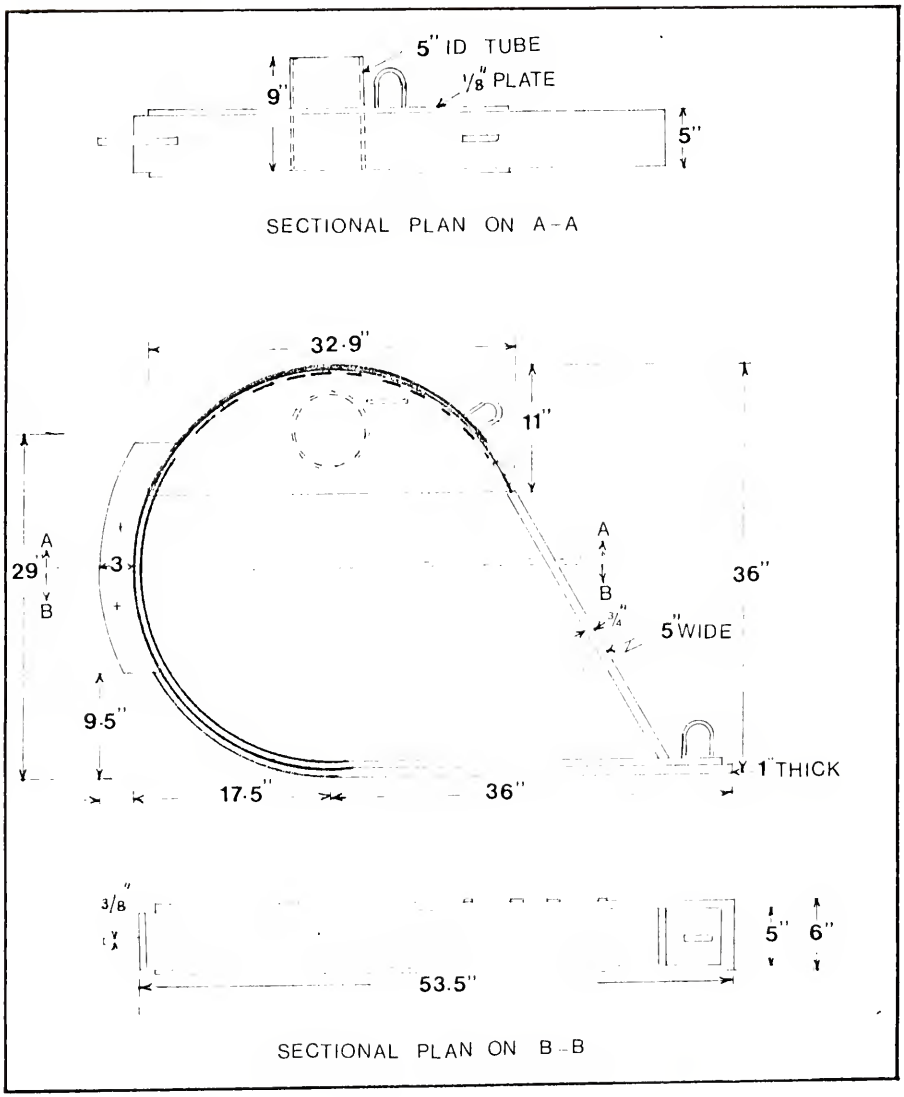

Figure 8.2. Trawl head.

interaction between the ocean bottom and the trawl does not affect the spread in the case of the beam trawl; whereas, in the case of the otter door trawl, the boards will tend to close with the result that the footrope tends to dig into the bottom; and the influence of tidal current is much less on a beam trawl than on the otter door trawl.

8.3 Design of the Beam Trawl

8.3.1 Beam

The length of the proposed beam was chosen as 30 ft, to suit trawlers operating along the coast of Florida. To reduce the weight of the assembly beam, aluminum was used instead of steel, wherever possible. The beam was designed by considering it as a continuous beam simply supported at three junctions (Fig. 8.3). The load acting on it was assumed to be uniformly distributed along the length. The maximum bending moment occurs at the midsection and is given by:

$$B.M. = 0.0313\ wL^2 \qquad (8.1)$$

where

B.M. = Bending moment in ft-lb

w = Load per unit length in ft/lb

L = Total length in ft

At a towing velocity of four knots, de Boer (1959) reports a resistance of 3700 lb for a 21-ft beam. By linear interpolation and adding a safety factor, the value of w for a

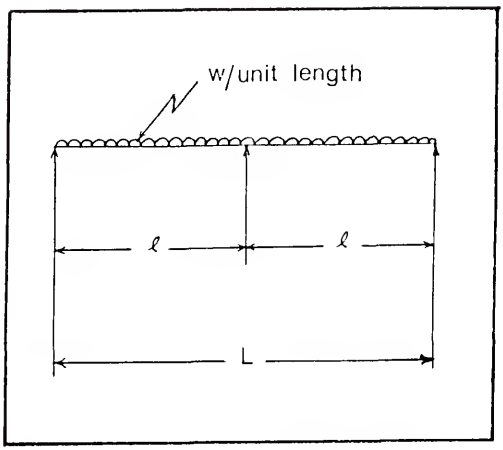

Figure 8.3. Continuous beam.

30-ft beam trawl was calculated to be 400 lb/ft. The design bending moment for the center section is found from Equation (8.1) and is equal to 11,268 ft-lb. Using aluminum 6061-T6, 5 in OD tube, the working stess σ is calculated by

$$\sigma = \frac{B.M.}{Z_m} \tag{8.2}$$

where

Z_m = Sectional modulus

and is given by

$$Z_m = \frac{1}{6}\left(D_o^3 - D_i^3\right) \tag{8.3}$$

in which

D_o = Outside diameter of tube

D_i = Inside diameter of tube

Substituting Equations (8.3) and (8.1) into (8.2), yields:

$$\sigma = 13.3 \text{ kips/in}^2 \tag{8.4}$$

which is less than the maximum allowable stress (35 kips/in^2). Similarly, the working stress for the side tubes is calculated to be:

$$\sigma = 12.33 \text{ kips/in}^2 \tag{8.5}$$

which is also less than the allowable stress.

The beam design can be analyzed for the possibility of vortex-generated vibration. If the frequency of the

vortices coincides with the natural frequency for the continuous beam, the drag will be substantially increased. The natural frequency for a simply supported continuous beam is:

$$\omega_n = \frac{\pi^2}{\ell^2} \sqrt{E'I/m''} \qquad (8.6)$$

where

E' = Modulus of elasticity

I = Moment of inertia

m'' = Mass per unit length

For the midsection tube,

$I = (8.735)(10^{-4})$ ft^4

$m'' = 0.258$ slugs/ft

$\ell = 15$ ft

$E' = (7.22)(10^4)$ lb/ft^2

and

$\omega_n = 0.686$ radians/sec

The towing velocity, which may create vortices shedding at this frequency, was computed by considering the Strouhal number, S_n, which is defined as:

$$S_n = \frac{n_f D_o}{V} \qquad (8.7)$$

where

n_f = Frequency of vortices

D_o = Outside diameter of tube

V = Velocity

When the Reynolds number of the flow is greater than 1000, Schlitchting (1969) gives a value of 0.21 for S_n. The towing velocity which causes vortices of frequency of 0.686 radians per second is:

$$V = \frac{n_f D_o}{S_n} = 1.36 \text{ fps} = 0.8 \text{ knots}$$

Similarly, for the end tubes, the towing velocity is 0.54 knots. In practice, the net is not towed at such low velocities. Therefore, this beam will not experience vortices causing vibrations. The final dimensions of the beam are given in Figure 8.1.

8.3.2 Trawl Head

The vertical distance between the center of the tube and the ground was fixed at 29 in which is a normal height for shrimping. The dimensions of the steel shoe, 1 in thick and 6 in wide, is the same as for the otter door. All the dimensions of the trawl head are given in Figure 8.2

The trawl head has different pad eyes to hook the lazyline, the headrope and the footrope. The tickler chains are attached by a shackle to the iron shoe. The position of the towing point may be varied depending upon the bottom condition.

8.3.3 Net

The net for the trawl is made from No. 15 nylon with a 2-in stretched mesh. The cutting diagram of the net is shown in Figure 8.4.

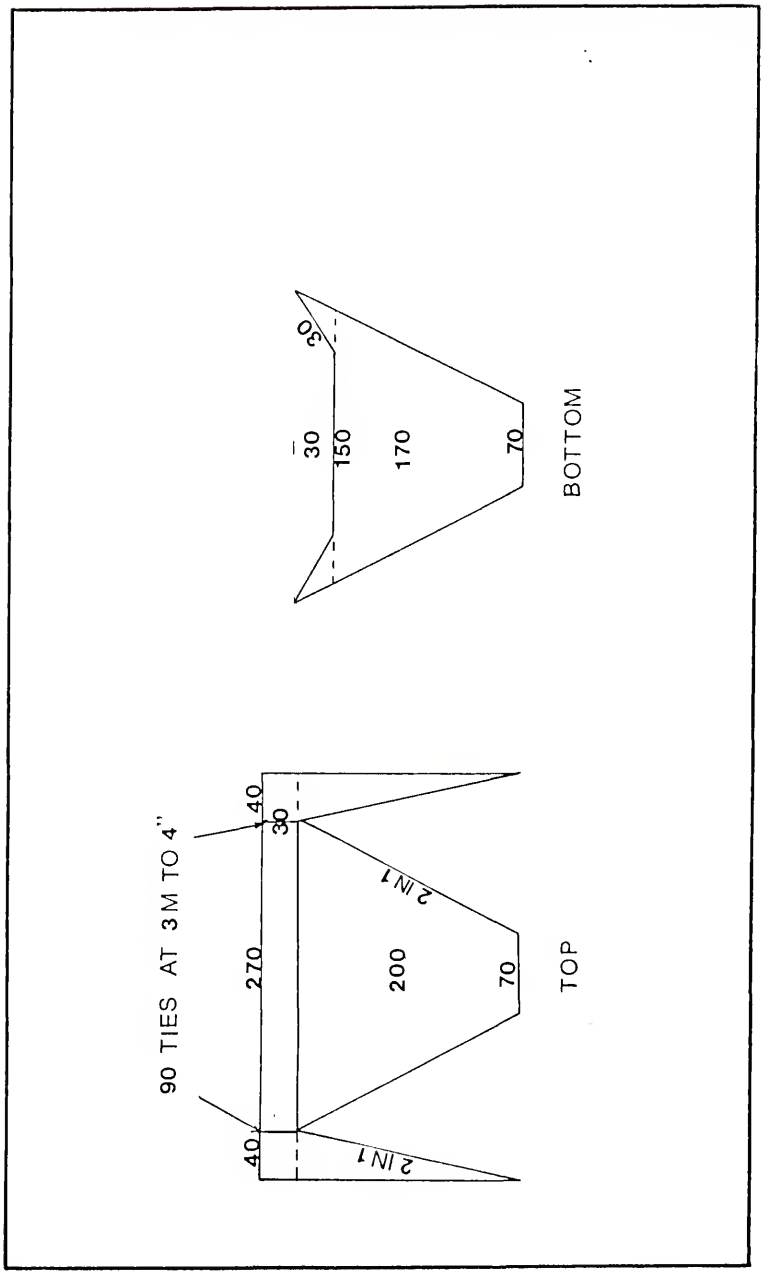

Figure 8.4. Prototype net for beam trawl.

8.4 Model and Field Experiments

In order to test the efficiency of the beam trawl to find the reduction in drag compared to the otter door trawl, a model of the designed beam trawl was built and tested in the flume. The basic length scale ratio is equal to 15.2. All other ratios are the same as for the otter door model and are summarized in Table 6.1. The model was built according to these scale ratios and the net diagram (Fig. 8.5). Cotton webbing of No. 9 thread with a 1-in stretched mesh was used in making the net. The dimensions of the model beam and the head were obtained by dividing the corresponding prototype dimensions by the length scale ratio.

8.4.1 Test Procedure and Results

The model beam trawl was tested in the flume by the same procedure adopted for testing the otter door trawl, as has been described in section 6.4. However, in this case, only the warp tensile force was measured. The height and spread of the net were fixed by the beam. The tensile forces were measured for different towing speeds with a 300-gram load cell. The values of the forces and the speeds are tabulated in Table 8.1. The model results of the beam trawl are projected to the prototype results in Table 8.1.

In order to compare the efficiency of the beam trawl with that of the otter door trawl, field tests were conducted in shallow water near St. Andrew Sound, southern Georgia. The trawler "Golden Isles," which has a double rig, was used.

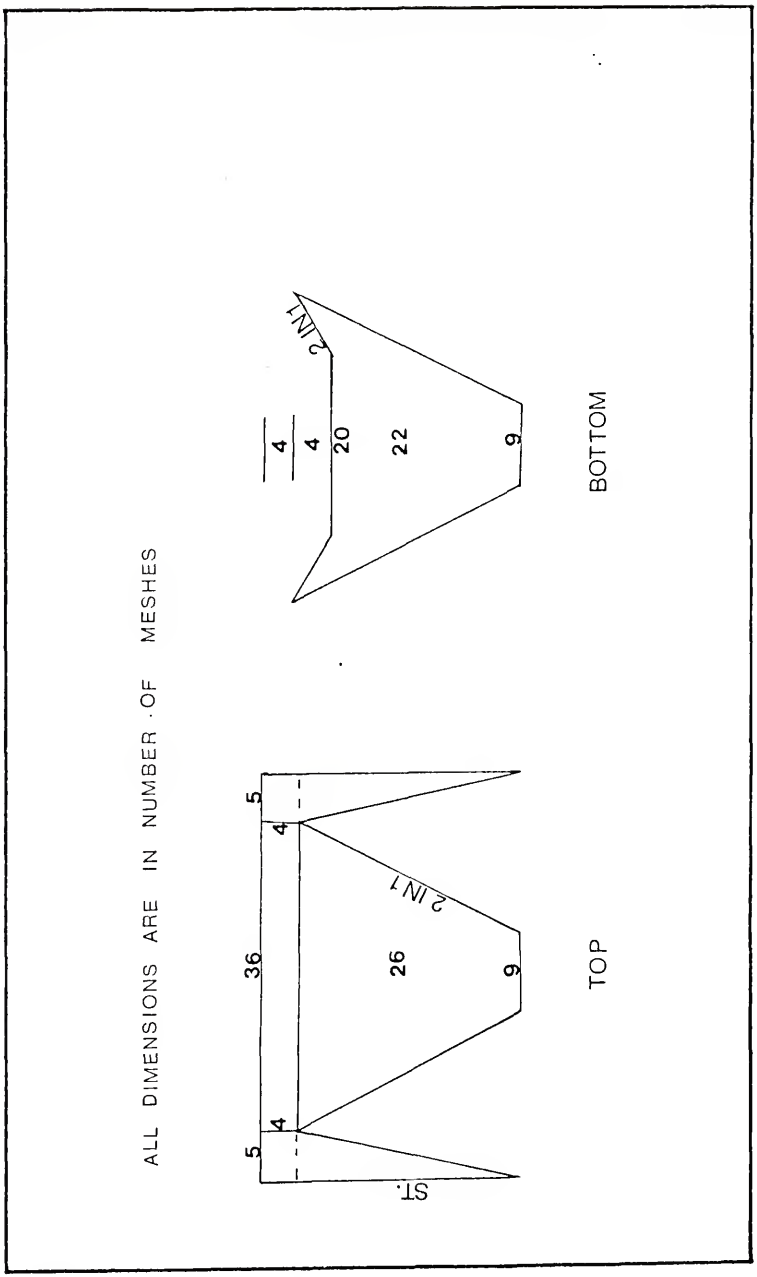

Figure 8.5. Model net diagram for beam trawl.

TABLE 8.1

MODEL TEST RESULTS OF BEAM TRAWL

Model Results		Projected to Prototype		
Velocity (fps)	Warp Tensile Force (gm)	Velocity (fps)	Velocity (knots)	Force (lb)
0.465	138.24	1.81	1.07	1101
0.642	200.00	2.50	1.48	1593
0.763	214.00	2.98	1.77	1705
0.932	220.00	3.63	2.15	1753
1.082	280.40	4.22	2.50	2234
1.207	360.00	4.71	2.79	2868

The beam trawl was attached to the port side rig of the trawler as shown in Figure 8.6. An otter door trawl was attached to the starboard rig. The net used for the otter door trawl was the same 50 ft flat net with 18 floats as was used in the previous field tests of the otter door trawl. The door size was 8' × 40" with a 1-in thick iron shoe. The trawler speed was measured with an Ott current meter, model V, and varied by changing the engine rpm of the trawler. The tensile force in the warps was measured with bolt load cells (Fig. 5.5) and recorded on a strip chart recorder. The door-spread was measured by means of triangulation as described in section 5.3.5. Table 8.2 summarizes the results of the field tests.

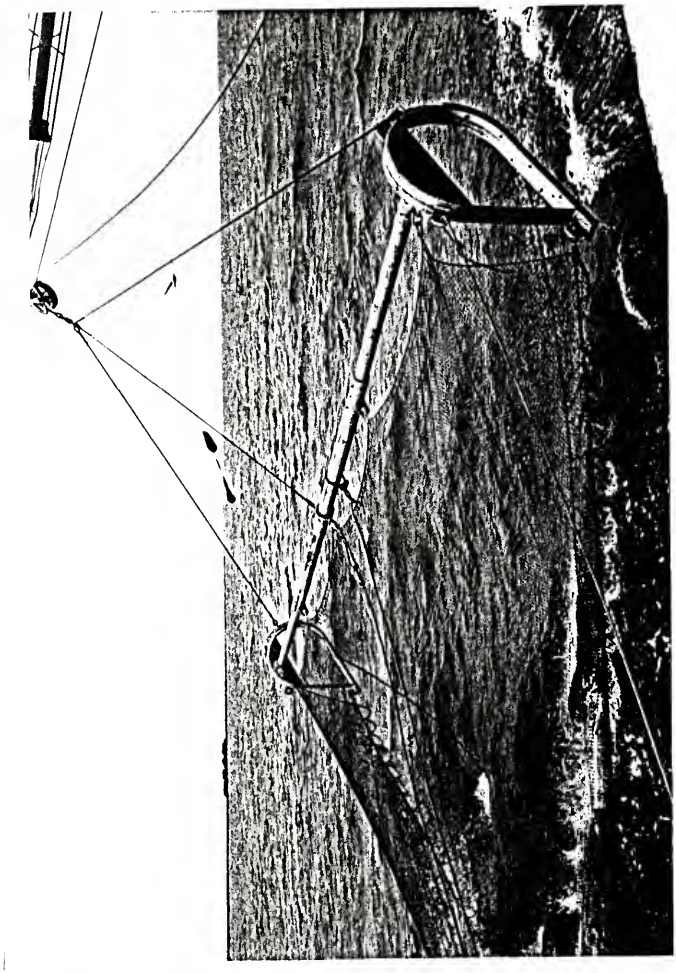

Figure 8.6. Ocean testing of beam trawl.

TABLE 8.2

RESULTS OF FIELD EXPERIMENTS

Velocity (fps)	Velocity (knots)	Force Beam (lb)	Force Otter Door (lb)	Spread Beam (ft)	Spread Otter Door (ft)
2.40	1.42	1398	1731	30	17.0
2.56	1.52	1595	1978	30	21.8
2.98	1.77	1669	2406	30	34.7

8.5 Discussion of Results

The results of the field tests show that the beam trawl can be towed with less drag than an otter door trawl. In order to compare the efficiencies between the two trawls, it is necessary to keep the net spread constant. The net spread is an important parameter in a fishing operation since the catch is proportional to the covered ground area. In Figure 8.7, the net spread for the otter door trawl is plotted against the trawler speed. From this relation, the towing speed, which will give a net spread of 30 ft, is found to be 2.84 fps.

Figure 8.8 shows the relationship between the warp tensile force and the towing speed of 2.84 fps is 2240 lb, while the corresponding value for the beam trawl is 1700 lb (see Fig. 8.9). Figure 8.9 also shows that the projected and observed values of field tests are in good agreement with each other.

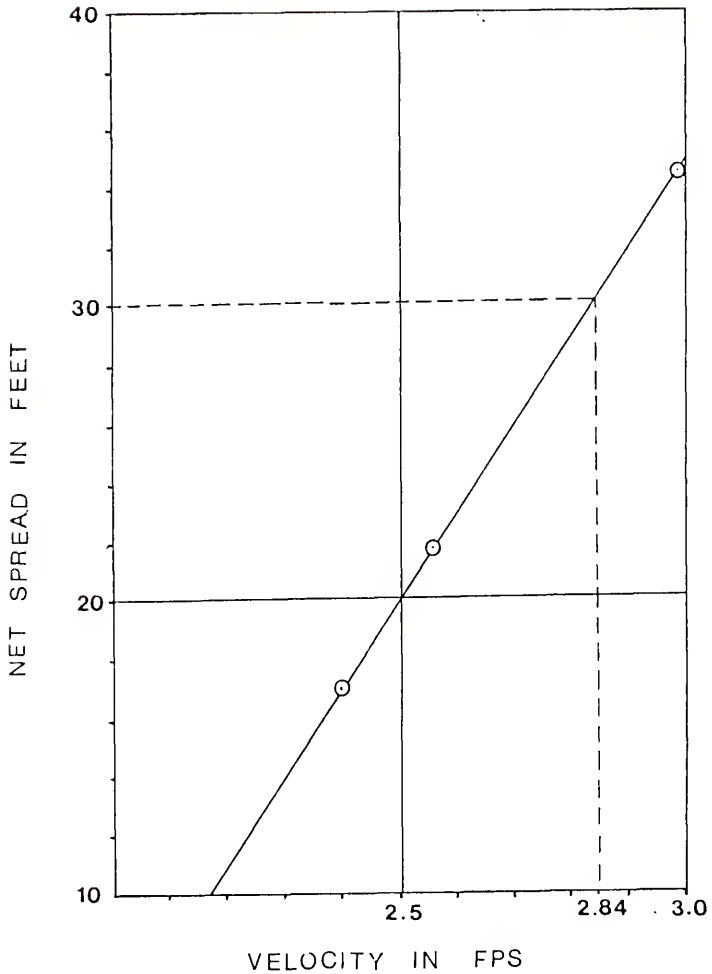

Figure 8.7. Relationship between net spread and trawler speed for otter door trawl.

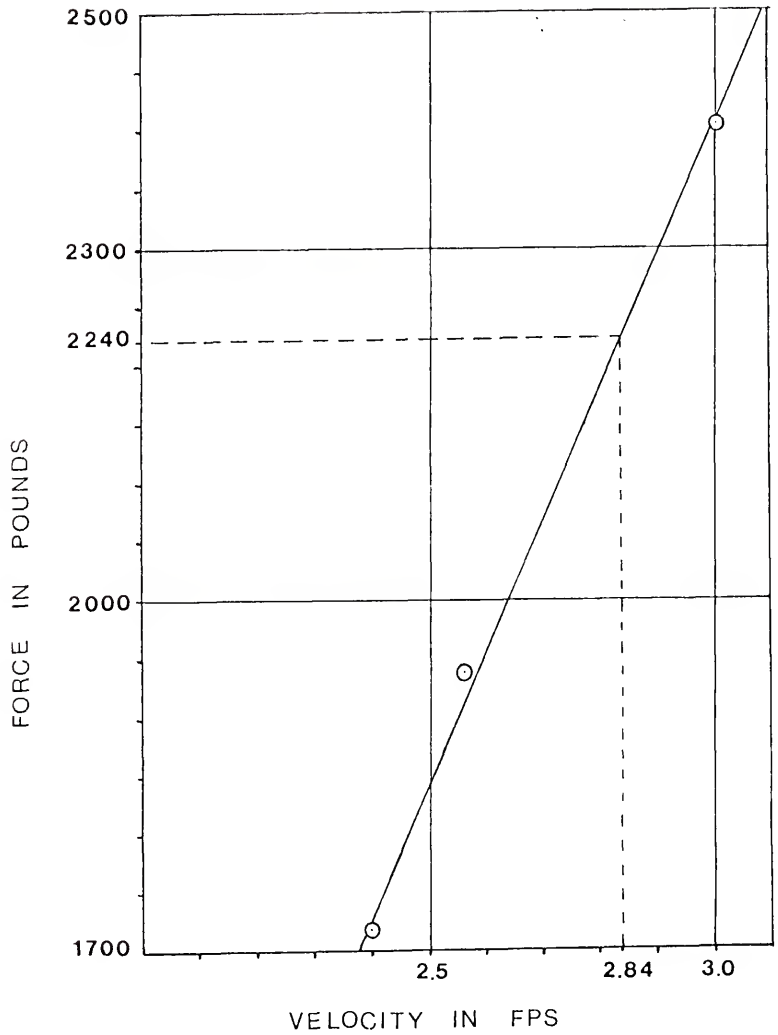

Figure 8.8. Relationship between warp tensile force and trawler speed for otter door trawl.

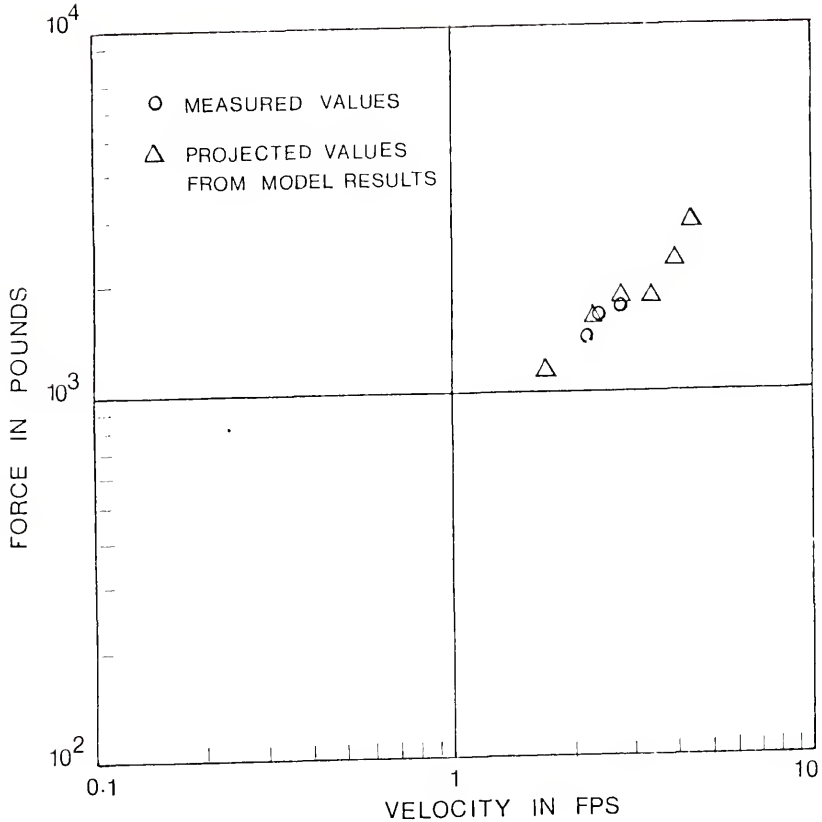

Figure 8.9. Relationship between warp tensile force and trawler speed for beam trawl.

The power P, required to pull the trawl, is calculated by the expression:

$$P = \frac{T_1 V}{33,000} \sqrt{1 - \left(\frac{D_w}{L_c}\right)^2} \qquad (8.8)$$

where

T_1 = Tension in cable in lb

D_w = Depth of water in ft

L_c = Length of towing cable

V = Velocity in ft/min

For the beam trawl,

$$P = \frac{(1700)(2.84)(60)}{33,000} \sqrt{1 - \left(\frac{28}{210}\right)^2}$$

$$= 8.70 \text{ hp}$$

and, for the otter door trawl,

$$P = 11.46 \text{ hp}$$

Therefore, by using a beam trawl instead of an otter door trawl, the power required to pull the trawl is reduced by 24 percent and the fuel saving should be substantial.

8.5.1 Conclusion

The results of the field tests show that the model approach can be effectively used in designing a new trawl.

Onshore field tests of the beam trawl indicate that the designed trawl is more efficient than an otter door trawl. Further tests of the beam trawl in deep water are necessary to evaluate the sea worthiness of the beam trawl.

CHAPTER 9

CONCLUSIONS AND RECOMMENDATIONS

Taking the stress-strain characteristics of the net materials into consideration, a new set of model laws were developed to simulate the flow around nets and trawls. Model experiments conducted in the flume yielded results comparable to those of the field tests, thereby confirming the validity of the developed model laws. Results of the model experiments also indicated that the uniform velocity profiles in the prototype must be modeled with similar uniform profiles in the flume in order to obtain the correct numerical transfer of model observations to the prototype conditions.

The model approach is well suited for development of new types of trawls as demonstrated by the design of a beam trawl for harvesting deep-water shrimp. The designed beam trawl can be towed with substantially less drag compared to an otter door trawl, thus reducing the fuel consumption of the trawler.

As discussed in Chapter 7, the existing numerical method for predicting the drag force acting on the net is not adequate. Further work is necessary to develop an equation which estimates the drag force acting on the belly. At present, model experiments conducted with a movable bed seem to be the only reliable method of testing fish nets.

APPENDIXES

The following abbreviations are used to denote the name of the journals.

B.F.C. - Bulletin of the Fisheries Research Board of Canada

B.F.H. - Bulletin of the Faculty of Fisheries, Hokkaido University

B.F.N. - Bulletin of the Faculty of Fisheries, Nagasaki University

B.S.F - Bulletin of the Japanese Society of Scientific Fisheries

B.T.L. - Bulletin of Tokai Regional Fisheries Research Laboratory

D.H.Z. - Deutsche Hydrographische Zeitschrift

F.F.B. - FAO Fisheries Bulletin

F.I.S. - Fishery Investigation (Supplementary Report), The Imperial Fisheries Experimental Station

J.A.P. - Journal of Applied Physics, Japan

J.F.I. - Journal of the Imperial Fisheries Institute

J.K.C. - Journal of the Kagoshima Fisheries College

J.O.S. - Journal of the Oceanographic Society of Japan

J.T.F. - Journal of the Tokyo University of Fisheries

M.A.K. - Memoirs of the College of Agriculture, Kyoto University

M.F.G.W. - Modern Fishing Gear of the World

M.F.K. - Memoirs of the Faculty of Fisheries, Kagoshima University

P.P.C. - Progress Report of the Pacific Coast Station

R.E.M. - Report of the U.S. Experimental Model Basin

R.T.M. - Report of the David W. Taylor Model Basin

R.U.M. - Report of the Faculty of Fisheries, Prefectural University of Mie

T.G.K. - Teiti-Gyogyo-Kai (The World of the Fixed Net Fisheries)

T.R.F. - Technical Report of Fishing Boat

APPENDIX A

BIBLIOGRAPHY ON CHARACTERISTICS OF FISHING TWINES AND THEIR TESTING

Arzano, R. 1959. "Man-made fibres." M.F.G.W., p. 13.

Carrothers, P. J. G. 1959. "The physical properties of netting and twines suitable for use in commercial fishing gear." M.F.G.W., p. 69.

E. I. Du Pont de Nemours and Co. 1959. "Synthetic fibres in the fishing industry." M.F.G.W., p. 147.

Imperial Chemical Industries, Ltd. 1959. "'Terylene' polyester fibre and its relation to the fishing industry." M.F.G.W., p. 43.

Japan Chemical Fibres Association. 1959. "The manufacture and testing of synthetic yarns and fibres used in Japanese fishing gear." M.F.G.W., p. 62.

Klust, G. 1959. "The efficiency of synthetic fibres in fishing, especially in Germany." M.F.G.W., p. 139.

Klust, G. 1964. "Standardization of terminology and numbering systems for netting twines." M.F.G.W., p. 3.

Kureha Kasei Co., Ltd. 1959. "Krehalon fishing nets." M.F.G.W., p. 57.

Lonsdale, J. E. 1959. "Nylon in fishing nets." M.F.G.W., p. 30.

Percier, A. 1959. "Specification of fishing gear." M.F.G.W., p. 260.

Reuter, J. 1959. "Some physical properties of manila rope." M.F.G.W., p. 59.

Reuter, J. 1959. "Testing of materials used in fishing." M.F.G.W., p. 82.

Shimozaki, Y. 1959. "Characteristics of synthetic twines used for fishing nets and ropes in Japan." M.F.G.W., p. 19.

Stutz, H. 1959. "Lateral strength and knot firmness of synthetic twines for fishing purposes." M.F.G.W., p. 87.

The Teikoku Rayon Co., Ltd. 1959. "Teviron fishing nets." M.F.G.W., p. 55.

van Wijngaarden, J. K. 1959. "Testing methods for net twines and nets, especially those manufactured from synthetic materials." M.F.G.W., p. 75.

Warenzeichenverband, P. 1959. "The technological characteristics of perlon for fishing equipment." M.F.G.W., p. 34.

APPENDIX B

BIBLIOGRAPHY ON MODEL LAW

Baranov, F. I. 1960. "Tekhnika promyshlennogo rybolovstva" (Industrial fishing techniques). Pishchepromizdat.

Fridman, A. L. 1964. "Usloviya podobiya rybolovnykh orudii" (Similarity conditions for fishing gear). Trudy Kaliningradrybvtuza, No. 18, Kaliningradskoe knizhnoe izdatel'stvo.

Fridman, A. L. 1964. "Opredelenie uslovii podobiya rhybolovnykh orudii i osnovnye napravleniya dal'neishikh issledovanii dlya obosnovaniya metodiki modelirovaniya" (Determination of the similarity conditions of fishing gear and main trends in further research to substantiate the methods of modeling). Trudy Kaliningradrybvtuza, No. 17, Kaliningradskoe Knizhnoe izdatel'stvo.

Fridman, A. L. and A. D. Yu. 1964. "Zavisimost' polozheniyanitok, kanatov i setel v potoke zhidkosti ot velichiny obobshchennogo kriteriya Fruda" (Dependence of the position of the twines, ropes and nets in liquid flow on the generalized Froude number. Trudy Kaliningradrybvtuza, No. 17, Kaliningradskoe Knizhnoe izdatel'stvo.

Fridman, A. L. 1966. "O primenenii metodov podobiya dlya sovershenstvovaniya orudii lova" (Application of similarity methods for improving fishing gear). Rybnoe Khozyaistov, No. 6.

Fridman, A. L. and A. D. Yu. 1967. "Soprotivlenie rybolovnoi seti, perpendikulyarnoi potoku" (Resistance of the fishing net perpendicular to the water flow). Rhybnoe Khozyaistvo, No. 9 and 10.

Idel'chik, I. E. 1954. "Gidravlicheski soprotivleniya" (Hydraulic resistance). Gosenergoizdat.

Kawakami, T. 1961. "On the law of mechanical similarity for drift gillnet." B.S.F., 27:124.

Kawakami, T. 1961. "Rule of enlarging or reduction of the scale of fishing net" (in Japanese). Suisan Kagaku (Fishery Science), 3:12.

Kawakami, T. 1968. "Development of mechanical studies of fishing gear." M.F.G.W., pp. 175-184.

Minakov, A. P. 1941. "Osnovy mekhaniki niti" (Fundamentals of the mechanics of twine). Trudy Moskovskogo Tekstil'nogo Instituta.

Sedov, L. I. 1954. "Metody podobiya i razmernosti mekhanike" (Similarity methods and dimensional analysis in mechanics). Gosizdat tekhnikoteroreticheskoi literatury.

Stengel, H. and H. I. Fischer. 1964. "Ergebnisse von stromunghtechnischen." Untersuchungen an Schleppnetzmodellen im Windkanal. Fischerei-Forschung, No. 1.

Tauti, M. 1934. "The force acting on the plane net in motion through the water." B.S.F., Vol. 3.

APPENDIX C

BIBLIOGRAPHY ON MODEL EXPERIMENTS

Parenthesized papers are written in Japanese. An asterisk before the title denotes that an English synopsis is given in addition to the Japanese text.

Dale, P. and S. Moller. 1964. "The development of a mid-water trawl." M.F.G.W., pp. 482-488.

Dickson, W. 1961. "A study relating models to commercial trawls." Marine Research, No. 1, Edinburgh.

Frey, K. and H. Sohle. 1934. "Model experiments with various forms of otter boards." Schiffbun, Schiffahrt and Hafenvau, Vol. 35.

Fujita, H. and T. Yokota. 1951. "The drag action on a net in a uniform current, I." J.A.P., 20:59.

Fujita, H. 1953. "The drag action on a net in a uniform current, II." M.A.K., 66:11.

Hamuro, C. 1954. *"A study of Danish seine by means of recording the height of entrance and direction of ground rope." B.S.F., 20:353.

Hamuro, C. and K. Ishii. 1956. *"Study on the automatic net depth meter, automatic net length meter for salmon gillnet and the results of measurement at sea." T.R.F., 8:29.

Hamuro, C. 1956. *"Study of the automatic net depth meter, net height meter for crab tangle net and its practical application." T.R.F., 8:183.

Hayashi, H. 1933. *"An investigation of a spreading device for trawling net." J.F.E., 3:37.

Honda, K. and Y. Matumoto. 1934. *"Model experiment on the sea fixed net for fishing amber-fish." B.S.F., 12:91.

Honda, K. and collaborators. 1955. "Model experiments on fixed nets for amber-fish, Seriora, used in the coast of Mie Prefecture." J.T.F., 41:195.

Hosino, S. and N. Sato. 1941. ("An experiment on the forms of the fishing net piece in the air currents.") F.I.S., 8:1.

Iitaka, Y. 1954. "Model experiments on the sardine purse seine operating in Hiuganada, I." B.S.F., 20:571.

Iitaka, Y. 1955. "Model experiments on the sardine purse seine operating in Hiuganada, II." B.S.F., 21:6.

Iitaka, Y. 1955. "Model experiments on the sardine purse seine operating in Hiuganada, III." B.S.F., 21:459.

Iitaka, Y. 1956. "Model experiments on the sardine purse seine operating in Hiuganada, IV." B.S.F., 22:389.

Imamura, Y. 1942. ("Model experiment of the British herring trawl.") B.S.F., 10:221.

Imamura, Y. 1942. ("Model experiments on a trawl net.") B.S.F., 11:61.

Inoue, M. 1954. "Model experiments on a sardine ringnet." B.S.F., 19:942.

Isouti, N. and T. Kawakami. 1957. "Mechanical characteristics of plate depressor for trolling." B.S.F., 23:354-356.

Isouti, N. and T. Kawakami. 1957. "Mechanical studies on the trolling gear, I. Estimation of the fishing depth." M.A.K., 76:1.

Kanamori, M. 1950. *"A tentative experiment on the improvement of yellow-tail setting net" (preliminary report). J.K.C., 1:4.

Kanamori, M. and S. Enami. 1952. *"Studies on the improvement of yellow-tail setting net on the model experiment of mid-layer trap-net, I." M.F.K., 2:2.

Kawakami, T. and H. Tubota. 1953. "On the configuration and distribution of tension of a rope in a uniform stream." M.A.K., 66:1.

Kawakami, T. 1953. "Mechanical action of the otter board of the trawl net." B.S.F., 19:228.

Kawakami, T. 1955. "Equilibrium configuration of a rectangular strip of net subjected to a uniform current." M.A.K., 72:1.

Kawakami, T. 1955. "Mechanical characters of the drag net." M.A.K., 72:5.

Kawakami, T. and K. Nakasai. 1962. "On the mechanical character of the drag net, II." B.S.F., 38:664-670.

Kobayashi, K. H. Takahashi, and M. Ueno. 1954. *"Fundamental studies on spherical glass floats for fishing nets, II: On the water resistance of glass floats." B.F.H., 4:348.

Kobayashi, K. 1956. *"An experiment on a mid-water trawl, IV: On its mechanism and a trial practice." B.F.H., 7:21.

Koga, S. 1955. *"On the extension of the wing of trawl net." B.F.N., 3:15.

Koike, A. 1953. *"Model experiments on a Teiso-hikiami (trawl net)." B.S.F., 19:8.

Kumarkori, T. and K. Ishii. 1954. *"Automatic net-height meter and automatic ground rope indicator for two-boat trawler and results of experiment for these apparatuses." T.R.F., 5:73.

Kumakori, T., C. Hamuro, and K. Ishii. 1955. *"Automatic net-height meter and automatic ground rope indicator for trawler and results of experiments for these apparatuses." T.R.F., 6:41.

Matunda, K. and T. Kawakami. 1968. "Experimental verification for similarity law on distorted model net." B.S.F., 34:23.

Miyamoto, H. 1934. *"The excess buoyance of gillnet and the tension of them." B.S.F., 3:147.

Miyamoto, H., M. Nomura, and Y. Shimozaki. 1952. *"Resistance of plane net against the flow of water, I: Effect of knot type on the resistance of net." B.S.F., 17:249.

Miyamoto, H. and M. Nomura. 1953. *"Resistance of plane net against the flow of water, II: Effect of different shapes of the mesh upon the resistance." B.S.F., 18:327.

Miyamoto, H. 1936. *"The model experiments on drifter drag net for fishing 'Sirauwo' in Lake Kasumigaura." B.S.F., 4:310.

Miyamoto, H. 1936. *"The model experiments on sailing trawl net used in Mikawa Bay." B.S.F., 4:391.

Miyamoto, H. 1936. *"Model experiments on trawl nets." B.S.F., 5:19.

Miyamoto, H. 1935. *"The form of amber-fish keddle net on the basis of model experiments." B.S.F., 4:153.

Miyamoto, H. 1936. *"Model experiments on sea fixed nets for fishing amber-fish, Seriola, I: Ettyu keddle net and ordinary keddle nets." B.S.F., 5:158.

Miyamoto, H. 1936. *"Model experiments on sea fixed net for fishing amber-fish, Seriola,II: Trap nets set on the fishing grounds under strong tidal currents." B.S.F., 5:227.

Miyamoto, H. 1937. *"Model experiments on sea fixed net for fishing amber-fish, Seriola, III: Trap nets." B.S.F., 5:361.

Miyamoto, H. 1937. *"Model experiments on sea fixed net for fishing amber-fish Seriola, IV: Keddle nets and trap net." B.S.F., 6:311.

Miyamoto, H. 1939. *"Model experiments on sea fixed net for fishing amber-fish, Seriola, V: The relation between the weight of sinkers and the deformation of amber-fish nets subjected to various currents." B.S.F., 7:319.

Miyamoto, H. 1941. *"Model experiments on sea fixed net for fishing amber-fish, Seriola, VI: Fishing gear in relation to the current prevailing on the fishing ground." B.S.F., 9:181.

Miyamoto, H. 1947. *"Model and full scale experiment on set net. Preliminary report, I: Double trap net for cod." B.S.F., 13:51.

Miyamoto, H. 1948. *"Model and full scale experiment on set net. Preliminary report, II: Double trap net for cod." B.S.F., 13:263.

Miyamoto, H. 1948. *"Model and full scale experiments on set net. Preliminary report, III: Trap net for sardine." B.S.F., 14:31.

Miyamoto, H. 1951. *"Study on the set-net." B.T.L., 2:1.

Miyazaki, T. 1939. *"Model experiments on fixed nets for fishing salmon in Kamchatka." B.S.F., 8:129.

Miyazaki, T. 1942. ("Model experiment on the leading net.") B.S.F., 11:287.

Miyazaki, T. 1942. ("Model experiment on a leading net, II.") B.S.F., 10:63.

Miyazaki, T. 1942. ("Model experiment on a fixed net.") B.S.F., 11:101.

Mori, Y. 1942. *"Model experiment on the sea fixed net for fishing amber-fish." B.S.F., 10:278.

Nakasai, K. and T. Kawakami. 1968. "On effect of edge boards attached to tips of plate depressor." B.F.N.

Narasako, Y. and M. Kanamori. 1964. "A large-sized experimental tank of twin symmetric elliptical circuits." M.F.G.W., pp. 205-208.

Nomura, M. and Y. Nozawa. 1955. *"Resistance of plane net against the flow of water, IV: On the inclination of threads in a current." B.S.F., 20:762.

Nomura, M. and K. Mori. 1956. *"Resistance of plane net against flow of water, III: Effect of kind of fibres on the resistance of net." B.S.F., 21:1100.

Nomura, M. and K. Mori. 1956. *"Resistance of plane net against flow of water, V: On the inclination of net in a current." B.S.F., 21:1114.

Nomura, M. 1951. *"Model experiments on two boat type trawl net." B.S.F., 16:347.

Nomura, M. and T. Yasui. 1953. *"Model experiments on trawl nets of various types." B.S.F., 18:727.

Ogura, M. 1954. *"Model experiment on a Tyuso-hikiami (trawl net)." B.S.F., 20:259.

Okuno, H. 1936. *"Model experiment on plates to sink an end of a trawl rope below the water surface or hydrofoil sinker." B.S.F., 5:155.

Okabe, G. 1938. *Model experiments of a fishing net, Anko-ami." B.S.F., 6:305.

Pack, Y. 1957. *"A model experiment of sardine trap net 'Hisago-ami'." B.S.F., 22:657.

Pack, Y. 1956. "Model experiments on a saury blanket net (Bouke-ami), I." B.S.F., 21:978.

Saito, T. 1941. *"Model experiments on the two kinds of sea bottom fixed nets for fishing 'Tara'." B.S.F., 2:185.

Saito, T. and H. Simizu. 1941. "Model experiments on 'Teguri-ami', a dragnet, for fishing 'Tara'." B.S.F., 10:11.

Sato, N. 1934. ("An experiment on the use of a surface trawl net.") F.I.S., 1:1.

Sato, N. 1943. ("An experiment with models of a surface seine net.") F.I.S., 9:35.

Sato, N. 1933. *"On a tank experiment with seine nets." J.F.E., 3:49.

Sato, N. 1943. ("An experiment with models of a surface seine net.") F.I.S., 9:35.

Sato, N. and I. Takayama. 1933. *"Experiments on hydrofoil sinker for a troll line." J.F.I., 3:73.

Sato, N. and S. Kurita. 1943. ("An experiment on the resistance and life for a float of a seine net.") F.I.S., 9:1.

Simizu, H. 1941. *"Model experiments on the sea bottom fixed nets for fishing 'Tara'," B.S.F., 9:191.

Sugano, S. 1936. *"The model experiments on fixed nets for fishing salmon in Kamchatka." B.S.F., 4:397.

Sugano, S. 1936. *"Experiments with models of a surface trawl net for fishing salmon." B.S.F., 5:12.

Takayama, S. and T. Koyama. 1964. "Increasing the opening height of a trawl net by means of a kite." M.F.G.W., pp. 185-195.

Uno, M. 1935. "The form and the tension on pursuing line, a mackerel ring-netused at Kosaito, Tyosen, as known by a model experiment." B.S.F., 4:147.

Walderhang, H. A. and A. Akre. 1962. "First IF report on otter board tests: The Norwegian ship model experiment tank." Proc. of IF Meeting, Hague.

Wang, Y. 1937. "Model experiments of Genziki-ami, a king of net for fishing shrimp." B.S.F., 5:369.

APPENDIX D

BIBLIOGRAPHY ON PROTOTYPE EXPERIMENTS

Parenthesized papers are written in Japanese. An asterisk before the title denotes that an English synopsis is given in addition to the Japanese text.

Baird, R. H. 1959. "Factors affecting the efficiency of dredges." M.F.G.W., p. 223.

Barraclough, W. E. and W. W. Johnson. 1956. "A new mid-water trawl for herring." B.F.C., p. 104.

Beardsley, A. J. and W. L. High. 1971. "Development of sorting trawls for use in the Pacific northwest shrimp fishery." Bureau of Comm. Fish., Expl. Fish & Gear Res. Base, Seattle, Washington.

Ben-Yami, M. 1959. "Study of the Mediterranean trawl net." M.F.G.W., p. 213.

Buckingham, H. 1973. "Design of trawls." World Fishing, Part 5, p. 48.

Carruthers, J. N. 1959. "Simple devices for studying the geometry of various gears and for relating some commercial fishing operations to the existing water movements. M.F.G.W., p. 254.

Chickamasa, H. and I. Kenji. 1959. "Studies on two-boat trawls and otter trawls by means of measuring instruments." M.F.G.W., p. 234.

Chickamasa, H. 1964. "Towing power, towing speed and size of bull trawl." M.F.G.W., p. 199.

Chickamasa, H. 1964. "Development of an improved otter trawl gear." M.F.G.W., p. 191.

de Boer, E. J. 1973. "Beam trawling: A study on the resistance of a beam trawl and measurement of the forces acting upon the rigging." Afdeling Technisch Onderzoek, Directie van de Visserijen.

Dickson, W. 1964. "Some comparative fishing experiments in trawl design." M.F.G.W., p. 165.

Fridman, A. L. and A. Danilov. 1967. "Yu ob osobennostyakh soprotivleniya rybolovnoi seti" (The special features of the resistance of the fishing net). Rybnoe Khozyaistvo.

Holmsen, A. 1967. "Comparative testing of mid-water rigs on small draggers." Dept. of Food and Res. Eco., Col. of Agri., University of Rhode Island, Kingston.

Kawakami, T. and Y. Iitaka. 1955. "On a simple instrument, Siomiito, for detecting underwater current. B.S.F., 20:962.

Ketchen, K. S. 1951. "Preliminary experiments to determine the working gape of trawling gear." P.P.C., 88:62.

Khanzohonkov, V. I. 1944. "Soprotivlenie setok" (Resistance of nets). Promyshlennaya Aerodinamika.

Kobayashi, K. and H. Takahashi. 1951. *"A study of fishing trawloperated in any depth of sea-water." B.F.H., 1:139.

Kobayashi, K. and H. Takahashi. 1951. *"A study on fishing trawl operated in any depth of sea-water: On the relations between the length of warp and the frontage of otter board." B.F.H., 2:86.

Kobayashi, K. and T. Deguchi. 1952. *"An experiment of a beam-type trawl net for fish larvae at the various depths of sea-water." B.F.G., 3:104.

Kumakori, T., C. Hamuro, K. Ishii, and O. Furuya. 1952. ("Catch gauge for two boat trawl.") T.R.F., 3:139.

Kumakori, T. and K. Ishii. 1952. ("Experiments on manufacturing of remote control towing thermometer for mid-water.") T.R.F., 3:159.

Kumakori, T., C. Hamuro, K. Ishii, and O. Furuya. 1953. ("Catch gauge for two boat trawler.") T.R.F., 4:112.

Luigi, C. 1959. "Studies to improve the efficiency of otter boards and trawl floats." M.F.G.W., p. 251.

Masaji, K. 1959. "A research on setnets." M.F.G.W., p. 256.

Miyamoto. H. 1959. "On the relation between otter trawl gear and towing power." M.F.G.W., p. 241.

Miyazaki, T. 1952. "Preliminary report on experiments with small trawl nets, I." R.U.M., 1:215.

Miyazaki, T. 1952. "Preliminary report on experiments with small trawl nets, I: Change in the height of square part of the mouth of the net with changes in tension of the rope of the net. R.U.M., 1:223.

Miyazaki, T. 1953. *"The relation between the mouth height of the square part of small trawl net and its pulling velocity." B.S.F., 19:223.

Nakasai, K. and T. Kawakami. 1968. "Mechanical studies on the mid-water trawl gear in operation." B.F.N.

Nicholas, E. 1964. "Suggestions for improved heavy trawl gear." M.F.G.W., p. 204.

Okonski, O. and S. Sadowski. 1959. "The headline, the footrope and their influence on the mouth of the trawl." M.F.G.W., p. 196.

Phillips, J. 1959. "The mouth of the trawl." M.F.G.W., p. 200.

Pode, L. 1950. "An experimental investigation of the hydrodynamic forces on stranded cables." R.T.M., p. 713.

Pode, L. 1951. "Tables for computing the equilibrium configuration of a flexible cable in a uniform stream." R.T.M., p. 687.

Pode, L. 1956. "Configuration and tension of a light flexible cable in a uniform stream." R.T.M., p. 717.

Sand, R. F. 1959. "Mid-water trawl design by underwater observations." M.F.G.W., p. 209.

Scharfe, J. 1959. "The use of echo-sounding as a means of observing the performance of trawling gear." M.F.G.W., p. 241.

Taber, R. E. 1970. "The dynamics of European wing trawls." University of Rhode Island, Marine Leaflet Series, #3.

Takayama, S. and T. Koyama. 1959. "Increasing the opening weight of a trawl net by means of a kite." M.F.G.W., p. 185.

Taniguchi, T. 1955. *"On the resistance of various fixed in a stream, I." B.S.F., 21:291.

Taniguchi, T. 1955. *"On the resistance of various fixed in a stream, II." B.S.F., 21:969.

Taniguchi, T. 1956. *"On the resistance of various fixed in a stream, III." B.S.F., 21:1107.

Taniguchi, T. 1957. *"On the resistance of various fixed in a stream, IV." B.S.F., 22:727.

Tauti, M., T. Miura, and K. Sugii. 1925. "Resistance of plane net in water. J.F.I., 21:11.

Tauti, M. 1930. ("Holding power of anchors.") T.G.K., 11:16.

Terada, T., I. Sekine, and T. Nozaki. 1915. ("Study on the resistance of fishing net against the flow of water.") J.F.I., 10:1.

Thews, J. G. and L. Landweber. 1936. "On the resistance of a heavy flexible cable for towing a surface float behind a ship." R.E.M., p. 418.

Thews, J. G. and L. Landweber. 1936. "The tension in a loop of cable towed through a fluid." R.E.M., p. 422.

Treschev, A. I. 1964. "Development of Soviet trawling techniques." M.F.G.W., p. 206.

U. S. Department of Commerce. 1971. "Progress reports on recent studies in developing a shrimp sorting trawl for use in Pacific northwest waters." Exploratory Fishing Gear Res. Base, Nat'l Marine Fish. Service, NAOAA, Seattle, Washington.

Verhoest, J. and A. Maton. 1964. "Double-rig shrimp beam trawling." M.F.G.W., p. 209.

APPENDIX E

CALCULATION OF FISHING NET DRAG BY THE NUMERICAL METHOD DEVELOPED BY KOWALSKI AND GIANNOTTI (1974)

The results of the field studies are used in the following to check the validity of the numerical method of computing fish net drag. Only a brief summary of the method pertinent to the present study is described. Other details are enumerated by Kowalski and Giannotti (1974). They assume that the total drag force acting on a net is comprised of the resistances of: (1) the cod end, (2) the belly, (3) the headrope (4) the footrope and (5) the floats.

$$F_{net} = F_{cod} + F_{belly} + F_{ropes} + F_{floats} \qquad (E.1)$$

where

F = Resistance

The resistances of the components of the net are computed by equations given in sections 2.1 and 2.2 as summarized below:

$$F_{cod} = (0.82)\left(\frac{\rho V^2}{2}\right)\left(\frac{\pi}{4} d_{cod}^2\right) n_1 + C_f \cdot \frac{\rho V^2}{2} \times \left(N_b \pi MD + N_k \pi D_k^2\right)\left(1 - n_1\right)$$

$$F_{belly} = C_{D\ panel} \left(\frac{\rho V^2}{2}\right) \left(S\pi ab\right) \left(1 - k_1\right)$$

$$F_{rope} = C_{D\ rope} \sin^3 \alpha \left(\frac{\rho V^2}{2}\right) H_r \ell_r$$

$$F_{float} = N_f\ C_{D\ float} \left(\frac{\rho V^2}{2}\right) A_p$$

All the symbols in the above equations have been defined in Chapter 2. For the Burbank Flat Net (Fig. 5.1), the above equations are used to calculate the drag forces.

E.1 Cod End

The surface area of a cod end with 178 meshes by 120 meshes is 23.11 ft^2. For time $t > 0$, $n_1 = 1$ and, therefore,

$$F_{cod} = \left(0.82\right)\left(\frac{1.988}{2}\right) V^2 \left(23.11\right) = 18.84\ V^2$$

$$F_{cod} = 18.84\ V^2 \qquad (E.2)$$

E.2 Belly

The solidity S for a 2 in mesh and a 0.06 in thick twine is calculated from Equation (2.13) and is equal to 0.146. The value of $C_{D\ panel}$ is 1.8 (from Equation (2.14)). For the flat net, the k_1 value is found to be as follows:

$$k_1 = \frac{6.626}{a}$$

Therefore,

$$F_{belly} = \left(1.8\right)\left(\frac{1.988}{2}\right) V^2 \left(0.146\right)\left(\pi ab\right)\left(1 - \frac{6.626}{a}\right)$$

$$F_{belly} = \left(0.82\right)\left(abV^2\right)\left(1 - \frac{6.626}{a}\right) \qquad (E.3)$$

where 2a and 2b are the door spread and net height, respectively.

E.3 Ropes

The resistances of the ropes to the flow are due to the drag of the headrope and footrope and the frictional resistance of the footrope to the ground. The values of H_p are equal to 0.5 in for both ropes. Assuming an angle of attack of 90°, the drag on the ropes is calculated as:

$$F_{rope} = \left(1.1\right)\left(\frac{1.988}{2}\right) V^2 \cdot \frac{1}{24}\left(50 + 24\right)$$

$$F_{rope} = 5.10\ V^2 \qquad (E.4)$$

The frictional resistance of the footrope with the bottom is approximated by

$$F_{friction} = (1.25)\ W \qquad (E.5)$$

where

W = Weight of rope

The footrope weighs 25 lb and, therefore, a frictional force of 31 lb should be added to the F_{rope}.

E.4 Floats

The projected area of one float is 0.223 ft^2. Because the floats were grouped together, the drag coefficient of the floats is assumed to be 0.93 (as justified in section 2.2.2). Therefore, the drag force acting on 21 floats is:

$$F_{float} = \left[21\right]\left[0.93\right]\left[\frac{1.988}{2}\right] V^2 \cdot \left[0.223\right]$$

$$F_{float} = (4.33)\ V^2 \qquad \text{(E.6)}$$

Therefore, the resistance of the net for different towing speeds can be calculated from Equations (E.1) to (E.6). Table E-1 itemizes the resistances of individual components.

TABLE E-1

CALCULATION OF THE NET RESISTANCE

Run number	1	2	3	4	5	6
Velocity (fps)	2.75	3.59	3.74	2.41	3.06	3.69
Net spread (2a)(ft)	26.66	27.73	28.80	23.00	25.00	27.00
Mouth opening (2b)(ft)	4.50	3.50	2.50	12.58	10.33	8.08
F_{cod} (lb)	142.5	242.8	263.5	109.4	176.4	256.3
F_{belly} (lb)	93.5	133.9	111.5	146.0	232.9	310.0
F_{rope} (lb)	38.6	65.7	71.3	29.6	47.8	69.4
$F_{friction}$ (lb)	31.0	31.0	31.0	31.0	31.0	31.0
F_{float} (lb)	0	0	0	25.1	40.5	59
F_{net} (computed)(lb)	305.6	473	477.3	341.7	528.6	725.7
F_{net} (measured)(lb)	450	800	1300	600	1100	1600

REFERENCES

Carrothers, P. J. G. and Baines, W. D. 1975. "Forces on screens inclined to fluid flow," Journal of Fluids Engineering, American Society of Mechanical Engineers, 1:116.

Christensen, B. A. 1975a. "Models and analogs," class notes of CE 624, Department of Civil Engineering, University of Florida.

Christensen, B. A. 1975b. "Sediment transport," class notes of CE 623, Department of Civil Engineering, University of Florida.

Christensen, B. A. and Snyder, R. M. 1975. "Physical modeling for scour initiation and sediment transport in distorted tidal models," Proceedings, Symposium on Modeling Techniques, American Society of Civil Engineers, p. 927.

Crewe, P. R. 1964. "Some of the general engineering principles of trawl gear design," Modern Fishing Gear of the World, p. 165.

Daily, J. W. and Harleman, D. R. F. 1966. Fluid Dynamics. Massachusetts: Addison-Wesley Publishing Company, Inc.

de Boer, P. A. 1959. "Trawl gear measurements obtained by underwater instruments," Modern Fishing Gear of the World, p. 225.

Dickson, W. 1959. "The use of model nets as a method of trawl gear," Modern Fishing Gear of the World, p. 166.

Dickson, W. 1971. "Trawl gear selection, design and construction in relation to fish behavior, vessel power and fishing conditions," Modern Fishing Gear of the World, pp. 336-347.

Fridman, A. L. 1973. "Theory and design of commercial fishing gear," U. S. Department of Commerce, National Technical Information Service, Springfield, Virginia.

Giannotti, J. 1973. A Model of Trawling Gear Interaction. Ph.D. thesis, Ocean Engineering, University of Rhode Island, Kingston.

Graf, W. 1971. Hydraulics of Sediment Transport. New York: McGraw-Hill Book Company, p. 385.

Hillier, A. 1974. Personal communication, University of Rhode Island, Kingston.

Kanamori, M. 1960. "On the physical analysis of the fixed fishing net resistance," Memoirs of the Faculty of Fisheries, Kagoshima University, 2:145.

Kawakami, T. 1959. "On the law of mechanical similarity for ropes of fishing nets," Bulletin of the Japanese Society of Scientific Fisheries, 10:795.

Kawakami, T. and Suzuki, O. 1959. "Studies on the kinetic behavior of the ground ripe of a trawl net 1," Bulletin of the Japanese Society of Scientific Fisheries, 6:413.

Kawakami, T. 1964. "The theory of designing and testing fishing nets in models," Modern Fishing Gear of the World, p. 471.

Kawakami, T. and Nakasai, K. 1968. "Theoretical derivation of characteristic curve of trawl nets," Memoirs of the Agriculture, College of the Agriculture, Kyoto University, Japan, No. 94.

Kowalski, T. and Giannotti, Jr. 1974. "Calculation of fishing net drag," Marine Technical Report No. 15, Sea Grant, University of Rhode Island, Kingston.

Miyake. 1927. "Research on the plane nets: Dragging resistance of plane net in water," Journal of Imperial Fisheries Institute (Japan), 2:125.

Motte, G. A. et al. 1973. "Bottom trawl performance study," Marine Technical Report Series No. 7, University of Rhode Island, Kingston.

Nicholls, J. 1964. "Trawl gear instrumentation and full scale testing," Modern Fishing Gear of the World, p. 147.

Nikuradse. 1933. "Gesetzmässigkeiten der turbulenten strömung in glatten rohren (Laws of turbulent flow in smooth pipes)," Verein deutscher Ingenieure, Forschungsheft No. 356, Berlin.

Revin, A. S. 1959. "Issledovanie vliyaniya struktury i formy tralovoi' setinaee soprotivlenie v potoke vody (Investigation of the effect of the trawl net structure and shape of its resistance in a water flow)," Trudy Vsesoyuznyi nauchnoissledovatel' skii institumorskogo rybnogo khozyaistva i okeanografii, Vol. 41, Pishchepromizdat, Russia.

Scharfe, J. 1959. "Experiments to decrease towing resistance of trawl gear," Modern Fishing Gear of the World, p. 245.

Schlitchting, H. 1968. Boundary Layer Theory. New York: McGraw-Hill Book Company, p. 32.

Streeter, V. L. 1961. Handbook of Fluid Dynamics. New York: McGraw-Hill Book Company, p. 13.

Suzuki, O. and Kawakami, T. 1960. "Studies on the kinematic behavior of the groundrope of the trawl net, II," Bulletin of the Japanese Society of Scientific Fisheries, 3:204.

Tauti, M. 1934. "A relation between experiments on model and full-scale of fishing net," Bulletin of the Japanese Society of Scientific Fisheries, 4:1.

Von Brandt, A. and Carrothers, P. J. G. 1964. "Test methods for fishing materials (Twines and netting)," Modern Fishing Gear of the World, p. 9.

Von Brandt, A. and Klust, G. 1971. "Synthetic net materials for bottom and midwater trawls," Modern Fishing Gear of the World, p. 318.

World Fishing. 1972. "After five years," May, p. 40.

BIOGRAPHICAL SKETCH

M. Krishnamurthy was born on May 4, 1945, in Srivilliputtur, Tamilnadu, India. He received the degree of Bachelor of Engineering in Civil Engineering in 1967 from the University of Madras. He entered the Indian Institute of Science, Bangalore, to pursue research work in hydraulic engineering and was awarded the degree of Master of Science in 1971 for his work on the erosion of cohesive soils.

Mr. Krishnamurthy came to the University of Florida in 1971 and worked as a graduate research assistant in the Coastal and Oceanographic Engineering Department until December, 1972. He obtained the degree of Master of Engineering from the University of Florida in August, 1972. Since 1973, Mr. Krishnamurthy has been specializing in the area of marine engineering as a graduate student in the hydraulics laboratory of the Civil Engineering Department.

Mr. Krishnamurthy is a member of the International Association for Hydraulic Research, American Society of Civil Engineers and the Marine Technology Society.

I certify that I have read this study and that in my opinion it conforms to acceptable standards of scholarly presentation and is fully adequate, in scope and quality, as a dissertation for the degree of Doctor of Philosophy.

B. A. Christensen
Professor of Civil Engineering

I certify that I have read this study and that in my opinion it conforms to acceptable standards of scholarly presentation and is fully adequate, in scope and quality, as a dissertation for the degree of Doctor of Philosophy.

Wayne C. Huber
Associate Professor of Environmental Engineering Sciences

I certify that I have read this study and that in my opinion it conforms to acceptable standards of scholarly presentation and is fully adequate, in scope and quality, as a dissertation for the degree of Doctor of Philosophy.

Z. R. Pop-Stojanovic
Professor of Mathematics

This dissertation was submitted to the Graduate Faculty of the College of Engineering and to the Graduate Council, and was accepted as partial fulfillment of the requirements for the degree of Doctor of Philosophy.

December, 1975

Dean, College of Engineering

Dean, Graduate School